DECOMPOSITION BEHAVIORS OF VARIOUS CRYSTALLINE CELLULOSES BY HYDROTHERMAL TREATMENT

ROSNAH ABDULLAH

Contents

CHAPTER 1
Introduction

1.1 The Significance of Lignocellulose for Biofuels

The current global issues on energy security and sustainability, as well as serious environmental impacts from global warming have enforced us to look for alternative energy resources. They are required to substitute petroleum-based fuels and products in a large scale in order to help remedy the issues, as well as to satisfy the increasing commodity needs of our society, particularly, in transportation sector (Ribeiro et al. 2007; IEA 2012).

Biomass is seen as potential resources for biofuels (Kheshgi et al. 2000; Fischer and Schrattenholzer 2001; UNEP 2009; IEA 2013). Its world primary production is estimated to be around 1,900 billion dried tons/year (Whittaker 1970). The plant biomass, known as lignocellulose, comprises cellulose, hemicellulose, lignin and other polymeric constituents. It is considered as the most abundant organic material on the earth and consists of non starch-based fibrous part of plant materials. Lignocellulose is a carbon-neutral renewable resource. It does not add to the greenhouse emission as it is environmentally benign which possibly reduces NOx and SOx depending on the fossil-fuels displaced. Moreover, it appears to have a significant economic potential given the fluctuating prices of the fossil fuels.

Due to the promising values of biomass for biofuel productions, policies and acts have been documented. These essentially triggered the development of biofuels demand by targets and blending quotas. Mandates for blending biofuels into vehicle fuels had been enacted worldwide (REN21 2005). The recent targets define higher levels of envisaged biofuels use in various countries. In general, most mandates require blending 10–15 % ethanol with gasoline (U.S. EPA 2011).

The Renewable Fuel Standard (RFS) program has been revised to increase the volume of renewable fuel blended into transportation fuel, from 34 billion litres/year in 2008 to 136 billion litres/year by 2022 (U.S. EPA 2011). The revised standards (RFS2) established new specific annual volume requirements for cellulosic biofuels, biomass-based diesel, advanced biofuels and totally renewable fuel in

transportation fuel. Biofuels could increase their penetration significantly in all long-term scenarios.

1.2 Cellulose as Feedstocks for Bioethanol Production

Cellulose production is approximated to be around 100 billion tons/year (Hon 1994; Klemm et al. 2005). It exists as the framework substance in lignocelluloses in the form of cellulose microfibrils, whereas hemicellulose presents as the matrix substance associated with the cellulose. Lignin, on the other hand, is the encrusting substance solidifying the cell wall associated with hemicellulose (Fujita and Harada 2001). The schematic diagram of cellulose microfibrils is shown in Fig. 1-1.

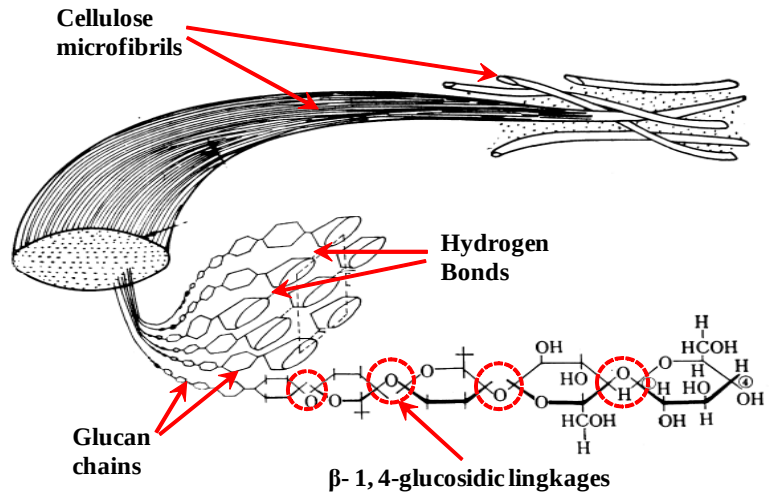

Fig. 1-1 The schematic diagram of cellulose mircrofibrils (Roelofsen 1965)

In recent decades, the cellulosic biofuel research, also known as "the advanced and conventional biofuels" has attracted much attention because of the availability of cellulose (40-50 wt% of dry substance) in most lignocellulosic biomass (Lynd et al. 1991; Fujita and Harada 2001). Due to the non-competing properties with food and feed resources, cellulose has been considered as potential feedstocks for bioethanol production.

In cellulose structure of the plant cell wall, identical to the building blocks, glucoses are linked together by β-1,4 glucosidic linkages. This consequently generates a linear, rigid and crystalline structure making it very resistant to biological

attack (Gray et al. 2006). These linkages can be broken down to form monomeric sugars, such as glucose, essential for fermentation process. The main stream for bioethanol production however is still based on food-based feedstocks, even though potential supply of cellulosic biomass is far higher than that of food crops.

When starch- or sugar-containing feedstocks, such as corn or sugarcane are used, the cost of raw material account for 40-70 % of the total ethanol production cost (Classen et al. 1999). The utilization of such starch or sugar for energy resources will compete with that for food products, leading to food shortage problems in the future. In contrast, when inedible feedstocks are used as raw materials, it is possible to produce large amounts of low-cost bioethanol (Wheals et al. 1999).

To attain the economical feasibility, a higher bioethanol yield is crucial. However, to date the development of bioethanol production from cellulosic biomass has been impeded by its great resistance to be hydrolyzed into sugars because of its crystalline structures. In converting cellulose to bioethanol, a pretreatment process is usually needed to render cellulose for more amenable and accessible towards hydrolysis through various ways such as chemical, physico-chemical, enzymatic and hydrothermal treatments. Though the cost of cellulosic biomass is perceived to be far lower than that of food-based crops, the cost to obtain sugars from cellulose prior to bioethanol production has historically been far too high to attract industrial interest.

Bioethanol production from cellulosic biomass generally follows these sequences: pretreatment, enzymatic saccharification, fermentation, product recovery and distillation. All the sequences steps are more or less the same, though various pretreatment methods can be used. The enzyme will hydrolyze cellulose to form fermentable sugars, and then convert to bioethanol by yeasts/bacteria.

1.3 Origin of Cellulose

Cellulose originates from a taxonomically diverse group of organisms including plants, bacteria, fungi, tunicate and protists (Nakashima et al. 2004). Wood plants are the general source of cellulose. The bacteria *Acetobacter xylinum* is a common non-plant source of cellulose; others comprise tunicate cellulose (e.g. *Microcosmus fulcatus*) which is produced by sea creatures, and protists which

mostly consist of unicellular microorganisms. All of them have the ability to biosynthesize cellulose (Favier et al. 1995; Nakashima et al. 2004; Stone 2005).

Table 1-1 Chemical composition of some typical cellulose-containing materials

Biomass source	Composition (g/g of oven-dried biomass basis)			
	Cellulose	Hemicellulose	Lignin	Others [a]
Japanese beech [b]	0.439	0.284	0.240	0.036
Japanese cedar [b]	0.379	0.227	0.331	0.043
Bamboo [b]	0.394	0.311	0.206	0.079
Rice husk [b]	0.360	0.173	0.241	0.199
Wheat straw [b]	0.371	0.340	0.200	0.077
Corn cob [b]	0.343	0.328	0.180	0.140
Miscanthus [b]	0.337	0.248	0.223	0.170
Baggasse [b]	0.383	0.309	0.224	0.074
Oil palm trunk [b]	0.306	0.284	0.282	0.112
Nipa frond [b]	0.324	0.291	0.196	0.155
Corn stalks [c]	0.350	0.250	0.350	0.050
Cotton [c]	0.950	0.020	0.009	0.004
Flax (retted) [c]	0.712	0.206	0.022	0.060
Hemp [c]	0.702	0.224	0.057	0.017
Istle [c]	0.735	0.070	0.174	0.019
Jute [d]	0.654	0.176	0.144	0.025
Ramie [e]	0.701	0.098	0.093	0.067
Sisal [f]	0.560	0.240	0.090	0.011

[a] Others include extractives, inorganics (ash), protein, wax and pectin; [b] Rabemanolontsoa and Saka 2013; [c] Hon 1996; [d] Wang et al.2008; [e] Kalita et al. 2013; [f] Fávaro et al. 2010

Despite the wide range of cellulose resources available, the current research for bioethanol production is highly concentrated on wood plant cellulose (Oilgae 2010; Bracmort 2013), which indirectly makes lignocelluloses as the major source of cellulose. Typical cellulose-containing materials with their chemical

composition are summarized in Table 1-1. Besides cellulose which is seen as the main components in woods, hemicellulose, lignin and a comparably small amount of other components such as extractives, inorganics (ash), protein, wax and pectin are also present.

1.3.1 Cellulose molecular structure

Cellulose is a linear homopolysaccharides consisting of β-1,4 D-glucopyranose units. The adjacent units are arranged so that glucosidic oxygens point in opposite directions to form cellobiose, the actual repeating unit of cellulose. The cellobiose units, illustrated in Fig. 1-2, are linked together to form an extended, linear chain.

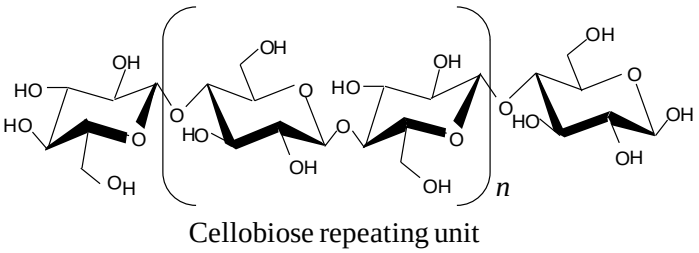

Fig.1- 2 The cellobiose unit of cellulose molecular structure

The parallel chains are later bonded each other by inter- and intra-molecular hydrogen bonds forming cellulose molecules. The presence of inter-molecular hydrogen bonds is responsible for the sheet-like nature of the native polymer, whereas the intra-molecular hydrogen bonds are relevant with regards to the single-chain conformation and stiffness. This resulted in aggregation of a highly crystalline and paracrystalline regions of cellulose microfibrils. The products on the combination of these microfibrils (~ 2-5 nm width) are cellulose fibers (Isogai 1994).

Due to the massive linkages, cellulose has becoming highly inert and resistant to hydrolysis. This may explain why oligomers with a degree of polymerization (DP) ≥ 6 are practically insoluble, despite that the molecule itself has a hydrophilic character. The physical properties, chemical reactivity and biological functions of cellulose are essentially determined by this compact structure. In terms of its density (1.5×10^3 kg/m^3), cellulose fibers are stiffer (Young Modulus 50-130 GPa) and

stronger (1 GPa), when measured along the polymer length, than nylon, silk, chitin, tendon, etc (Ashby et al. 1995).

The DP indicates the number of glucopyranose units in cellulose molecules. On average, the DP of native celluloses is higher than that of the treated celluloses. Table 1-2 reveals some examples to show the differences of DP on native and treated celluloses (Heinze 1998; Zugenmaier 2008).

Table 1-2 Average DP evaluated from the molecular mass distribution of some selected celluloses ([a] Heinze 1998; [b] Zugenmaier 2008).

	Cellulose	DP
Native cellulose	Cotton [b]	10,000-15,000
	Bacterial cellulose [b]	4,000-6,000
	Ramie [b]	10,000
	Flax [b]	9,000
	Valonia [b]	25,000
	Wood cellulose [b]	6,000-10,000
Treated cellulose	Cotton linters bleached [b]	1,000 -5,000
	Avicel [a]	280
	Chemical pulp bleached [b]	700
	Sulfate pulp [a]	900-2000
	Cellophane [b]	300
	Rayon [b]	300-500
	Cellulose acetate [b]	200-350

The DP of the treated celluloses on average is seen to be shorter i.e., < 5,000. The soluble oligosaccharides are shorter fragments of cellulose with DP up to 12, which are soluble and only slightly soluble for $DP \leq 6$ and $6 < DP < 12$, respectively (Pereira et al. 1988; Zhang and Lynd 2004; Ehara and Saka 2005). The DP of a molecule portrays its character, thus DP is seen as an important property for cellulosic materials. There are many established DP test methods for cellulose, for instance, cellulose dissolution in cupriethylenediamine solution (TAPPI 1982),

organic solvents or inorganic acids followed by derivatization or ionic solutions. The DP of cellulose may be represented in terms of the number-average, weight-average or viscosity-average and measured by diverse instruments such as osmometry, size-exclusion chromatography or determination of reducing-end concentration, cryoscopy etc (Zhang and Lynd 2005).

1.3.2 Crystalline structure

The crystalline structure of cellulose has been demonstrated by studies with X-ray diffractometry (XRD), electron diffractometry, infrared (IR) spectroscopy, Raman spectroscopy etc (Marchessault and Liang 1960; Sugiyama et al. 1991a, 1991b; Horii 2000; Fujita and Harada 2001). The cellulose crystallites are imperfect in terms of crystallinity, crystalline size, cellulose molecules orientations and crystalline purity (Isogai 1994). To determine the coordinates of all heavy atoms of cellulose in a unit cell, various crystallographic planes are used to describe the unit cell of cellulose (Gardiner and Sarko 1985; Isogai 1994; Langan et al. 2001; Nishiyama et al. 2002, 2003; Wada et al. 2004a). In this chapter, the [001] direction on an *a*-*b* plane is used to describe the projection of unit cells of cellulose.

1.3.3 Cellulose polymorphs

There have been extensive studies devoted for the investigation on cellulose polymorphs (Gardner and Blackwell 1974; Hayashi et al. 1975; Sarko et al. 1976; Isogai et al. 1989; French et al. 1993; Isogai 1994; Nishiyama et al. 2002, 2003; Wada et al. 2004a, 2004b). The interest arises due to the vast abundance of cellulose in nature and their technological utilization on a very large scale. Each of the polymorphic form has a significant difference from the technological point of view, and their presence in a cellulose-based product markedly affects their properties.

There are six known polymorphs of cellulose, namely celluloses I, II, III_I, III_{II}, IV_I, and IV_{II}, identified by their characteristic XRD patterns as well as ^{13}C nuclear magnetic resonance (NMR) spectra. These celluloses can be prepared by various methods and may be interconverted (Isogai 1994). The interconversion process of these cellulose polymorphs is shown in Fig. 1-3 (Kroon-Baternburg et al. 1996).

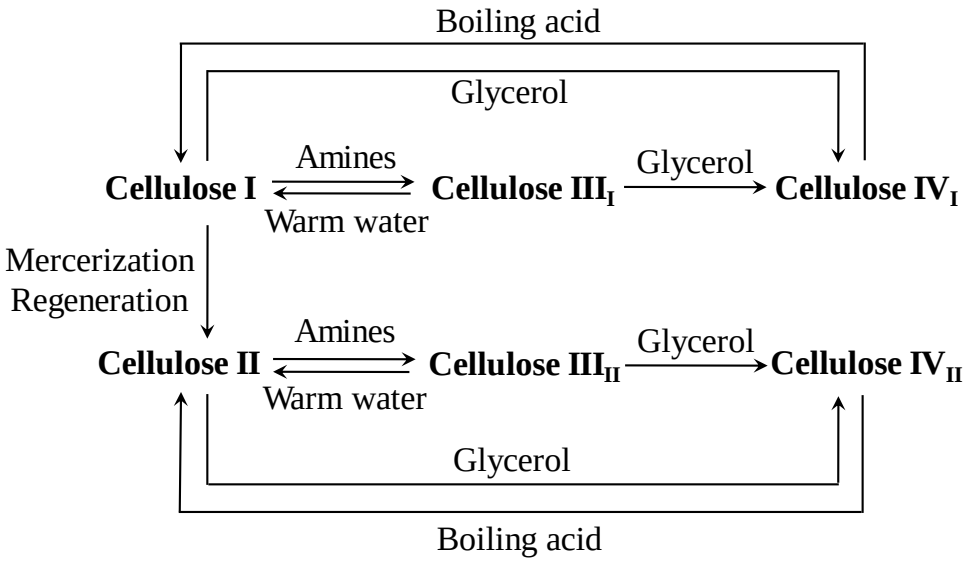

Fig. 1-3 Polymorphy of celluloses (Kroon-Baternburg et al. 1996)

Native cellulose, also known as cellulose I, is abundant in nature and has parallel arrangement of chains, whereas cellulose II can be prepared by two distinct routes: mercerization by alkali treatment and regeneration through solubilization and subsequent recrystallization. It is thermodynamically more stable in structure with an antiparallel arrangement of the strands and some inter-sheet hydrogen bonds. Celluloses III_I and III_{II} can be prepared from celluloses I and II, respectively, by treatment with liquid ammonia or organic amines. The swelling of cellulose from the treatment is a simple and classical way to increase the accessibility of crystalline cellulose (Da Silva Perez et al. 2003). On the other hand, celluloses IV_I and IV_{II} can be obtained by heating celluloses III_I and III_{II}, respectively, at 260 ˚C in pressurized glycerol (Hayashi et al. 1975; Isogai 1994; O'Sullivan 1997).

1.3.3.1 Cellulose I

Cellulose I has a monoclinic unit cell with space group $P2_1$ and parallel arrangement of chains (Meyer and Misch 1937). It could be further classified into two polymorphs, celluloses I_α and I_β, whose detailed structures have been established recently through synchrotron X-ray and neutron fiber diffraction studies (Atalla and VanderHart 1984; Sugiyama et al. 1991a; French et al. 1993; Nishiyama et al. 2002, 2003). They are differences in their resonances of C-1 atoms i.e., singlet for

cellulose I_α and a doublet for cellulose I_β. This rather small difference indicates a different hydrogen bonding pattern of the glucosidic linkages. Cellulose I_α is described as a triclinic structure, with one cellulose chain per unit cell, whereas a monoclinic with two chains per unit cell for cellulose I_β. Their unit cell projections in [001] directions are shown in Fig. 1-4.

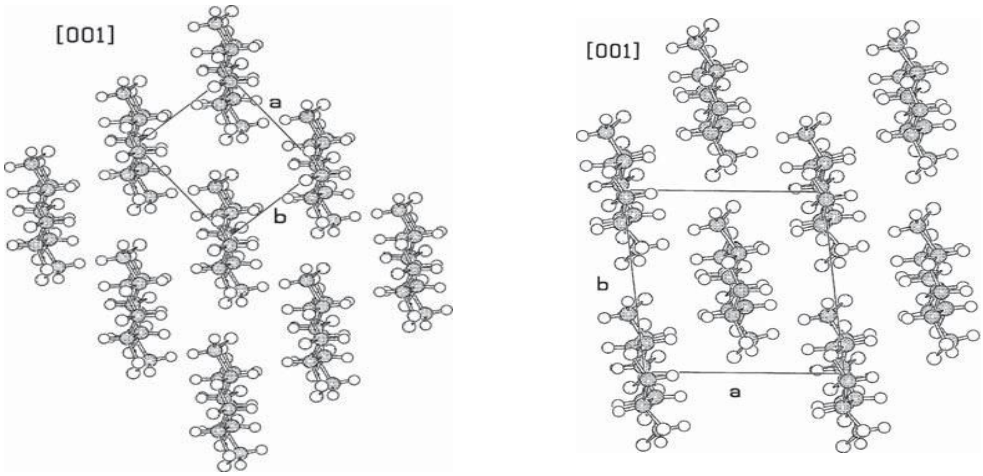

Cellulose I_α Cellulose I_β

Fig. 1-4 Sheet-like arrangements of celluloses I_α (Nishiyama et al. 2003) and I_β (Nishiyama et al. 2002)

Marine algal and bacterial celluloses are found to be rich in cellulose I_α with the average mass ($\bar{m}$) of 63% (Isogai 1994), while ramie, cotton and wood are dominated by cellulose I_β with $\bar{m}$ of about 80%. Cellulose I_β chains are packed in a more stable form in its unit cell than that of I_α (Yamamoto and Horii 1993). It has also been shown that cellulose I_α is entirely transformed into cellulose I_β phase without losing its crystallinity, by hydrothermal treatment or by treatments with various solvents (Wada et al. 2004a).

1.3.3.2 Cellulose II

Cellulose II has a two chain unit cell with space group $P2_1$ and has parallel chain arrangement. It can be prepared from cellulose I by mercerization process, i.e., the intra-crystalline swelling of cellulose I in 17-22 % (w/v) aqueous sodium

hydroxide (NaOH), followed by decomposition of the intermediate via washing out the NaOH (Kolpak et al. 1978; French et al. 1993; Zugenmaier 2008). The swelling allows for reorganization of the chains and results in cellulose II when the swelling agent is removed. Nevertheless, the molecular mechanism of the conversion during the swollen state is largely unknown. It can also be prepared by regeneration process by dissolving cellulose in a derivative-forming solvent and then reprecipitating it by diluting in water. Both procedures lead to the same unit cells. The conversion of cellulose I to cellulose II is generally considered to be irreversible. The unit cell projection of cellulose II is shown in Fig. 1-5.

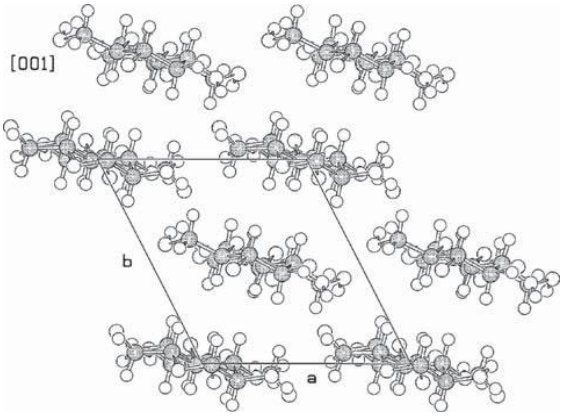

Fig. 1-5 Sheet-like arrangements of cellulose II (Langan et al. 2001)

1.3.3.3 Cellulose III

Cellulose III is an important cellulose allomorph because it is the basis for composite cellulose. It is a low-temperature modification structure of cellulose (Kulshreshtha 1979). Two crystalline cellulose structures III_I and III_{II} that can be prepared by treating cellulose I and cellulose II, respectively, with liquid ammonia or organic amines, followed by washing with alcohol and drying in air (Marrinan and Mann 1956; Hayashi et al. 1975; Chanzy et al. 1983; Isogai 1994). This conversion, however, is reversible (Kroon-Baternburg et al. 1996; Wada 2001). The unit cells for both allomorphs are found to be very similar, with some differences in intensities of the meridional reflections only (Sarko et al. 1976). These findings were recently

supported by a comparison of the two similar X-ray fiber patterns of celluloses III_I and III_{II}. However, it is assumed that the two structures pack in quite different fashion, parallel arrangements in cellulose III_I and anti-parallel in cellulose III_{II}. This is concluded from the fact that cellulose III_I can revert back by boiling water for 30 min (Roche and Chanzy 1981) or through a solvent complex to the parallel-packed cellulose I and that cellulose III_{II} can be converted by the same heat treatment to antiparallel-packed cellulose II.

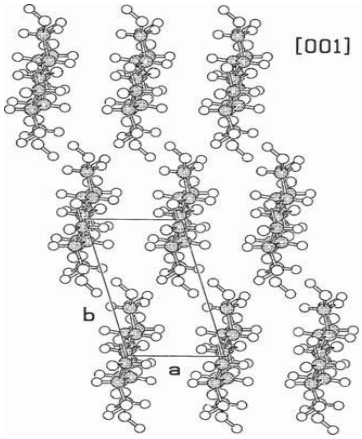

Fig. 1-6 Sheet-like arrangements of celluloses III_I and III_{II} (Wada et al. 2004b)

Similar X-ray diagrams for celluloses III_I and III_{II} were found and a two-chain unit cell for cellulose III_I was proposed as in Fig. 1-6 (Wada et al. 2004b). This idea was motivated by the necessity for two anti-parallel running chains in cellulose III_{II} and the almost identical X-ray patterns of the two structures.

1.3.3.4 Cellulose IV

In contrast with cellulose III, cellulose IV is a high modification structure of cellulose (Kulshreshtha 1979). Celluloses IV_I and IV_{II} are produced by heating celluloses III_I and III_{II}, respectively, in a pressurized glycerol treatment for 30 min at 260 ˚C (Hayashi et al. 1975; Isogai, 1994). Glycerol acts as a protective plasticizing medium, allowing the cellulose molecules to retain sufficient mutual mobility in order to arrange themselves into another stable lattice at 250 ˚C. There is no additional compound of cellulose and glycerol is formed during this conversion.

Figure 1-7 shows the structure of celluloses IV_I and IV_{II}. The XRD patterns of celluloses IV_I and IV_{II} and their unit cells are very similar but their derived structures can be distinguished upon heterogeneous acetylation. It is necessary to convert cellulose I to cellulose III_I before its transformation into cellulose IV_I because of fibrillation of cellulose microfibrils. It makes them more accessible to the reaction for conversion to cellulose IV_I that occurred through the change to cellulose III_I. The perfection of cellulose IV_I depends on the crystallinity of the original sample either the starting material being celluloses I or III_I.

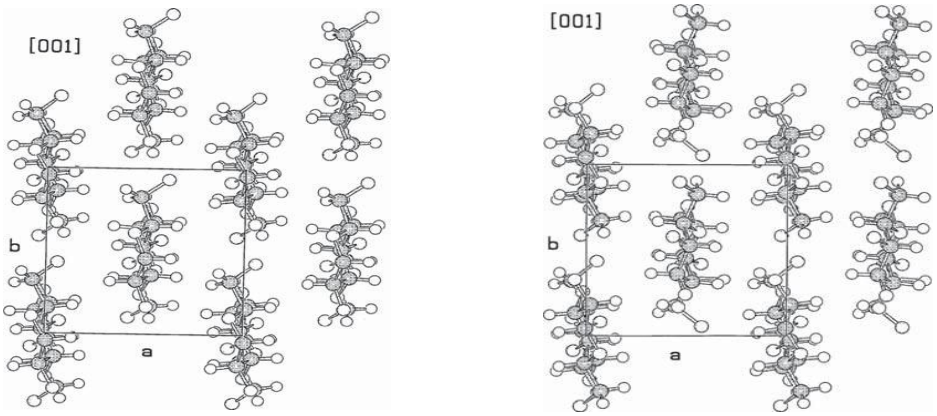

Cellulose IV_I Cellulose IV_{II}

Fig. 1-7 Projection of the celluloses IV_I and IV_{II} (Gardiner and Sarko 1985)

In a recent study using *clodaphora*, the structure of cellulose IV_I was revealed to contain lateral disorder of cellulose I (Wada et al. 2004a), agreeable with other findings that cellulose IV_I comprise mixtures of celluloses IV_I (~ 60 %) and I (Marrinan 1956; Isogai 1989; Newman 2008). In either case, the structure cannot be termed as cellulose I, thus, it seems acceptable to consider it as cellulose IV_I, like in the literatures (Chanzy et al. 1979; Gardiner and Sarko 1985). A study was done on disencrusted cellulose sub-elementary fibrils of the primary cell wall of cotton and rose cells which lead to the conclusion that the two observed diffraction spots on the equator agreed with that of cellulose IV_I but not cellulose I (Chanzy et al. 1979).

The morphology of the heavily treated initial cellulose may facilitate a rearrangement of the chains during the conversions as observed by Wada et al. (2004a), which may be hindered through morphological restraints. In the case of the

sub-elementary fibrils studied by Chanzy et al. (1979) the lateral disorder seemed to be an intrinsic property of the fibrils and cannot be erased by treatments normally leading to cellulose I (Zugenmaier 2008).

1.4 Decomposition of Cellulose for Bioethanol and Biochemical Productions

The decomposition of cellulose has been receiving considerable attention for both bioethanol and biochemical productions. Hydrolysis of cellulose, especially involving high temperature and pressure, is very often not only producing sugars alone, but also other degraded products (through dehydration and fragmentation) such as furfural, erythrose etc (Antal and Mok 1990a; Ehara et al. 2002; Phaiboonsilpa et al. 2010). For this reason, it is safe and valid to define the process of breaking down of cellulose as *decomposition of cellulose* which literally includes either/both hydrolysis or/and degradation processes.

Numerous methods on physico-chemical, chemical, enzymatic and hydrothermal treatments have been utilized worldwide for decomposition of cellulose, in order to obtain sugar molecules, particularly, glucose for further fermentation process (Eriksson 1982; Bobleter et al. 1983; McMillan 1994; Bjeree et al. 1996; Ando et al. 2000; Aden et al. 2002; Kumar et al. 2010; Mittal et al. 2011). In literatures, the methods are mostly described as pretreatment steps for lignocellulosic materials because cellulose is associated with hemicellulose which is encrusted with lignin.

This study focuses on cellulose, thus it would rather be described as treatment technology for cellulose decomposition. Some selected well-known treatment technologies that will be discussed broadly are classified into chemical, enzymatic and hydrothermal treatments. It is also common to have one or more combinations of treatment methods for cellulose decomposition such as acid hydrolysis followed by enzymatic treatment etc.

Despite of various methods available and applied, the two main key limiting factors for cellulose decomposition are still on existing, (1) the accessibility of the surface contact of cellulose and (2) cellulose crystallinity (Xiao et al. 2011). The reduction on these factors would significantly improve the decomposition process (McMillan 1994). In addition, better sugar yields can be obtained if the formation of

sugars or the ability to subsequently produce sugars by enzymatic hydrolysis can be improved and the degradation or loss of carbohydrates can be avoided during the process of cellulose decomposition (Sun and Cheng 2002).

1.4.1 Chemical treatments

1.4.1.1 Acid/alkali hydrolysis

The acid/alkali hydrolysis methods are widely used for cellulose decomposition. These treatments increase surface area and reduce the cellulose crystallinity due to structural swelling and dissolution. There are two types of cellulose swelling involved, inter-crystalline and intra-crystalline. Inter-crystalline swelling can be affected by water, whereas intra-crystalline swelling requires a chemical agent for breaking the hydrogen bonding of the cellulose.

Acid hydrolysis can be performed with several types of acids, including sulfuric, hydrochloric, phosphoric, formic etc and can be either concentrated or diluted (Harris and Beglinger 1946; Camacho et al. 1996). Processes involving concentrated acids are operated at low temperature and give high yields (e.g., 90 % of theoretical glucose yield). However, a large amount of acids used cause problems associated with toxicity to the environments, corrosion and energy demand for acid recovery process (Jones and Semrau 1984). The concentrated acid must be recovered after hydrolysis to make the process economically feasible (Sivers and Zacchi 1995). On the other hand, dilute acid hydrolysis requires high temperature treatment for acceptable conversion rates of cellulose to glucose. Unfortunately, acidity and high temperature increase both the rate of cellulose hydrolysis and the rate of decomposition of glucose products (Jones and Semrau 1984; McMillan 1994).

Alkali hydrolysis is usually used to enhance enzymatic hydrolysis of cellulosic materials (Karr and Holzapple 2000). The main reagents used for this process is NaOH, ammonia, calcium hydroxide, and oxidative alkali. Dilute NaOH aqueous solution causes disruption of carbohydrate linkages and swelling of cellulose, a reduction of cellulose crystallinity, an increase in surface area and a decrease in the DP.

1.4.1.2 Ionic liquid

Ionic liquids are a group of new organic salts that exist as liquids at a relatively low temperature. They are chemically and thermally stable, non-flammable and have low volatility (Zhu et al. 2006). These properties can be tuned to dissolve/liquefy a wide variety of compounds including cellulose.

Liquefaction of cellulose in ionic liquids, such as 1-ethyl-3-methylimidazolium chloride (Miyafuji et al. 2009), 1-butyl-3-methylimidazolium chloride (Sievers et al. 2009), 1-allyl-3-methylimidazolium chloride (Zhu et al. 2006), 1-ethyl-3-methylimidazolium acetate (Lee et al. 2009; Cetinkol et al. 2010) etc. and their subsequent regeneration to amorphous cellulose by using anti-solvent such as water, ethanol, methanol, acetone has gained many research interests. Cellulose crystalline structure is observed to be gradually broken down in ionic liquid treatment (Miyafuji et al. 2009). The hydrolysis rate of regenerated cellulose is significantly increased and the initial rates of hydrolysis are approximated to be in the order of magnitude higher than that of untreated cellulose (Dadi et al. 2006). While, a nearly complete conversion of the carbohydrate fraction into water-soluble (WS) products is readily observed at 120 ˚C in ionic liquids, which is lower than the temperatures typically applied for aqueous-phase hydrolysis (Sievers et al. 2009). After regeneration of celluloses, the ionic liquids can be recovered and reused, however the cost and recycling of ionic liquid are the major disadvantage of the process.

1.4.2 Enzymatic treatments

Enzymatic treatment, also known as enzymatic saccharification, is a slow process and the extent of hydrolysis is influenced by the structural properties such as cellulose crystallinity, surface area, DP and porosity (Mittal et al. 2011). It is carried out by a highly specific enzyme called cellulase (Béguin and Aubert 1994). The products of the treatment are usually monosaccharides such as glucose, though some cellobiose could still present in the end results as products.

The enzymatic hydrolysis has low energy consumption because it is usually conducted at mild conditions (pH 4.8-5.0, ≤ 50 ˚C), has low waste disposal and no

corrosion problems (Duff and Murray 1996; Mittal et al. 2011). However, some challenges such as the retardation of hydrolysis rate, high cellulose loading and little knowledge about the cellulose kinetics are very commonly faced. The cellulase can be produced from both bacteria and fungi, however the cellulase excreted from bacteria is more complicated than that of fungi as it is produced as intracellular enzyme. These microorganisms can be aerobic or anaerobic, mesophilic or thermophilic.

Bacteria belonging to species such as *Clostridium, Cellulomonas, Thermomonospora, Ruminococcus* etc can produce cellulase (Bisaria 1991). Among those, *Cellulomonas fimi* and *Thermomonospora fusca* have been extensively studied for cellulase production. Many cellulolytic bacteria, particularly the cellulolytic anaerobes such *as Clostridium thermocellum and Bacteroides cellulosolvens* produce cellulases with high specific activity but do not produce high enzyme titres (Duff and Murray 1996). They have a very low growth rate and require anaerobic growth conditions, thus, most research for commercial cellulase production has focused on fungi. Fungi that have been reported to produce cellulases include *Sclerotium rolfsii, Phanerohaete chrysosporium and* species of *Trichoderma, Aspergillus* and *Penicillium* (Fan et al. 1987; Duff and Murray 1996). From these, *Trichoderma* has been most extensively studied for cellulase production (Sternberg 1976).

Cellulases are usually composed of 3 major components that are involved in the treatment process: (1) endoglucanase - attacks regions of low crystallinity in the cellulose fiber to create free chain-ends; (2) cellobiohydrolase - degrades the molecule further by removing cellobiose units from the free chain-ends; and (3) β-glucosidase - hydrolyses cellobiose to produce glucose (Sun and Cheng 2002). During the treatment, cellulose is decomposed by the cellulase to reducing sugars from its long chains, which can be fermented by yeasts/bacteria to produce ethanol (Wright 1998).

1.4.3 Hydrothermal treatments

1.4.3.1 Sub/supercritical water

Water has a relatively high critical point (374 ˚C/22.1 MPa) due to the strong interaction between the molecules that are caused by numerous hydrogen bonds. Liquid water below the critical point is referred as subcritical water whereas water above the critical point is termed supercritical water. Both density and dielectric constant of the water medium play major roles in solubilizing different compounds. At these conditions, water becomes a good solvent for cellulose so that its decomposition can take place without any catalysts, resulting in the efficient conversion into various WS saccharides (Antal and Mok 1990b; Minowa et al. 1998; Ando et al. 2000; Sasaki et al. 2002; Kamio et al. 2006).

When water is heated, hydrogen bondings start to weaken, allowing the dissociation of water into acidic hydronium ions (H_3O^+) and basic hydroxide ions (OH^-). The structure of water changes significantly near the critical point because of the breakage of infinite network of hydrogen bonds (Kalinichev and Churakov 1999). In fact, dielectric constant of water decreases considerably near the critical point, which causes a change in the dynamic viscosity and also increases self-diffusion coefficient of water (Marcus 1999).

In the sub/supercritical region, higher ionic products exist, therefore, higher H^+ and OH^- ion concentrations compared to ambient water, which offers a highly interesting reaction medium for hydrolysis process. Acid neutralization is not required because the H^+ ion concentration is a function of temperature and decreases when the temperature is lowered.

The intermediates formed during the reactions show a high solubility in sub/supercritical water; hence reaction steps are mainly homogeneous. Diffusion related problems such as mass transfer through the interface are not encountered in homogeneous reaction (Kruse and Gawlik 2003; Peterson et al. 2008). The physical properties such as viscosity, ionic products, density, dielectric constant and heat capacity, change dramatically in the sub/supercritical regions with only a small change in the temperature or pressure, resulting in a substantial increase in the rates of chemical reactions (Franck 1987; Savage 1999). These substantial changes in the

physical and chemical properties of water in the vicinity of its critical point can be utilized advantageously for cellulose decomposition (Dinjus and Kruse 2004; Peterson et al. 2008).

Sasaki et al. (2000, 2003) suggested that cellulose hydrolysis at high temperature takes place with liquefaction in water. This is probably because of the cleavage of intra- and inter-molecular hydrogen bondings in the cellulose crystal. The decomposition rate of cellulose in subcritical water treatment was found to be extremely high, however, the hydrolysis rate of cellulose was much lower than the degradation rate of glucose and its oligomers (Sasaki et al. 1998). While in another study (Saka and Ueno 1999), cellulose was rapidly decomposed in supercritical water for 5-10 s to produce cellobiose, glucose and levoglucosan. However, glucose was further degraded due to the high temperature of the supercritical water treatment.

1.4.3.*2* Hot-compressed water

Several years ago, it was clarified that high pressure (40-70 MPa) and high temperature (350-400 ˚C) enhanced the dehydration of glucose to 5-hydromethylfurfural (5HMF) that caused inhibitory effect to the subsequent fermentation process (Aida et al. 2007). Moreover, the economic and environmental constrains limit the applicability of these subcritical/supercritical methods (Liu and Wyman 2005). As a result, hot-compressed water (HCW) appears as a better option for decomposition of cellulose.

The HCW refers to the water at sub/supercritical state, or at sufficiently high pressure and temperature (Phaiboonsilpa 2010). It has a milder condition process with high ionic products as compared to sub/supercritical water treatment, environmentally friendly characteristics and attractive reaction media for a variety of applications (Ando et al. 2000; Rogalinski et al. 2008).

The HCW system can be categorized as batch- and flow-type systems (Kusdiana et al. 2002). The decomposition reaction of cellulose is dominant in batch-type reaction; therefore, a flow-type HCW treatment is preferable (Ehara et al. 2002; Liu and Wyman 2003). Another kind of HCW system is a semi-flow type. It resulted better digestible cellulose (Xiao et al. 2011), greater removal of lignin (Tirtowidjojo et al. 1988), higher sugar recovery from hemicelluloses (Bobleter et al.

1983) and less inhibitors in the hydrolyzed liquid as compared with the conventional batch and co-current flow systems (Liu and Wyman 2003).

Recently, the two-step semi-flow HCW treatments were used to study the chemical conversion of lignocellulosic biomass (Lu et al. 2009; Phaiboonsilpa 2010; Phaiboonsilpa et al. 2010, 2011) and revealed that 230 ˚C/10 MPa/15 min and 270 ˚C/10 MPa/15 min were, respectively, the optimum conditions for decomposition of hemicellulose and cellulose. It was shown that the main reaction of saccharides involve hydrolysis, dehydration and fragmentation.

1.5 Summative Description of This Dissertation

While cellulose decomposition has been prominent for bioethanol and biochemical productions around the world, the study on the decomposition has been primarily limited to only celluloses I, II and III_I by using conventional methods. Therefore, it is the aim of this dissertation to study in depth on decomposition behaviors of various crystalline celluloses (I, II, III_I, III_{II}, IV_I and IV_{II}) by hydrothermal treatment. It specifically focuses on the fundamental understanding of the reactions involved in the treatment by investigating the hydrothermal conversion of various crystalline celluloses and additionally, to determine quantitatively various hydrolyzed and degraded products obtained.

The *Chapter 1* of this dissertation has been covered as introduction that discussed on the importance of lignocellulosic resources, cellulose backgrounds and the trends on cellulose decomposition treatments by diverse methods starting with conventional to the newly developed technologies, discussion of their advantages and weaknesses, as well as the issues that lead to the importance of the current study.

In *Chapter 2*, various crystalline celluloses were prepared as feedstocks. By using semi-flow HCW system as the treatment medium, decomposition behaviors of the celluloses at 230-270 ˚C/10 MPa/2-15 min were studied thoroughly. This chapter focused principally on understanding the changes in the physical characteristics of these celluloses such as the DP and crystallinity. It was observed that the crystallinity remained unaffected during the treatment, whereas the DP decreased with treatment temperatures. This study revealed that the decomposition behaviors were dependent on the different crystalline forms of the starting celluloses.

In contrast, decomposition behaviors of the celluloses were also explored by means of lower pressure and temperature treatment i.e., through enzymatic saccharification. Here, the well-known cellulase complex of the mesophilic soft rot fungus *Trichoderma viride* was used. The similar parameters such as DP and crystallinity of the celluloses were considered. The crystallinity, DP and the residue were observed to be decreasing with treatment times. The details of the study were discussed in *Chapter 3*.

As a further approach, using mainly data obtained from the WS portions, the hydrothermal decomposition of the celluloses as treated by semi-flow HCW were explored in *Chapter 4*. The hydrothermal decomposition and its decomposition kinetics were found to be dependable on treatment temperature as well as crystalline form of celluloses. The hydrothermal decomposition of the celluloses was found to be similarly following the decomposition pathways of cellulose I (Phaiboonsilpa et al. 2010). In this treatment, hydrolysis reaction was shown better because less degradable products were obtained.

Cellulose III is an important cellulose allomorph as it is the basis for composite cellulose. Thus, a comprehensive examination was conducted for the polymorphs of the cellulose in HCW treatments and reported in *Chapter 5*. It was found that celluloses III_I and III_{II} were reconverted into their respective parent celluloses and were dependent on pressures and temperatures within HCW condition limits.

For *Chapter 6*, the molecular dynamics (MD) simulation was examined for the decomposition behaviors of the crystalline models cellulose I_β, II, III_I and IV_I under the HCW condition. The MD simulation, however, can only illustrate how the crystalline celluloses decompose qualitatively, but not quantitatively, and the procedure was unable to differentiate the biochemicals produced in the WS portions. The study shows that the hydrogen bonding interactions play important roles in the process and the decomposition behaviors were due to different crystalline form of celluloses, in good agreement with the experimental data reported in *Chapter 2*.

Finally, the decomposition behaviors of the celluloses based on the studies presented earlier were summarized and concluded in *Chapter 7*. Prospects for the future studies to fulfill this present research were moreover proposed in this chapter.

CHAPTER 2

Decomposition Behaviors of Celluloses as Studied for the Residues

2.1 Introduction

For the past three decades, hydrothermal treatment, such as hot-compressed water (HCW), has attracted much attention due to its suitability as a non-toxic, an environmentally benign, a non-catalytic and an inexpensive medium for lignocelluloses hydrolysis (Bobleter et al. 1976; Bobleter et al. 1983; Yu and Wu. 2010). About 4-22 % of cellulose was decomposed in HCW (200-230 ˚C/34.5 MPa/15 min) by using flow-type treatment (Mok and Antal 1992). Bobleter and coworkers (1976, 1983) have shown that passing HCW continuously through a stationary biomass bed, also known as, semi-flow HCW treatment, resulted better digestible cellulose (Xiao et al. 2011), greater removal of lignin (Tirtowidjojo et al. 1988), higher sugar recovery from hemicelluloses and less inhibitors in the hydrolyzed liquid as compared with the conventional batch and co-current flow systems (Liu and Wyman 2003).

Previously, the two-step semi-flow HCW treatments of lignocelluloses biomass (Lu et al. 2009; Phaiboonsilpa et al. 2010, 2011) have suggested that 230 ˚C/10 MPa/15 min and 270 ˚C/10 MPa/15 min were optimum conditions for decomposition of hemicelluloses and cellulose, respectively. Thus, the objective of this work is to investigate comprehensively the hydrothermal decomposition behaviors of various crystalline celluloses as treated by semi-flow HCW through their residues at 230-270 ˚C/10 MPa/2-15 min.

The original publication is available at Springer via http://dx.doi.org/10.1007/s10570-013-0022-4

2.2 Materials and Methods

2.2.1 Preparation of various crystalline celluloses

The celluloses were prepared from cotton linter (Buckeye 1AY-500), which, in its native form is cellulose I (cell I). Mercerized cellulose with crystalline form of cellulose II (cell II) was prepared from cell I by soaking it into 20.0 % of aqueous NaOH solution for 24 h at ambient temperature, followed by washing thoroughly with water and freeze-drying (Isogai et al. 1998). Samples with the crystalline forms of celluloses III_I (cell III_I) and III_{II} (cell III_{II}) were prepared from cell I and cell II, respectively, by soaking them in 100 % ethylenediamine (EDA) for 24 h at ambient temperature, washed with dried methanol and kept under vacuum.

The prepared cell III_I and cell III_{II} were further used for the preparation of celluloses IV_I (cell IV_I) and IV_{II} (cell IV_{II}). They were firstly soaked in glycerol for 3 days at ambient temperature and then heated in a reaction vessel at 260 ˚C/0.6 MPa/30 min (Isogai et al. 1989). After cooling down to ambient temperature, the product was washed with water and acetone successively and dried in vacuum. To simplify, the cotton linter (cell I) was converted into group I (celI I, cell III_I, cell IV_I) and group II (cell II, cell III_{II}, cell IV_{II}) celluloses. The chemical compositions of these celluloses were also analyzed and all the cellulose samples were found to contain similar components of about 99.9 wt% glucose and 0.1wt% xylose.

To evaluate decomposition behaviors for the celluloses by semi-flow HCW treatment, celluloses with similar degree of polymerization (DP) are appropriate for their comparison. Consequently, these celluloses were adjusted by trials and errors for their DPs. Cell I were heated in HCW conditions at 100-200 ˚C/10 MPa/10-15 min prior to the preparation processes above and measured the DP. This is repeated until the DP is almost similar.

2.2.2 Determination of degree of polymerization and crystallinity of the celluloses

The DP is an important parameter to be considered in order to study the decomposition behaviors. The viscosities of the celluloses were measured by using 0.5M cupriethethylenediamine (Cuen) (TAPPI, 1982) in a Cannon Fenske capillary

viscometer. The viscosity average DP of the cellulose samples was calculated from the intrinsic viscosity [η] according to the Eq. (2-1) (Sihtola et al. 1963):

$$DP^{0.905} = 0.75[\eta] \qquad \text{Eq. (2-1)}$$

Apart from the DP, the crystallinity of the celluloses is another essential parameter. The X-ray diffraction (XRD) patterns of these celluloses were recorded by X-ray diffractometer Rigaku RINT 2200 equipped with monochrometer. About 20 mg of cellulose was placed on a glass sample holder and flattened carefully, then mounted on the sample holder. X-ray diffraction was conducted on reflectance modes through a 2θ range between 7.5 ˚ and 32.5 ˚ by Cu-K_α radiation (λ=0.1542 nm), operated at 40 kV and 30 mA at ambient temperature. Gaussian functions were used to deconvolute the XRD patterns of various crystalline celluloses. The crystallinity was then calculated from the ratio of the area of all crystalline peaks with less background to the total area (Park et al. 2010).

The diffraction angles of each XRD pattern and their assignment diffraction planes are summarized based on a newly proposed conventional indexing for various unit cells of cellulose (French 2014). Here, the unit cells were mainly referenced to the orientation along *c*-axis, whereby various data from literatures and experimental approaches were used, thus some variations may occur (Gardiner and Sarko 1985; Isogai 1994; Langan et al. 2001; Nishiyama et al. 2002, 2003; Wada et al. 2004a, 2004b).

2.2.3 Fourier transform-infrared analysis of residual celluloses

The Fourier Transform-Infrared (FT-IR) analysis was carried out for the residues of the celluloses obtained after HCW treatments. The spectra of the dried sample pellets in KBr were recorded using a Shimadzu IR-8000 spectrophotometer. All the spectra were recorded with an accumulation of 64 scans, revolution of 4 cm^{-1}, in a range from 4000 to 400 cm^{-1}.

2.2.4 Treatment of the celluloses by semi-flow hot-compressed water

The prepared celluloses (about 0.4 g) as starting materials were treated individually within a 5 ml reaction vessel in a semi-flow HCW system at temperatures of 230, 250 and 270 ˚C under 10 MPa for 2-15 min. The semi-flow HCW conversion system and its operational procedures as explained elsewhere were adapted for this study (Lu et al. 2009; Phaiboonsilpa et al. 2010, 2011). Briefly, the ambient distilled water from a water tank was flown through the reaction vessel by a pump in order to pressurize the system at 10 MPa controlled by a back-pressure regulator. To raise the temperature, the preheating unit monitored by thermocouples was used to reach at the designated temperature of 230, 250 and 270 ˚C for about 20 min under 10 MPa and remain constant for additional 15 min, totally 35 min. In vaddition, another heating unit was installed at the reaction vessel to maintain the designated temperature in the reaction vessel, into which the HCW was passed through at the flow-rate of 10 ml/min.

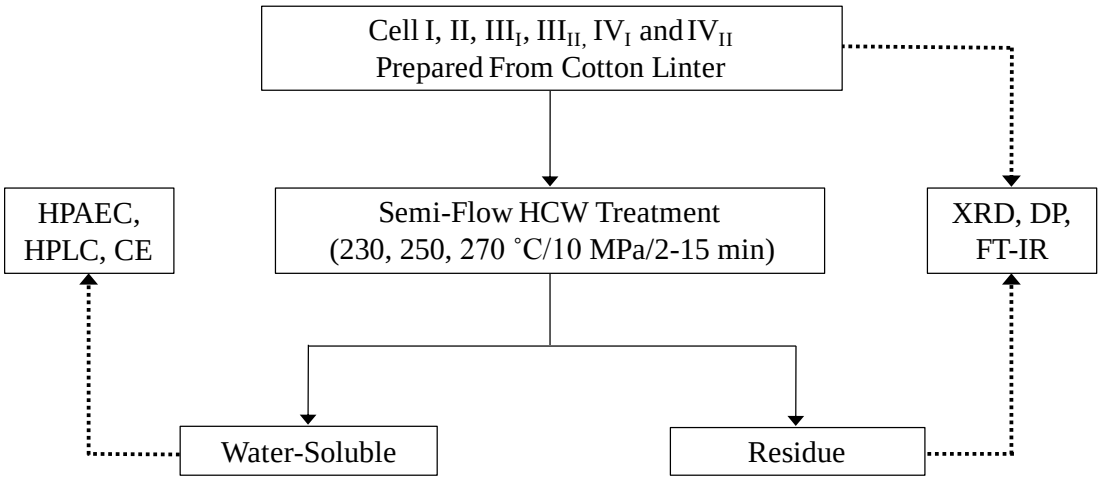

Fig. 2-1 The experimental process to study the decomposition behaviors of the prepared celluloses

The treatments yielded residues of celluloses and water-soluble (WS) portions. The analysis on WS portions will be discussed in details in *Chapter 4*. After the HCW passing through reaction vessel, the WS portions were cooled down immediately by the cooling system to terminate all reactions. The WS portions

collected every 5 min were allowed to settle in ambient temperature and pressure for a minimum of 12 h, before filtering them by 0.45 μm membranes prior to subsequent analysis. The residues of celluloses left in the reaction vessel were, conversely, collected, dried unless otherwise mentioned and evaluated for its DP and crystallinity, again (Ehara and Saka 2002; Kumar et al. 2010). The experimental process for the study is illustrated in Fig. 2-1.

2.3 Results and Discussion

2.3.1 Characteristics of the starting celluloses

The XRD patterns and the DP of the starting celluloses obtained after the adjustments are demonstrated in Fig. 2-2 and Table 2-1, respectively.

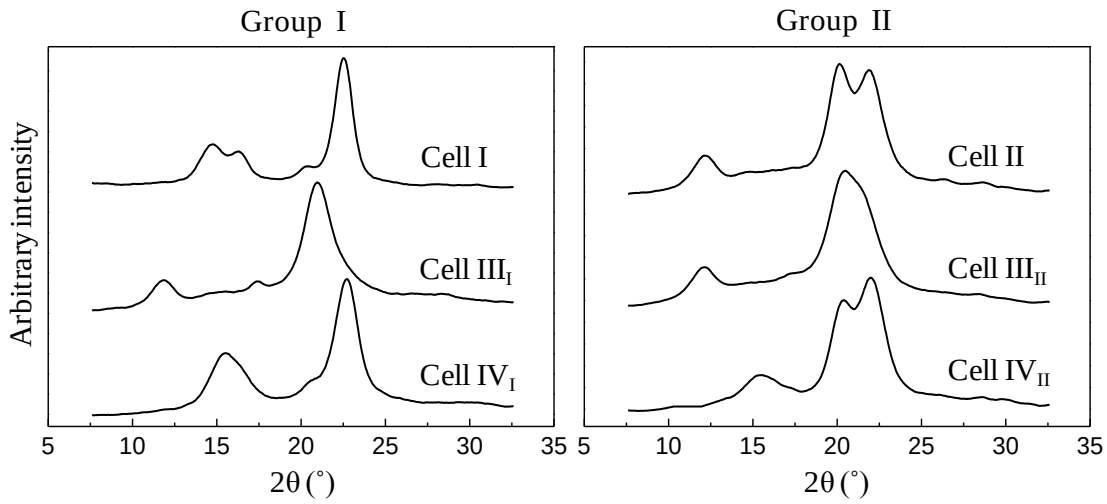

Fig. 2-2 The XRD patterns for the celluloses prepared for this study

The diffraction angles of each XRD pattern and their assignment diffraction planes are summarized in Table 2-2. For the celluloses in Fig. 2-2 and Table 2-1, the semi-flow HCW treatments were carried out at 230-270 ˚C/10 MPa/2-15 min.

Table 2-1 The DP and crystallinity for the prepared celluloses

	Cell	DP	Crystallinity (%)
Group I	I	176	91.8
	III_I	164	86.0
	IV_I	167	89.6
Group II	II	173	85.3
	III_{II}	176	87.2
	IV_{II}	164	85.0

Table 2-2 The diffraction planes and angles in XRD patterns of the celluloses

	Cell	Diffraction planes / Diffraction angles, 2θ (˚)		
Group I	I	$\bar{1}10$ / 14.4	110 / 16.3	200 / 22.5
	III_I	010 / 11.7	100 / 20.8	$1\bar{1}0$ / 20.8
	IV_I	$1\bar{1}0$ / 15.4	020 / 21.8	200 / 22.2
Group II	II	$\bar{1}10$ / 12.1	110 / 19.7	020 / 22.0
	III_{II}	010 / 12.1	100 / 20.4	$1\bar{1}0$ / 20.4
	IV_{II}	$1\bar{1}0$ / 15.1	012 / 20.6	200 / 22.5

I, II and III_I according to French (2014)

2.3.2 Evaluation of the residues of celluloses

The XRD patterns recorded for the residues of celluloses in group I and group II after XRD analysis are shown in Figs. 2-3 and 2-4, respectively. In Fig. 2-3, the XRD patterns of the residues from cell I are observed to remain the same as in the starting cell I, in contrast with the XRD patterns of residues from cell III_I and cell IV_I. Two equatorial reflections of cell III_I at $2\theta \approx 11.7$ and 20.8 ˚ indexed as 010 and $1\bar{1}0$, respectively, can be observed at the starting of cell III_I. After the HCW treatments at 230-270 ˚C/10 MPa/15 min, the peak at $2\theta \approx 11.7$ ˚, for all residues from cell III_I was totally disappeared, whereas a peak at $2\theta \approx 20.8$ ˚ was noticeably becoming smaller at elevated temperatures.

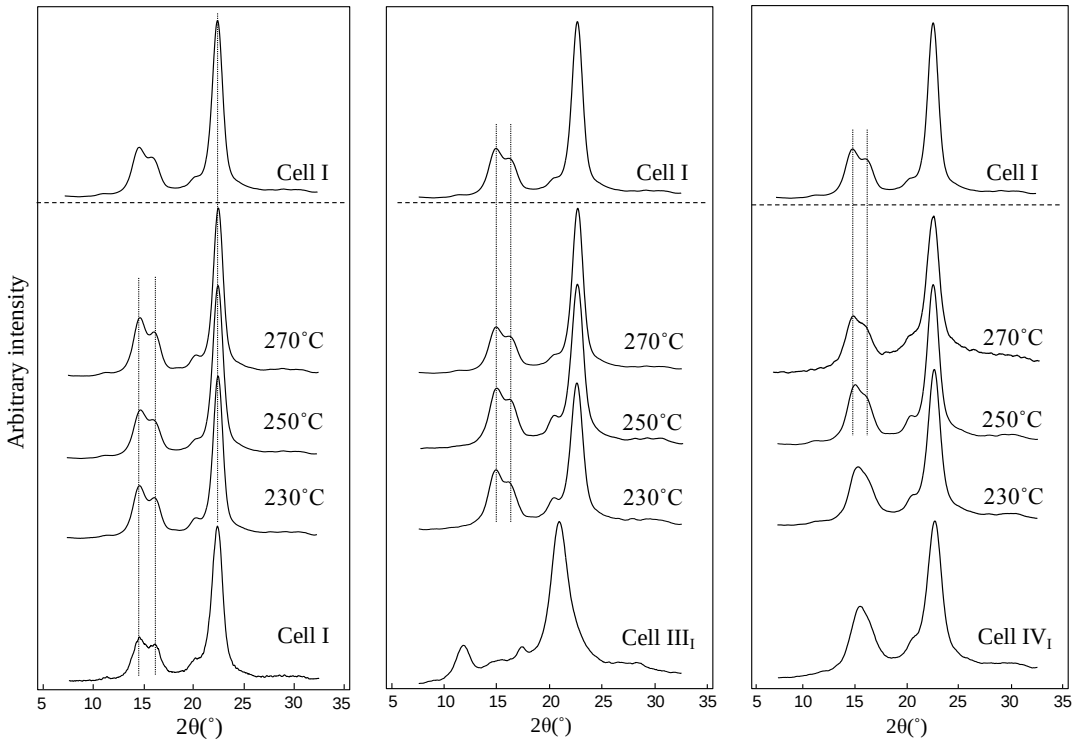

Fig. 2-3 The XRD patterns for the residues from cell I, cell III_I and cell IV_I (*from left to right*) treated by semi-flow HCW at 230-270 ˚C/10 MPa/15 min

In addition, the XRD peaks at $2\theta \approx 14.4$, 16.3 and 22.5 ˚ were intensively appeared. These peaks were similar to those of cell I, indexed as $\bar{1}10$, 110 and 200, respectively. Here, therefore, all residues from cell III_I were observed to be totally

converted to cell I. A similar result is reported for cell III_I treated in EDA to be reversed and converted into cell I by treatment in warm water, whereas cell III_I treated with liquid ammonia (140 ˚C/12 kPa) was found to be stable to boiling water for a few hours (Sueoka et al. 1973; Roche and Chanzy 1981; Yatsu et al. 1986; Wada 2001; Wada et al. 2008).

Whereas for cell IV_I, the peak at $2\theta \approx 15.4$ ˚ (indexed as $1\bar{1}0$) was shown to slowly emerge into two peaks as it was treated in the elevated temperatures. Although the changes were not seen for residue from cell IV_I at 230 ˚C, this corresponding peak started to be transformed at 250 and 270 ˚C, which was found to be corresponded to that of cell I; indexed as $\bar{1}10$ and 110.

This behavior of cell IV_I converted to cell I by HCW is a fairly new observation. Previously, it was only known that the similar conversion occurred by boiling acid (2.5 N HCl/below 1 h) treatment (Chidambareswaran et al. 1982). Though there are credible proofs that showed cell IV_I is not a genuine allomorph (Wada et al. 2004a; Isogai 1989; Newman 2008), however, the decomposition behavior after HCW is not the same as in cell I (see also later in *Chapter 4*). In this case, it is believed that the prepared cell IV_I has assisted the decomposition process during HCW treatment. During the treatment, it could be speculated that the prepared cell IV_I (contained lateral disorder structure of cell I) rearranged itself slowly and recrystallizing to cell I structure. However, a more detail investigation on this part is necessary to confirm the assumption.

As for the residues from group II shown in Fig. 2-4, the XRD patterns of residues from cell II and cell IV_{II} remained the same. On the other hand, the residues from cell III_{II} were observed to be transformed to other crystalline form. The peak at $2\theta \approx 12.1$ ˚ (indexed as 010) for all residues from cell III_{II} was shown to have no changes compared with the control cell III_{II}. However, a peak at $2\theta \approx 20.4$ ˚ was completely emerged into two peaks at $2\theta \approx 19.7$ and 22.0 ˚, as can be seen with residues from cell III_{II}.

These peaks corresponded, respectively, to crystalline peaks at 110 and 020 of cell II. Moreover, a small peak at $2\theta \approx 15.1$ ˚ was noticed and became more prominent at 270 ˚C, which also matched up with crystalline peak of cell IV_{II} that

indexed as $1\bar{1}0$. Thus, these outcomes of residues from cell III_{II} after HCW treatments comprised a mixture of cell II and cell IV_{II}.

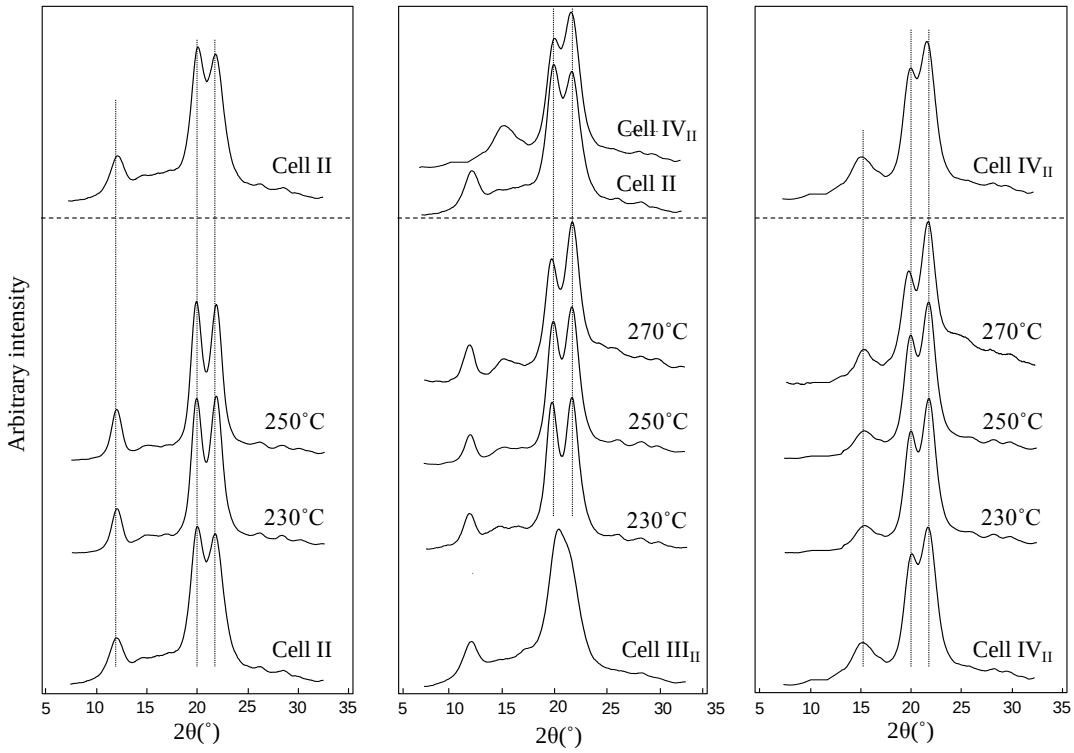

Fig. 2-4 The XRD patterns for the residues from cell II, cell III_{II} and cell IV_{II} (*from left to right*) treated by semi-flow HCW at 230-270 ˚C/10 MPa/15 min

All XRD patterns on residues from celluloses in Figs. 2-3 and 2-4 were recorded and compared for the dried residues. The XRD analyses were also performed for the wet residues from celluloses of cell III_I, cell IV_I and cell III_{II}, consequently resulted the same.

Figure 2-5 shows the obtained XRD patterns of residues from cell III_I as treated by semi-flow HCW at lower temperature, 230 ˚C/10 MPa/2-15 min. It seems apparent that cell III_I has started to be converted to cell I at an early stage of the HCW treatment. The peaks for $1\bar{1}0$ of cell III_I were disappearing even after 2 min treatment. Similar observations were recorded for cell III_I treated at the higher temperature (250-270 ˚C/10 MPa/2-10 min). Upon examination on wet residues of the celluloses, the results showed that they had already been converted as well.

The same was performed for cell IV_I and cell III_{II}, at 230-270 ˚C/10 MPa/2-10 min (data not shown) and they were found to behave in a similar manner. Cell IV_I has started to be converted to cell I at 10 min treatments under 250-270 ˚C/10 MPa, whereas for cell III_{II}, the conversion has occurred even at 2 min treatment under 230 ˚C/10 MPa to cell II mainly and to cell IV_{II} to some extent. All these results showed that they have already been converted at the early stage of the HCW treatment at 230-270 ˚C/10 MPa. Since cell III_{II} was observed to be converted to cell II and cell IV_{II}, further treatments for cell II were also performed at 270 ˚C/10 MPa/2-10 min in order to check whether it would be converted to cell IV_{II}. However, no significant crystallographic changes was observed, thus it remained as cell II at 270 ˚C/10 MPa/2-10 min.

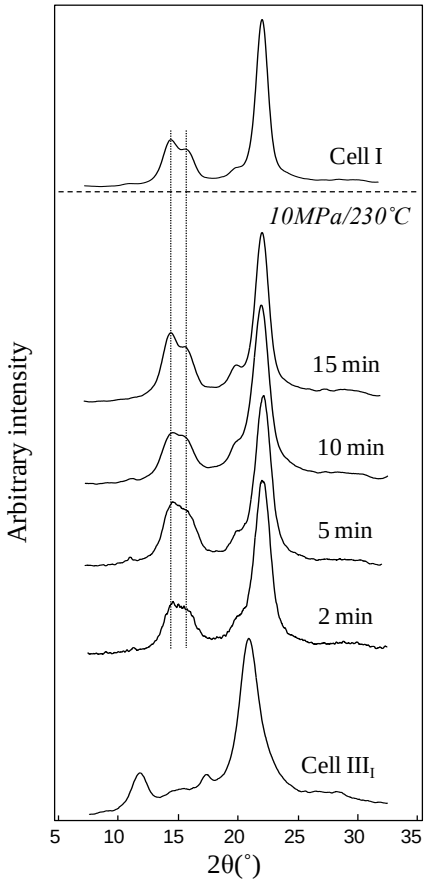

Fig. 2-5 The XRD patterns for the residues from cell III_I as treated by semi-flow HCW at 230 ˚C/10 MPa for different treatment times

In relation to the residues from cell III_I, cell IV_I and cell III_{II} in Figs. 2-3 to 2-5, the FT-IR measurements were also performed. Here, the FT-IR spectra focused only on the OH stretching regions before and after the HCW treatments, as Fig. 2-6. The extensively discussed bands in literatures at 3,480, 3,300 and 3150 cm^{-1} were found in the spectra of cell III_I, whereas the residues of celluloses were found to be similar as those of halocynthia and ramie which are cell I (cell I_β type) (Wada, 2001; Kokot et al. 2002; Zugenmaier, 2008). The bands at 3,720 cm^{-1} was clearly observed showing that cell III_I has been converted to cell I.

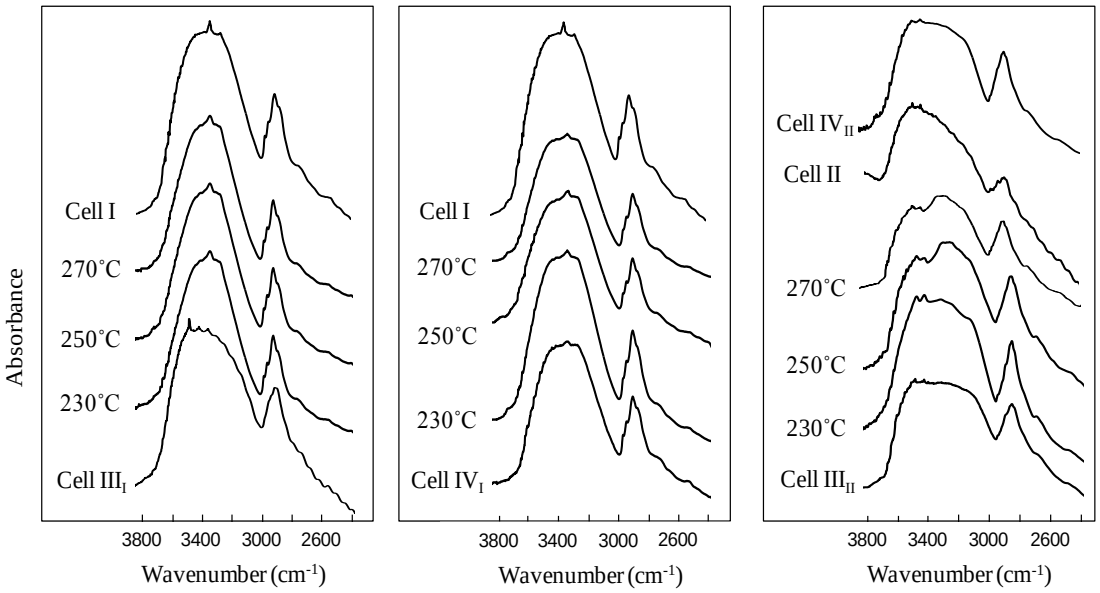

Fig. 2-6 The FT-IR spectra for the residues from cell III_I, cell IV_I and cell III_{II} (*from left to right*) treated by semi-flow HCW at 230-270 ˚C/10 MPa/15 min

In contrast, neither cell IV_I nor cell III_{II} was regularly discussed in literatures. The residues from cell IV_I that consisted of a mixture of cell I and cell IV_I, usually has higher proportion of cell IV_I (Marrinan and Mann 1956; Zugenmaier, 2008). Despite the presence of a high proportion of cell IV_I, there seems to be no distinctive absorption which could be attributed to cell IV_I. It is, therefore, assumed that the spectra of the residues from cell IV_I resemble that from cell I, whereby the structure consisted of cell I structure in lateral disorder form.

The cell III_{II} spectrum has close resemblance with that of cell II as suggested by Marrinan and Mann (1956) that the distance of the hydrogen bonding must be very similar in the two forms. The general appearance of FT-IR spectra of cell IV_{II} spectrum resembled that of cell II. There was somehow no clear shift could be seen with the FT-IR spectra obtained after HCW, only, a decrease in intensity of the spectra for 270 ˚C/10 MPa/15 min. The appearance of different bands, as compared with that of controls cell II, III_{II} and IV_{II}, in between 3200 to 3600 cm^{-1} were observed with spectra from 250 and 270 ˚C, which could be ascribed from the decomposition process.

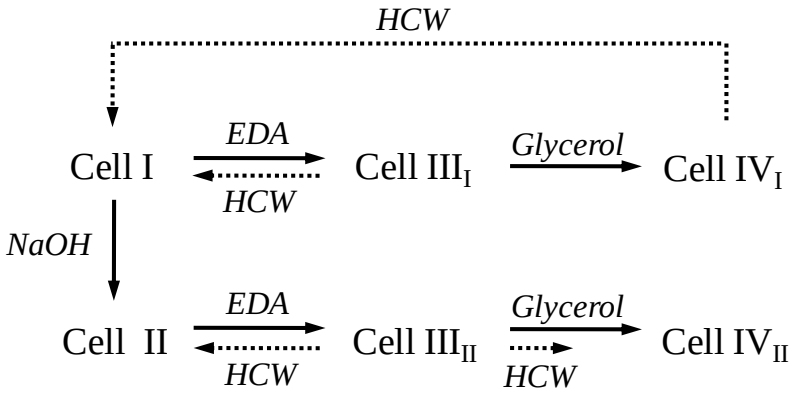

Fig. 2-7 The possible interconversion pathways for various crystalline celluloses. *Solid line*: Preparation process; *Dotted line*: Transformation by HCW treatment

All the observations above showed that the interconversion of cell III_I, cell IV_I and cell III_{II} has occurred at either early or later stage of the HCW treatments. From these results, a possible interconversion for the preparation process and transformation of celluloses by HCW treatments can be summarized as in Fig. 2-7.

In spite of the crystallographic changes occurred for the residues from cell III_I, cell IV_I and cell III_{II}, the changes in crystallinity and DP for residues of celluloses after HCW treatments were demonstrated in Fig. 2-8. The crystallinity for residues from cell III_I, cell IV_I and cell III_{II} was evaluated from the obtained XRD patterns as treated by the corresponding temperatures. The overall results were found out to be increased slightly and remained almost constant approximately at 90 %. The slight increase could be due to the combined effects of an aqueous environment that removed the paracrystalline portions of celluloses during hydrolysis (Weimer et al.

1995) and annealing that could take place on the cellulose at temperature between 220 and 280 ˚C (Yamamoto and Wu 1993).

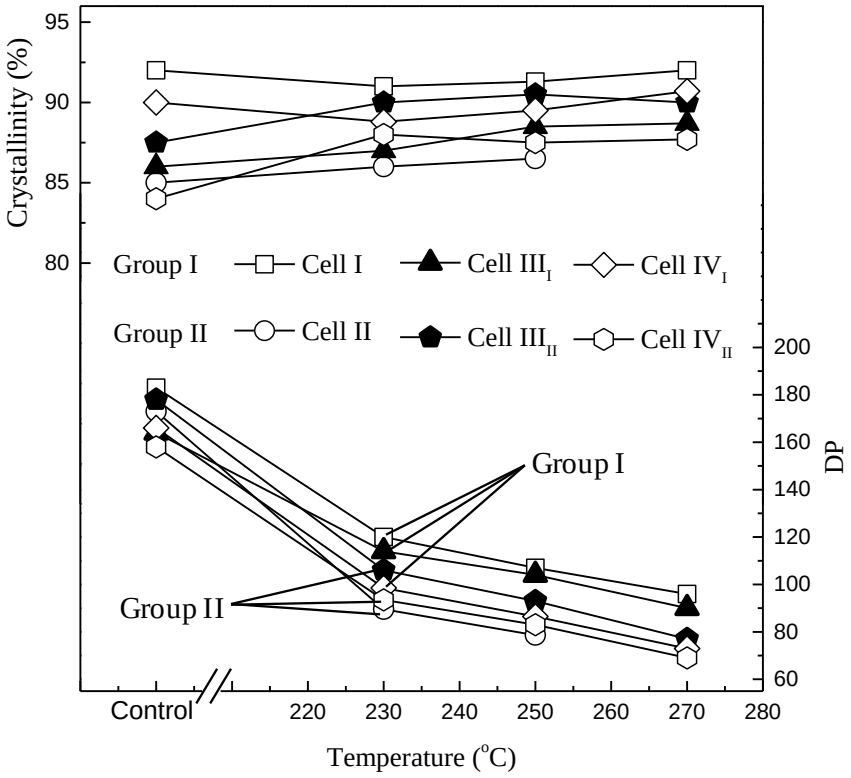

Fig. 2-8 The changes on crystallinity and DP for the residues from the celluloses as treated at 230-270 ˚C/10 MPa/15 min by semi-flow HCW

This observation agrees with previous studies, that even at a severe treatment temperature 270 ˚C, the crystallinity was observed to remain almost unchanged (Sasaki et al. 2000; Jollet et al. 2009; Kumar et al. 2010, Tolonen et al. 2011). One study emphasized that (i) crystallinity and (ii) changes in the crystalline form of a cellulose; as the two of the main determining factors efficacy of hydrolysis of biomass (Cetinkol et al. 2010). However, it is generally thought that drying could lead to the formation of new hydrogen bonds and recrystallization, which would increase the crystallinity rather than reducing it (Tolonen et al. 2011).

Contrary to the crystallinity results, the DP for all residues of celluloses was seen to decrease slightly with increase in temperature (Tolonen et al. 2011). The expectation that the lower DP celluloses such as cell IV_{II} would be easier to decompose due to their shorter average lengths of molecules, however, was not

observed in Fig. 2-8. The DP was decreasing and leveling off to about 70, which is obvious with group II celluloses, even after the treatment at 270 ˚C/10 MPa/15 min. In literatures, the degradation cellulose II from cotton linters of DP 3100 by hydrolysis may decrease to a DP of ~ 85 to 70 (Schulz and Husemann, 1942; Jörgensen 1950; Shibazaki et al. 1997).

The present interpretations suggested that the crystalline structure of the celluloses were still rigid, but only broken down into shorter-chain of cellulose molecules. As temperature increases, the DP decreases which would raise the solubility of cellulose in water and conversion of cellulose to the hydrolyzed and degraded products (Sasaki et al. 2000; Yu and Wu 2009). In Fig. 2-8, the DP of group I celluloses was observed to be generally higher than that of group II. This shows that group II is easier to be decomposed as compared with group I. Also, based on visual examination, the fibers as the starting materials have been changed into powder-liked residues after the HCW treatment.

Figure 2-9 illustrates the relationship of DP and residues of celluloses after HCW treatments. Both are seen to decrease as the treatment temperatures were increased. It has also been reported in previous studies that the DP of residues gradually decreased with increasing cellulose decomposition (Sasaki et al. 2000; Tolonen et al. 2011).

The overall yield of the residues after semi-flow HCW treatment for various types of celluloses is shown in Fig. 2-10. These residues notably decreased with the increase in temperatures. The residues of the celluloses obtained particularly at treatment condition of 230 ˚C/10 MPa/15 min were still quite high in yield (70-90 wt%), agreeable with earlier studies that the condition was known not to hydrolyze the crystalline cellulose in wood (Lu et al. 2009; Phaiboonsilpa et al. 2010; 2011).

Since in the present study, the starting DP was adjusted to be the same for all celluloses, a direct comparison can be made for decomposition behaviors of the celluloses. As DP in the residues of celluloses is a function of cellulose decomposition, the observed changes on residues were only due to the different crystalline structures of celluloses as starting materials. The various crystalline celluloses prepared as the starting materials have assisted the decomposition process in HCW treatments even though the interconversion of some celluloses has occurred.

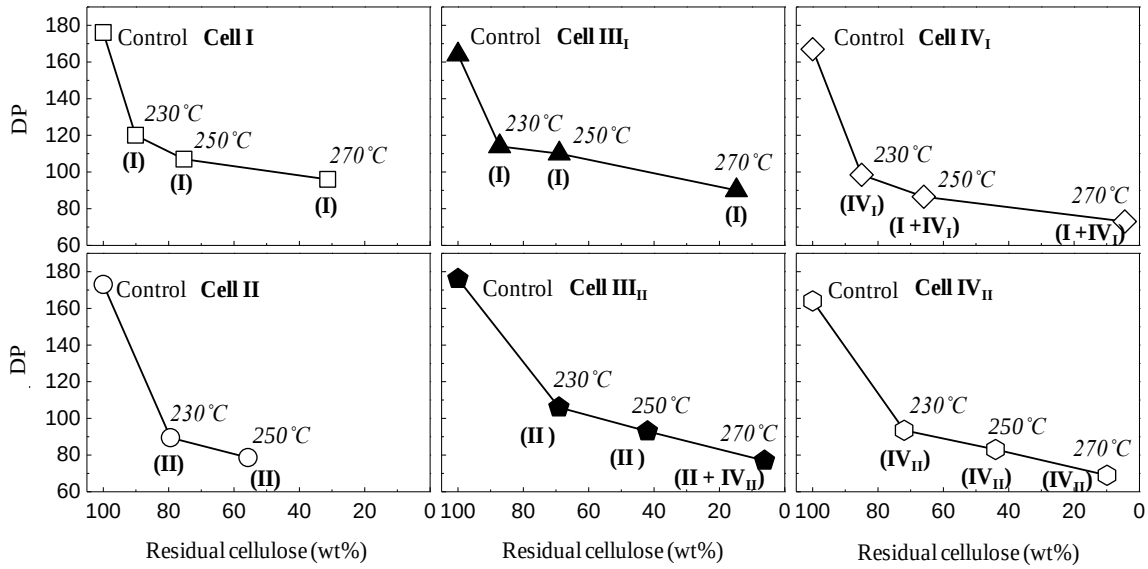

Fig. 2-9 The relationship between DP and residues from the celluloses as treated by semi-flow HCW at 230-270 ˚C/10 MPa/15 min

Cell I yielded the highest residue among the celluloses used in this study followed by cell III_I and cell IV_I, as in Fig. 2-10. At 230 and 250 ˚C, both cell III_I and cell IV_I behaved very similarly, however, cell IV_I decomposed more at 270 ˚C as compared with cell III_I. This trend was later followed by cell II, cell III_{II} and cell IV_{II}. Both cell III_{II} and cell IV_{II} behaved in the same manner, whereas, more decomposition was observed for cell IV_{II} at 270 ˚C as compared with cell III_{II}. Cell II was observed to have no residues left at 270 ˚C, thus crystallinity and DP values were recorded in Fig. 2-8.

To sum up, cell I in native crystalline form was found to be the most resistant against decomposition, while cell II, cell III_{II} and cell IV_{II} were decomposed the most as compared with the other types of celluloses such as cell III_I and cell IV_I. This could be an indication of the easiness for decomposition of the celluloses and it seemed likely that group I celluloses (cell I, cell III_I and cell IV_I) had higher resistance to be decomposed as compared with group II celluloses (cell II, cell III_{II} and cell IV_{II}).

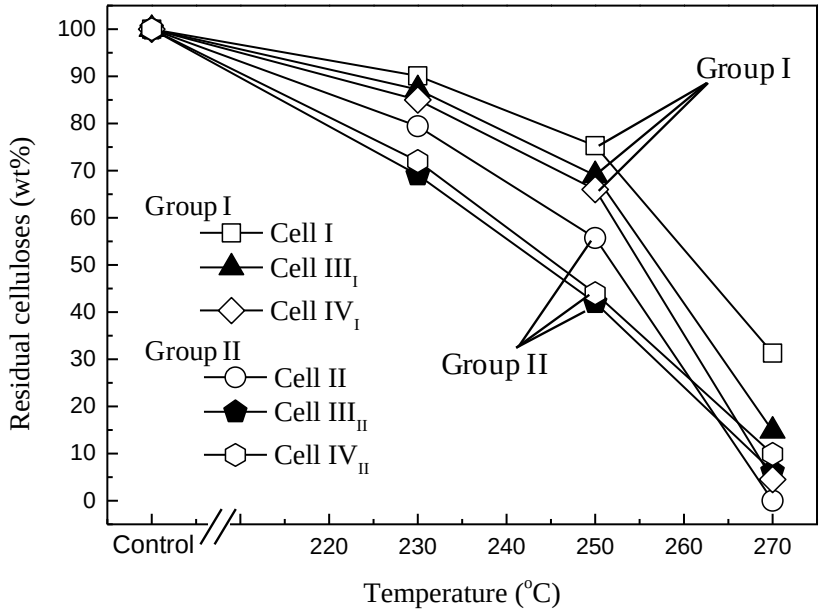

Fig. 2-10 The changes on the residues from the celluloses as treated at 230-270 ˚C/10 MPa/15 min by semi-flow HCW

2.4 Concluding Remarks

The decomposition behaviors on various types of crystalline celluloses were investigated at 230-270 ˚C/10 MPa/2-15 min. To compare directly the effect of the treatment, the DP of the celluloses was adjusted by trial and error to be similar prior to the treatment. Based on the results of the residues, crystallographic changes were found to be occurred during the HCW treatment for cell III_I, cell IV_I and cell III_{II}. In general, group I celluloses (cell I, cell III_I, cell IV_I) have been converted to cell I and group II (cell II, cell III_{II}, cell IV_{II}) to cell II. Despite of these changes, the overall results of residues showed that group I has higher resistance to be decomposed than group II.

It was clear that the decomposition behaviors were due to their different crystalline forms of celluloses. All these data are useful to understand the behaviors of different types of crystalline celluloses that could provide information for efficient use of lignocelluloses.

CHAPTER 3

Decomposition Behaviors of Celluloses by Enzymatic Treatment

3.1 Introduction

Numerous studies involving cellulases on celluloses have discovered the mechanisms of enzyme degrade cellulose (Fan et al. 1980; Lee et al. 1983; Hsu 1996; Cao and Tan. 2002; Yoshida et al. 2008; Hall et al. 2010: Ward 2011). Different cellulases changed the degree of polymerization (DP), solubility towards aqueous alkali solution and crystallinity of cellulose during enzymatic hydrolysis (Reese et al. 1957; Sasaki et al. 1979; Puri 1984). Cellobiose yield was increased by using non-continuous hydrolysis process without further addition of enzyme (Vanderghem et al. 2010), while treated celluloses with alkali or anhydrous liquid ammonia affected enzyme digestibility based on the relative crystallinity (Mittal et al. 2011).

There are many works on enzymatic hydrolysis of celluloses, however, they focussed on either one or few allomorphs, explored their kinetics, studied their molecular simulations and used bacteria for their treatment (Weimer et al. 1991; Wada et al. 2010; Beckham et al. 2011; Mittal et al. 2011). Up to date, no reports are yet available that describes the comparison of enzymatic hydrolysis behaviors using various celluloses with retention of constant degree of polymerization (DP). Therefore, in this study, hydrolysis behavior of the various crystalline celluloses during treatment by cellulase of *Trichoderma viride* is investigated, in addition, to compare them with the decomposition behaviors of the celluloses from the HCW treatments.

The original publication is available at Springer via http://dx.doi.org/10.1007/s10570-014-0410-4

3.2 Material and Methods

3.2.1 Various crystalline celluloses and enzyme

The celluloses were prepared according to the methods described in *Chapter 2*. They were adjusted to similar DP which is necessary for comparing and evaluating the decomposition products from this work.

The cellulase in lyophilized powder from *Trichoderma viride* Sigma C9422 was purchased from Nacalai Tesque, Japan. The activity of the enzymes was expressed in international units (U), i.e., one international unit of enzyme is defined as the amount that catalyzes the formation of one μmol of product per min under the defined conditions. The activity was found to be 11.4 U/ml.

3.2.2 Enzymatic hydrolysis for celluloses

In a 20 ml glass vials were added 35 mg/ml cellulose, 0.35 U/mg cellulose of cellulase and 0.05 M sodium acetate buffer of pH 5.0 (thermostated before at 50 ˚C) until 3 ml final volume. The pH value was adjusted using 1 M hydrochloric acid (HCl), if necessary (Bommarius et al. 2008). The controls together with the reaction mixtures were placed in an incubator at 50 ˚C and continuously stirred using magnetic stirrers. No β-glucosidase supplement was used in this study (Kadam et al. 2004). At the designated treatment times, the samples were removed and the enzyme reactions were terminated by quenching in ice bath, followed by centrifugation at 8000 × *g* for 2 min. The supernatant was immediately filtered, then refrigerated until subjected to analysis (Van Wyk 1997; Bommarius et al. 2008; Yang 2010). All chemicals used in this study were of reagent grade without purification. Enzymatic treatments were performed in duplicates.

3.2.3 Analyses of cellulose residues

The DP of the residues was measured using the molecular weight distribution of celluloses as phenyl carbamate derivatives. The procedure was modified from prior published methods (Evans et al. 1989; Mormann et al. 2002). Cellulose (5 mg) and phenyl isocyanate (0.2 mL) were added to pyridine (2 mL), and its mixture was heated up to 80 ˚C under continuous stirring for 24 h to become a yellow transparent

solution. Methanol (0.5 mL) was then added to terminate the reaction, and the solvent was removed by evaporation in vacuum to give dark yellow syrup.

The syrups of the phenyl carbamate derivatives were dissolved in tetrahydrofuran (THF). The solutions were then filtered through 0.45 μm microcentrifuge membrane filters prior to analysis by gel permeation chromatography (GPC) Shimadzu LC-10A under the following chromatographic conditions: column, Shodex LF-804; column temperature, 40 ˚C; eluent, HPLC grade THF; flow-rate, 1.0 ml/min and detector, UV_{254nm}. Polystyrene standards were used to calibrate retention time for its molecular weight. The DP of cellulose was then calculated by dividing the molecular weights of the carbanilated cellulose by that of its repeating unit (=519) with the degree of substitution of 3.0. All reported values were based on the average of duplicate samples.

The evaluation of crystalline by using the X-ray diffraction (XRD) patterns was recorded by X-ray diffractometer Rigaku RINT 2200, as in section 2.2.2.

3.2.4 Analysis of the supernatants

The total sugar productions i.e., the total hydrolyzed products, cellobiose and glucose, in supernatant for each hydrolysis time points were measured by high performance liquid chromatography (HPLC) system (Shimadzu, LC-10A). The chromatographic conditions were: column, Bio-Rad Aminex HPX-87P; detector, UV_{254nm}; eluent, deionized water; flow-rate, 0.6 ml/min and oven temperature, 85 ˚C. The sample injection volume was 10 μl and the running time was 30 min.

3.3 Results and Discussion

3.3.1 Evaluation of cellulose residues

To evaluate and compare directly their hydrolysis behaviors, it is essential for the starting materials to have a common DP. As a result, the adjusted DP and the corresponding crystallinity of the celluloses are summarized in Table 3-1. The XRD patterns of these celluloses are similar to Fig. 2-2 in *Chapter 2*.

Table 3-1 The DP of the celluloses as starting materials

	Cell	DP	Crystallinity (%)
Group I	I	174	91.8
	III_I	174	86.0
	IV_I	168	89.6
Group II	II	172	85.3
	III_{II}	170	87.2
	IV_{II}	169	85.0

Each of these celluloses was then treated with cellulase at pH 5.0 and 50 ˚C with solid concentration set to 35 mg/ml and enzyme loading of 0.35 U/mg cellulose. As the substrate is pure cellulose, higher loading of enzyme is unnecessary. The time courses of residues obtained from the celluloses after enzymatic hydrolysis is presented in Fig. 3-1. During the 17 days hydrolysis treatment, the residues obtained from the celluloses were decreasing, with its higher rate during the first week treatments.

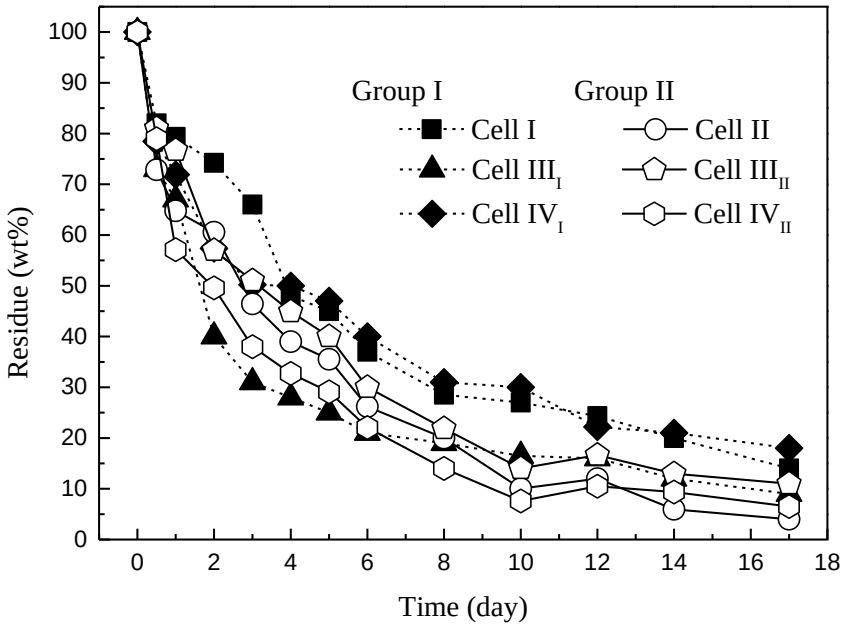

Fig. 3-1 The residues obtained from the celluloses after enzymatic hydrolysis

In group I, cell III_I hydrolyzed the most, and it has lesser residue than that of cell I and cell IV_I, which behave quite similarly. On the other hand, all celluloses in group II reach more or less similar yields and are seemingly equivalent to that of cell III_I. Generally, group II celluloses are easier to hydrolyze than those of group I, except for cell III_I.

Figure 3-2 shows the XRD patterns of group I celluloses after enzymatic hydrolysis. In Fig. 3-2 (*left*), the XRD patterns of the residues from cell I are observed to remain almost unchanged even after 17 days hydrolysis treatment. However, the intensity at $2\theta \approx 22.5^\circ$, is decreasing as enzymatic hydrolysis is prolonged and the peaks at $2\theta \approx 14.4^\circ$ and 16.3° are not sharp as observed in the control. This is seen in the progressive decrease in crystallinity in Fig. 3-5 (below) and may be due to the enzymatic attacks onto the structure of the cell I (Lee et al. 1983; Cao and Tan 2005).

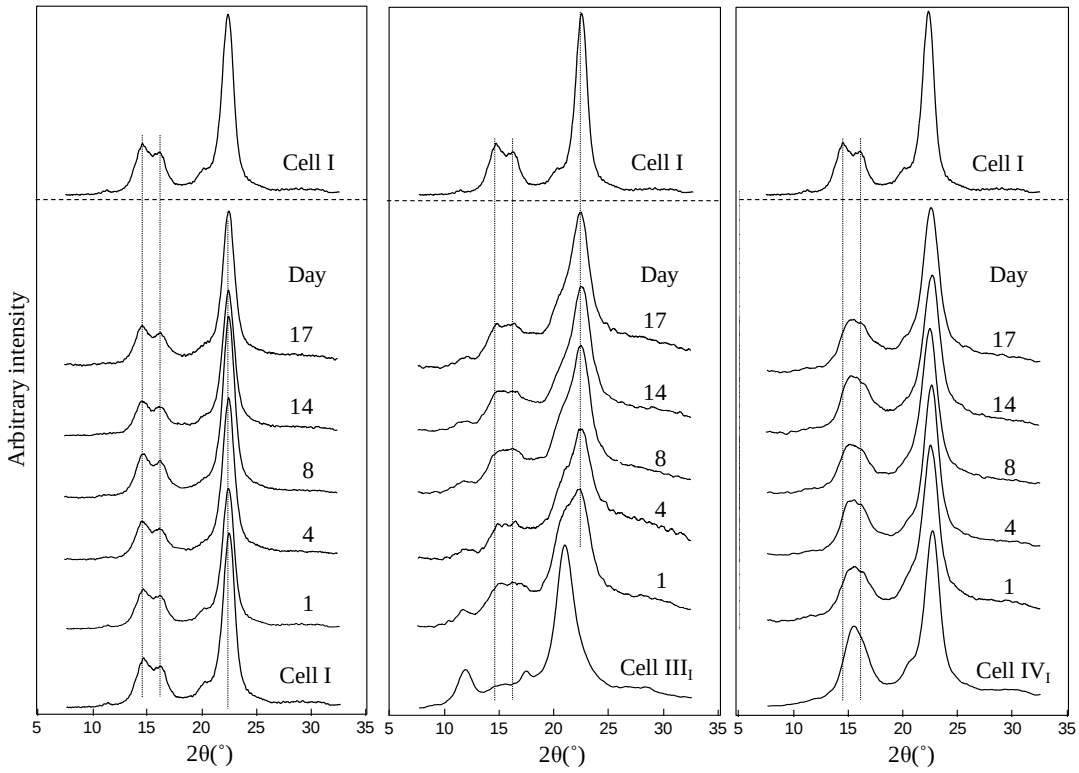

Fig. 3-2 The XRD patterns of group I celluloses; cell I (*left*), cell III_I (*middle*), cell IV_I (*right*), after enzymatic hydrolysis

In Fig.3-2 (middle), the XRD patterns of residues from cell III_I demonstrate that the cell III_I is slowly converted back to cell I. Yet, the full XRD pattern of cell I is not obtained. During the treatment, the residues from cell III_I are observed to be gradually modified to a mixture of cell I and cell III_I. As for the XRD pattern of the residues from cell IV_I, in Fig. 3-2 (*right*), no significant changes are observed, apart from, the peak $2\theta \approx 15.1^\circ$. The peak was becoming broader and slowly imitated the characteristic peaks of cell I. In both cases cell III_I and cell IV_I, some enzymatic attacks could also have taken place.

Figure 3-3 shows the XRD patterns of group II celluloses after enzymatic hydrolysis. Though there is no significant change observed from the XRD patterns of cell II, in Fig 3-3 (*left*), the intensity at $2\theta \approx 19.7^\circ$ and 22.0° decreases as enzymatic treatment time is prolonged. The XRD patterns of residues from cell III_{II}, in Fig. 3-3 (*middle*) and cell IV_{II}, in Fig. 3-3 (*right*), were slowly converted into their parent, cell II.

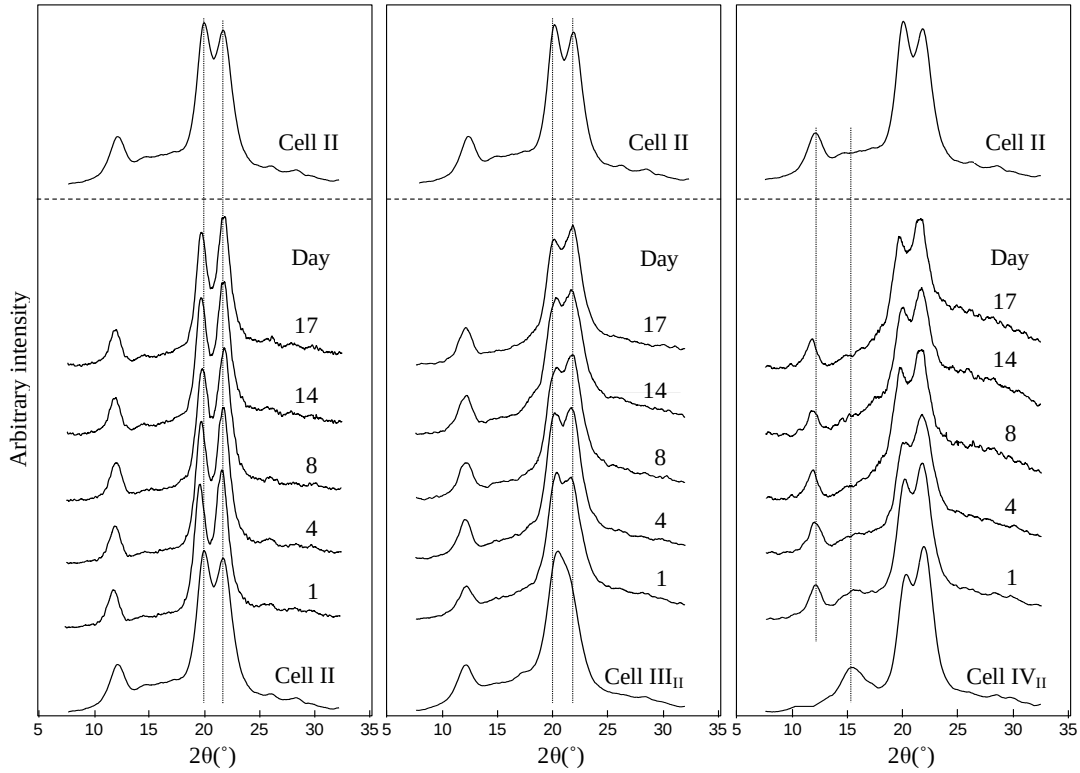

Fig. 3-3 The XRD patterns for group II celluloses; cell II (*left*), cell III_{II} (*middle*), cell IV_{II} (right), after enzymatic hydrolysis

For cell III_{II}, in Fig. 3-3 (middle), two peaks at $2\theta \approx 20.1^{\circ}$ and 21.6° emerge during the time of hydrolysis, comparable to the control, cell II. In contrast with Fig. 3-3 (*right*), the peak at $2\theta \approx 15.1^{\circ}$ for cell IV_{II} disappears after 1 a few days' treatment, replicating the control cell II. Thus, from cell III_{II}, in Fig. 3-4 (*middle*) and cell IV_{II}, in Fig. 3-3 (*right*), mixtures comprising cell III_{II} and cell II, also cell IV_{II} and cell II, are present during the treatments. These behaviors of cellulose residues from cell III_I in Fig. 3-2 (*middle*); cell IV_I in Fig. 3-2 (*right*); cell III_{II} in Fig. 3-3 (*middle*) and cell IV_{II} in Fig. 3-3 (*right*) are also examined under wet conditions by X-ray diffractometry with similar results.

Figure 3-4 shows the comparison between XRD patterns of residues from cell III_I treated *with* and *without* enzyme. In these data, the changes from cell III_I into cell I occur *with* or *without* cellulase. However, the peaks at $2\theta \approx 14.4^{\circ}$ and 16.3° appear at a much slower rate *with* enzyme. Somehow, the enzymatic attacks must interfere with the conversion process.

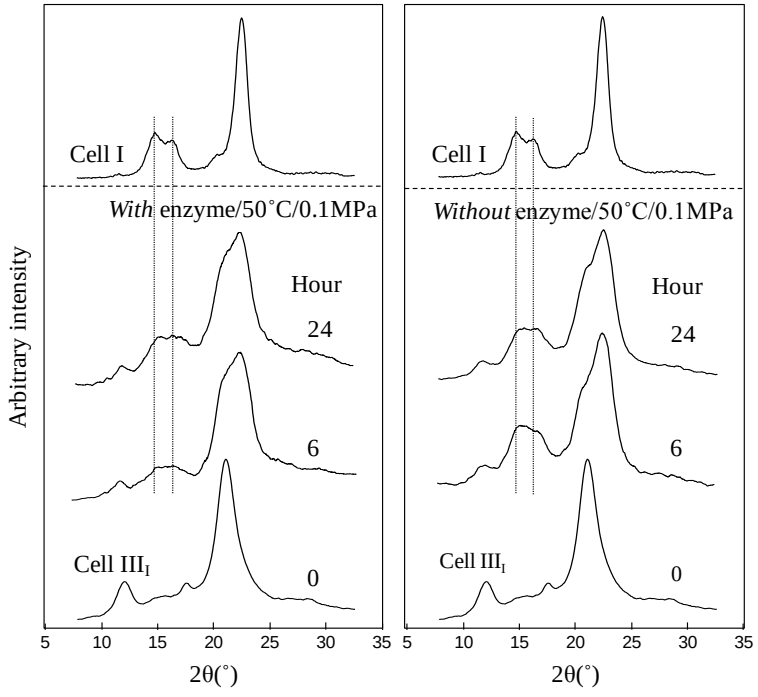

Fig. 3-4 The comparison between XRD patterns of residues from cell III_I when treated *with* and without enzyme

According to the literatures, the immersion of cell III_I in a polar solvent could obtain cell III_I or cell I (Loeb and Segal 1955; Wada et al. 2008). Similar conversion of the crystalline form to its parent cellulose is also detectable with cell IV_I, cell III_{II} and cell IV_{II}, but is insignificant for cell IV_I, when it is treated *without* enzyme.

Figure 3-5 shows the relationship between DP and crystallinity of the celluloses after enzymatic hydrolysis. The crystallinity is observed to drop slowly after 1 day of treatment and then soon starts to decrease faster. The enzyme could probably attack first the paracrystalline regions of the celluloses, hence the crystallinity dropped slower at first, and then later would attack the crystalline parts. As for the DP, it is observed to decrease with treatment time. With celluloses in the modified forms (cell III_I, cell IV_I, cell III_{II}, cell IV_{II}), enzymatic hydrolysis reaction is shown to be more effective, compared with the cellulose in the cell I form. This agrees with the previous work by Igarashi et al. (2007). Figure 3-5 shows more changes occurred with group II than group I celluloses, and the changes during hydrolysis reaction were closely related to the initial state of cellulose structure.

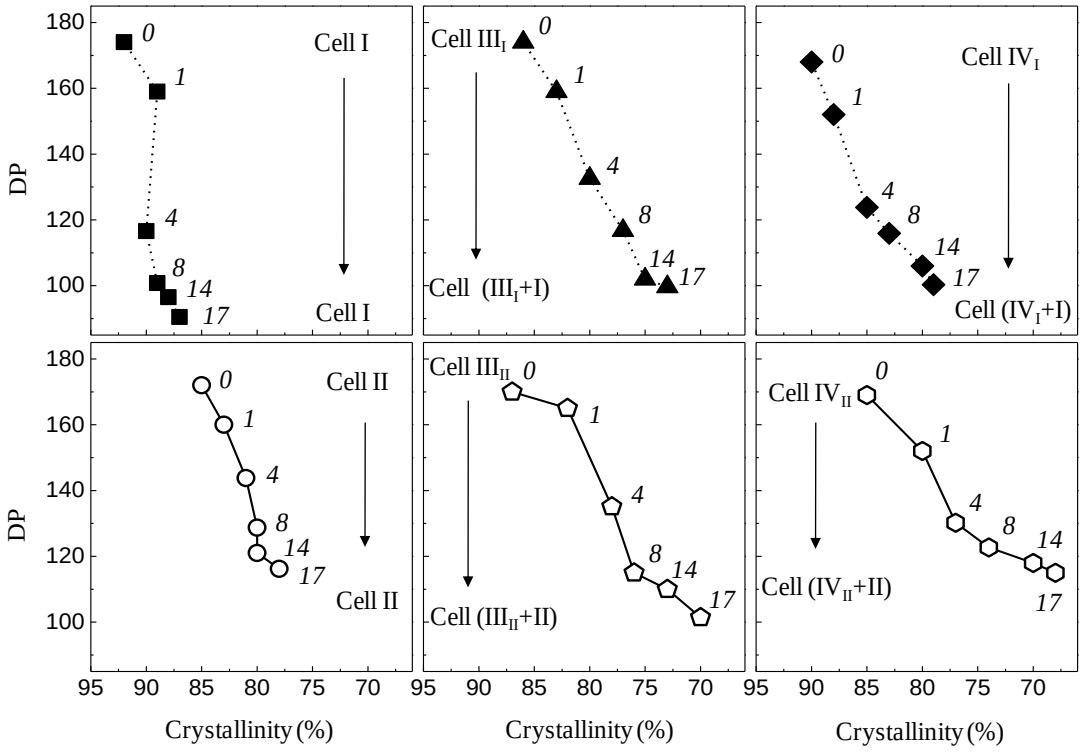

Fig. 3-5 The changes in DP and crystallinity of the celluloses after enzymatic hydrolysis

3.3.2 Evaluation of the supernatants

The analysis of supernatant shows that enzymatic hydrolysis produces hydrolyzed products (total sugar) such as cellobiose and glucose. On average, more than 75 wt% of the total sugar consists of glucose. The results on total sugar obtained for the celluloses after enzymatic hydrolysis are shown in Fig. 3-6. Overall, cell III_I and group II celluloses produced similar total sugar yields, higher than those of cell I and cell IV_I. This confirms earlier findings that hydrolysis yield rates produced of cellulose III_I were much higher than for cellulose I (Igarashi et al. 2007), but for a more complete range of polymorphs and controlled DP.

Moreover, in this work, it is found that comparable yields of total sugar are obtainable from enzymatic hydrolysis of cell II and cell III_I, disagreeing with the previous work in which similar DPs were not considered for the starting materials (Mittal et al. 2011). The comparable behavior of cell I and cell IV_I could be because of the structures of cell IV_I and cell I are analogous (Wada et al. 2004b).

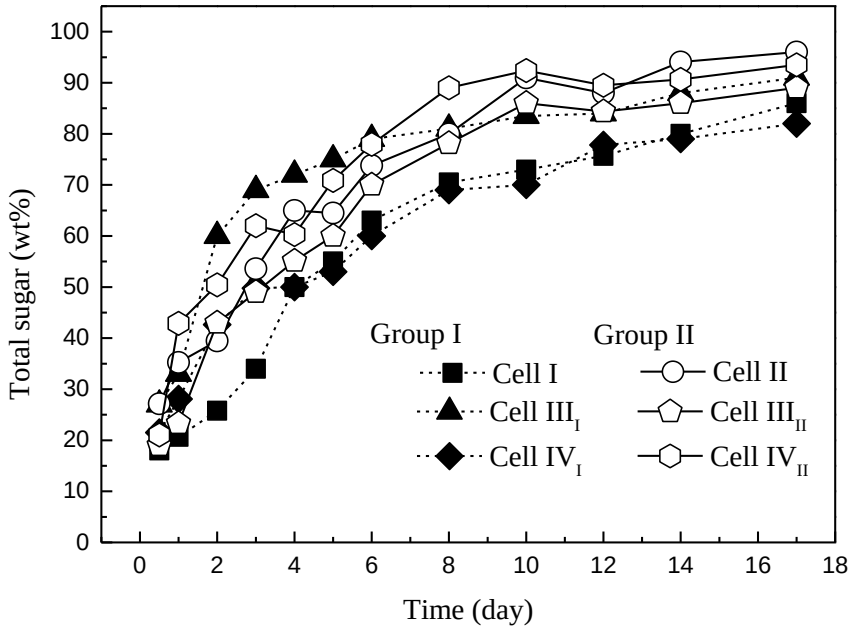

Fig. 3-6 The yield of total sugars from the celluloses after enzymatic hydrolysis

Matsuoka et al. (2011) previously showed thermal glycosylation converts the reducing ends into more stable glycosides with alcohol, which what would probably happened during the preparation of cell IV_I. The reducing ends in the paracrystalline

regions were suggested to be more reactive than those in the crystalline regions. In Fig. 3-6, some sugars can be obtained as result of enzymatic hydrolysis of cell IV_I (as the starting material). This could possibly be due to the enzymatic attack that facilitated the cell IV_I to convert into cell I (Fig. 3-2) and thus uncapped its reducing ends, as well as, the attacking of enzyme at the reducing ends of the paracrystalline regions.

The behaviors of the celluloses are seen to be dependable on the initial hydrolysis reactions. Given that the interconversion processes for some celluloses are most probably independent of the enzyme reaction, thus, the trends of total sugar productions are most likely due to intrinsic properties of the starting materials.

3.4 Concluding Remarks

In order to enhance enzymatic hydrolysis sugar production, various forms of crystalline celluloses were used as the starting materials. The modification of cellulose crystalline structures somehow assists the enzyme to perform better during hydrolysis reaction, although interconversion processes of the celluloses have occurred. In addition, considering constant DP for starting materials was necessary to improve the evaluation of enzymatic treatment of the various cellulose forms. From the results above, it is concluded that enzymatic hydrolysis treatment is better for cell III_I and group II celluloses, compared to native cellulose. Thus a recommendation can be made to either convert cell I into cell III_I or group II celluloses for enzymatic hydrolysis.

CHAPTER 4

Decomposition Behaviors of Celluloses as Studied for the Water-Soluble Products

4.1 Introduction

In *Chapter 2*, the decomposition behaviors of various crystalline celluloses as treated by semi-flow hot-compressed water (HCW) at 230-270 ˚C/10 MPa/2-15 min were conducted and the analysis on the residues were carefully discussed based on the physical characteristics such as degree of polymerization (DP) and crystalinity. The overall results of residues showed that group I celluloses have higher resistance to decompose than group II celluloses.

In addition to the above work (Abdullah et al. 2013), many other studies have been done on the analysis of cellulose hydrolysis by using HCW treatments (Mok and Antal 1992; Adschiri et al 1993; Sasaki et al. 1998; Saka and Ueno 1999; Ehara and Saka 2002; Sakaki et al. 2002; Liu and Wyman 2003; Schacht et al. 2008; Kumar and Gupta 2008; Lu et al. 2009; Phaiboonsilpa et al. 2010, 2011), however, the comprehensive investigation has been rarely conducted on various crystalline celluloses as the feedstocks. As a further approach, the primary objective is of this work is to study quantitatively the decomposition from the celluloses by hydrothermal treatment i.e., semi-flow HCW through the yields of the water-soluble (WS) portions. It is anticipated that this line of informative evaluations would help to understand the impact of semi-flow HCW treatment on these celluloses and judge the feasibility of such processing on downstream bioethanol process.

4.2 Materials and Methods

4.2.1 Various crystalline celluloses preparation

The preparation of the celluloses and the adjustment the DP followed the procedure as already described in *Chapter 2*.

The original publication is available at Springer via http://dx.doi.org/10.1007/s10086-014-1401-7

4.2.2 Degree of polymerization and crystallinity of the celluloses

The DP of the celluloses was analyzed and calculated based on previous studies (Sihtola et al. 1963; TAPPI 1982). For the crystallinity determination, Gaussian functions were used to deconvolute the X-ray diffraction (XRD) patterns of the celluloses (Park et al. 2010). These XRD patterns were recorded by X-ray diffractometer Rigaku RINT 2200 (as in *Chapter 2*).

4.2.3 Treatment of the celluloses by semi-flow hot-compressed water

The prepared celluloses as starting materials were then treated individually in a semi-flow HCW system. The details of the treatments have been described previously in section 2.2.4 of *Chapter 2*. The treatments yielded residues of celluloses and WS portions, at which the residues analyses have been discussed expansively.

4.2.4 Analytical methods

The WS portions collected were analyzed and characterized by using high-performance anion exchange chromatography (HPAEC), high-performance liquid chromatography (HPLC) and capillary electrophoresis (CE). The HPAEC system (Dionex ICS-1000 system) equipped with the CarboPac PA-1 column (4 mm x 250 mm) and electrochemical detector for pulsed amperometric detection was employed and operated at 35 ˚C and flow-rate of 1.0 ml/min under the helium atmosphere for monosaccharides and cello-oligosaccharides in the WS portions. The mobile phase was a gradient-programmed mixture of deionized water, 0.2 M NaOH and 2.0 M CH_3COONa, as eluents. All eluents contained in 3 separate reservoirs were degassed by an aspirator and subsequently purged with helium to prevent the absorption of CO_2.

The HPLC system (Shimadzu, LC-10A) equipped with a Shodex Sugar KS-801/Ultron PS-80P columns and refractive index/UV-Vis detector was applied. The eluent used was deionized water at a flow-rate of 1.0 ml/min and oven temperature was set to be 80 ˚C for the columns. The CE (Agilent; Germany) was used to assay the low molecular weight organic acids. A fused-silica capillary

(Agilent; 75 μm diameter, 104 cm total length, 95.5 cm effective length) was used at 15 ˚C.

Concentrations of the products in the WS portions were calculated based on the peak areas on chromatograms obtained from HPAEC, HPLC and CE. A set of standards with known concentrations, containing the compounds that were to be identified both quantitatively and qualitatively, was prepared and analyzed together with the samples by using the relevant analytical equipment as mentioned above (Lu et al. 2009; Phaiboonsilpa et al. 2010; Yu and Wu 2010).

4.3 Results and Discussion

Having similar DPs for the celluloses as starting materials is essential so that a direct comparison between the celluloses can be made. The crystallinity and DP for the celluloses are similar to that listed in Table 2-1 (as in *Chapter 2*). Treatments by semi-flow HCW were then carried out for these celluloses at 230-270 ˚C/10 MPa/15 min.

4.3.1 Decomposition kinetics of various crystalline celluloses

The semi-flow HCW treatment decomposed the celluloses either partially or completely to the WS portions. The yield on WS portions from the celluloses as shown in Fig. 4-1, is a function of treatment temperatures. During the treatment, the yield on WS portions increased as the treatment temperature increased. They were measurable even at lower temperature, 230 ˚C/10 MPa, with approximately 10-30 wt% and increased to more than 70 wt% at higher temperature, 270 ˚C/10 MPa. At 270 ˚C/10 MPa/15 min, cell II was shown to be totally decomposed to WS portions as compared with other celluloses. The overall results from Fig.4-1 illustrated that higher yields were obtainable for group II celluloses than group I.

Figure 4-2 shows the Arrhenius plot of the present results according to the pseudo-first-order reaction kinetics. The relationship between natural logarithms of reaction constants, ln *k*, and T^{-1} shows good linear fits with the results indicating that the decomposition follows the pseudo-first-order reaction kinetics. Cellulose hydrolysis is classically defined by a pseudo-homogeneous kinetics model, a term

that in reality reflects that the hydrolysis process is heterogeneous (Olanrewaju 2012). Every parameter used such as time, pressure and DP on the celluloses were kept constant, satisfying the assumption that the Arrhenius-plot is temperature dependent. Though, the data points obtained in this study are only based on three different temperatures profile, the degree of decomposition could be determined reliably and the comparison of kinetics on the celluloses can be done directly.

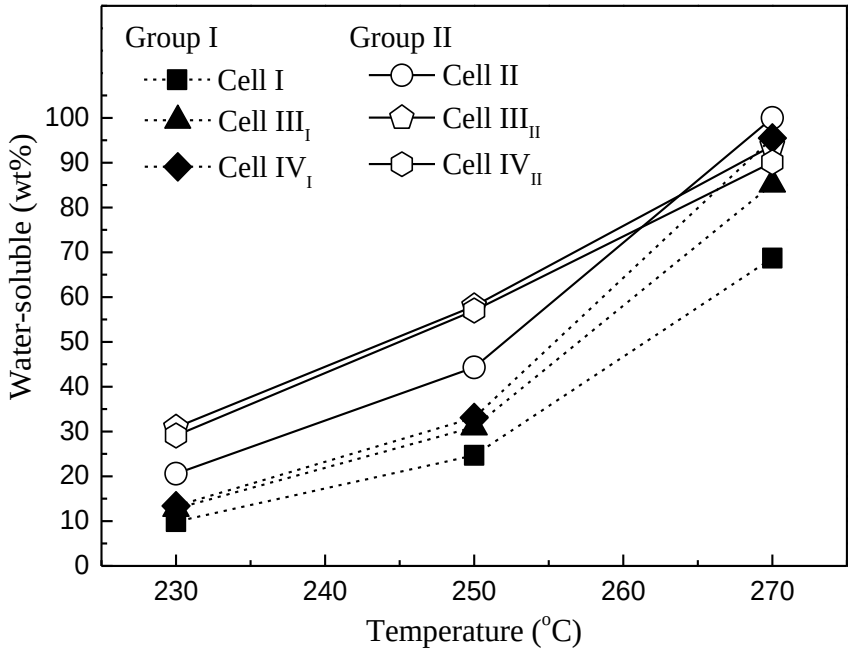

Fig. 4-1 The yield on WS portions obtained from the celluloses as treated by semi-flow HCW at 230-270 ˚C/10 MPa/15 min

The apparent activation energies, Ea, for the celluloses can be calculated from Fig. 4-2. Activation energy of any reaction mainly explains its degree of temperature-sensitiveness; reactions with higher E_a are high in temperature-sensitiveness, while the reactions with lower E_a are low temperature-sensitive (Xin et al. 2009). It can also be said that E_a is defined as the minimum energy required for decomposition to occur. The smaller E_a for decomposition of cellulose signifies the requirement of less energy for its decomposition and *vice versa*. In the figure, it was shown that different slopes obtained for each of the celluloses suggested different E_a for cellulose decomposition in the studied temperature range.

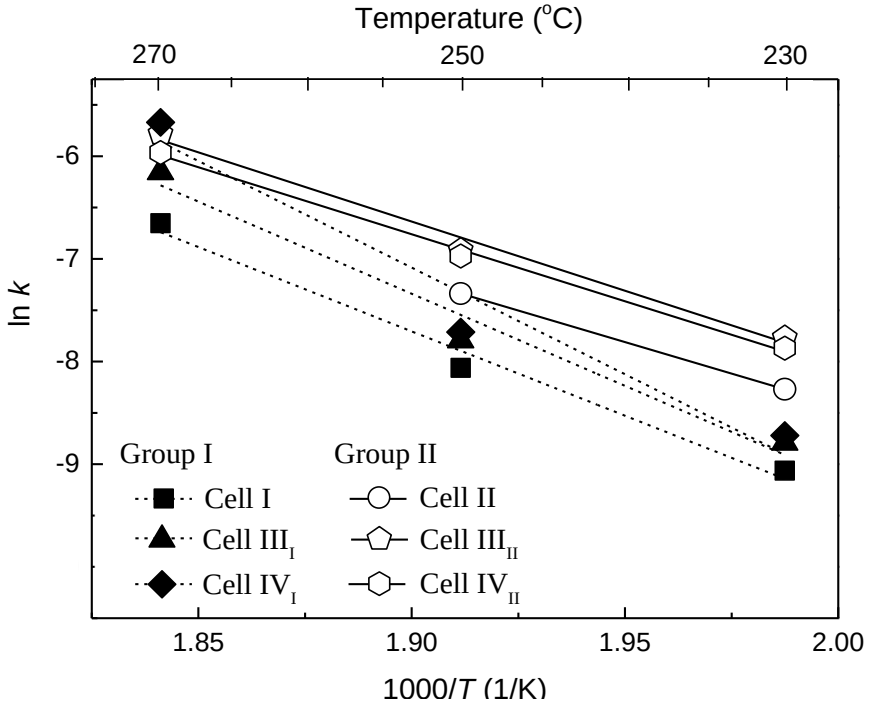

Fig. 4-2 The Arrhenius plot for the celluloses using pseudo-first order reaction kinetics as treated by semi-flow HCW at 230-270 ˚C/10 MPa/15 min

Table 4-1 shows the obtained Ea for all celluloses within the treatment temperatures. The E_a for group I and group II celluloses are, respectively, greater than 130 and 100 kJ/mol. It is apparent that the celluloses in group I have higher E_a than those in group II, which implies an easier decomposition process for group II celluloses by semi-flow HCW treatment. However, due to the aforementioned limitations such as limited numbers of experiments carried out in a relatively narrow temperature range, the obtained E_a must be judged critically. The acquired E_a was based on the best fit curves. As a result, a higher E_a was obtained for cell IV_I as compared with cell I and cell III_I. Since comparison of E_a was done between group I and group II, the above observation of group I having higher Ea than group II is valid.

These Ea are lower than previously reported, 164 kJ/mol (Schacht et al. 2008) and 145 kJ/mol (Sasaki et al. 2004) without catalysts, whereas, 144 kJ/mol and 100 kJ/mol (Mok et al. 1992) in dilute sulfuric acid catalyst. The differences in E_a could be due to various definitions of decomposition processes and of cellulose hydrolysis only at elevated temperatures (above 290 ˚C/25 MPa), treatment

conditions used. For instance, Sasaki et al. (2004) studied just the kinetics whereby in this work the kinetics of various cellulose decomposition were measured at 230-270 ˚C/10 MPa.

Table 4-1 The activation energies of the celluloses as treated by semi-flow HCW at 230-270 ˚C/10 MPa/15 min

	Cellulose	Activation energy, E_a (kJ/mol)
Group I	Cell I	137
	Cell III_I	149
	Cell IV_I	172
Group II	Cell II	102
	Cell III_{II}	112
	Cell IV_{II}	108

The observed decomposition of cellulose in subcritical water appears to be as good as that occurring in dilute sulphuric acid hydrolysis (Mok et al. 1992). Cellulose firstly undergoes a rapid weight loss and followed by a slow hydrolysis step of the remaining cellulose. The high reactivity is associated with accessible paracrystalline regions in cellulose that are more vulnerable to chemical attacks than the crystalline regions (Sasaki et al. 2000).

The reaction temperature has influence on the solvent properties of water (Kruse and Dinjus 2007; Marshall and Franck 1981). It has been suggested that the shift in solvent properties affects the kinetics of cellulose decomposition (Sasaki et al. 2002; Deguchi et al. 2008). However, in this present work, the constant E_a implies that the reaction mechanism of the hydrothermal decomposition is not distinctly affected. The lower E_a obtained indirectly showed that the decomposition of the celluloses in this system is a catalytic process, in agreement with the literature (Mok et al. 1992).

4.3.2 Quantification of the water-soluble portions

Figure 4-3 below shows the reaction scheme of cellulose I decomposition into hydrolyzed and degraded products as treated by semi-flow HCW treatment, adapted from (Abdullah et al. 2013). In the present work, the WS portions for the celluloses obtained from each treatment were found to follow a similar decomposition pathway as in Fig. 4-3. It is important to know the decomposition pathway of cellulose as the degraded products inhibit the fermentation process for ethanol production (Palmqvist and Hann-Hägerdal 2000).

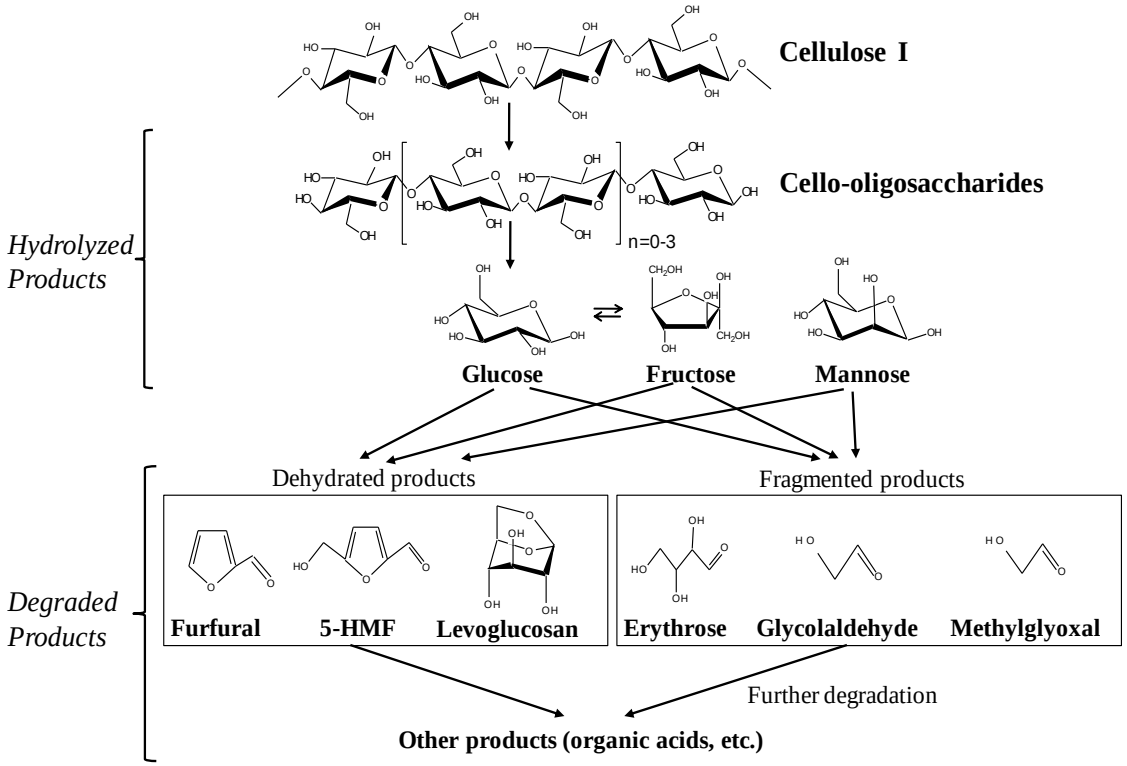

Fig. 4-3 Decomposition pathway of crystalline cellulose as treated by semi-flow HCW (Phaiboonsilpa et al. 2010)

Under the HCW conditions, the ionization constant of water increases with temperature and the amount of dissociation also increases, compared with normal temperature and pressure. The glucosidic linkages of cellulose are cleaved and cellulose starts to hydrolyze into cello-oligosaccharides, and subsequently, hydrolyzed to monosaccharide of glucose (Antal and Mok 1990a; Kruse and Gawlik

2003; Phaiboonsilpa et al. 2010). Isomerization of glucose occurred producing fructose and mannose. These monosaccharides are unstable at high temperature and thus some parts of them are further converted into their degraded products such as furfural, 5-hydroxymethyl furfural (5HMF), levoglucosan through dehydration, and erythrose, glycolaldehyde, methylglyoxal through fragmentation (Antal and Mok 1990b). Prolonged treatment, however, allows further degradation to take place, generating other products such as organic acids.

The resulted WS portion percentages based on the dried weight of cellulose samples are summarized in Table 4-2. It was clearly indicated that the celluloses have been converted to the hydrolyzed and degraded products. The hydrolyzed products are comprised of cello-oligosaccharides, glucose, fructose and mannose, whereas the degraded products consist of dehydrated and fragmented products, as well as organic acids. Their productions were recorded higher in hydrolyzed products as compared with degraded products, and more yields were obtained as treatment temperatures increased.

These WS portions were calculated similarly as in the previous studies (Lu et al. 2009; Phaiboonsilpa et al. 2010). The cello-oligosaccharides were consisted of cellobiose, cellotriose, cellotetraose, cellopentaose, cellohexaose and other cello-oligosaccharides with the higher DP. The more existence of the cello-oligosaccharides with the higher DP shows that the cellulose has more resistance against hydrolysis by semi-flow HCW treatment. In addition to cello-oligosaccharides and glucose, a smaller amount of fructose was also detected and only traces of mannose were identified. A much lower yield of the WS portions obtained at 230 ˚C/10 MPa/15 min was due to the difficulty of the crystalline structures of celluloses to be hydrolyzed at such lower temperature (Phaiboonsilpa et al. 2011). The cello-oligosaccharides observed could be obtained from the paracrystalline cellulose. The observed fructose is not a sugar component in cotton linter, but it maybe isomerized from glucose after hydrolysis from cellulose (Kabyemela et al. 1999; Srokol et al. 2004).

Table 4-2 The summarized yields of WS portions and water-insoluble residues from the celluloses as treated by semi-flow HCW at 230-270 ˚C/10 MPa/15 min

	Semi-flow HCW treatments under 10MPa/15min	Yield (wt%)									
		Water-soluble portions									Water-insoluble residue
		Hydrolyzed products				Degraded products			Unknown	Total	
		Cello-oligo-saccharides	Glucose	Fructose	Mannose	Dehydrated	Fragmented	Organic acids			
Group I	**Cell I**										
	230˚C	3.4	1.2	0.1	0.0	0.2	0.1	0.0	4.9	9.9	90.1
	250˚C	12.3	6.2	0.6	0.0	1.6	0.9	0.2	2.9	24.7	75.3
	270˚C	31.8	17.8	2.4	0.0	7.1	2.3	1.1	6.2	68.7	31.3
	Cell III_I										
	230˚C	5.0	2.2	0.1	0.0	0.3	0.1	0.4	4.7	12.8	87.2
	250˚C	12.0	6.1	0.5	0.0	1.2	0.4	0.5	10.3	31.0	69.0
	270˚C	31.3	17.9	3.5	0.0	7.1	2.7	0.8	21.9	85.2	14.8
	Cell IV_I										
	230˚C	8.1	3.1	0.2	0.0	0.4	0.1	0.2	1.3	13.4	86.6
	250˚C	13.5	6.5	0.6	0.0	1.5	0.9	0.3	9.8	33.1	66.9
	270˚C	43.4	19.6	4.0	0.0	7.5	3.0	0.6	17.4	95.5	4.5
Group II	**Cell II**										
	230˚C	6.4	2.2	0.1	0.0	0.9	0.0	0.5	10.5	20.6	79.4
	250˚C	19.4	12.1	0.7	0.0	2.5	1.2	0.5	7.9	44.3	55.7
	270˚C	34.7	26.0	6.6	0.0	11.4	6.4	1.0	13.9	100.0	0.0
	Cell III_{II}										
	230˚C	15.6	3.9	0.1	0.0	0.5	0.1	0.1	10.6	30.9	69.1
	250˚C	31.0	10.7	4.8	0.0	3.8	0.8	0.3	6.6	58.0	42.0
	270˚C	46.4	17.6	7.0	0.0	6.8	1.6	0.5	13.9	93.8	6.2
	Cell IV_{II}										
	230˚C	6.1	3.5	0.1	0.0	0.4	0.6	0.1	18.3	29.1	70.9
	250˚C	30.2	9.3	0.6	0.0	2.1	2.0	0.4	12.4	57.0	43.0
	270˚C	49.4	15.0	2.6	0.0	5.8	6.0	0.8	10.5	90.1	9.9

The Table 4-2 can clearly showed that the decomposition products obtained from cell IV_I has lower residue yields and higher WS portions than that of cell I, supporting the evidence on *Chapter 2*. The prepared cell IV_I as the starting materials aided the decomposition process in HCW treatment.

To evaluate the decomposition behavior of the celluloses in details, the results from 270 ˚C/10 MPa/15 min would be more appropriate, as this was suggested as the optimum condition for cellulose decomposition (Phaiboonsilpa et al. 2010; Phaiboonsilpa et al. 2011). Table 4-3 shows the comparison between hydrolyzed and degraded products for the two groups of cellulose samples at 270 ˚C/10 MPa/15 min.

Table 4-3 The total hydrolyzed and degraded products of WS portions from the celluloses as treated by semi-flow HCW at 270 ˚C/10 MPa/15 min

	Cellulose	Hydrolyzed product (wt%)	Degraded product (wt%)
Group I	Cell I	52.0	10.5
	Cell III_I	52.7	10.6
	Cell IV_I	67.0	11.1
Group II	Cell II	67.3	18.8
	Cell III_{II}	71.0	8.9
	Cell IV_{II}	67.0	12.6

It can be seen that for both group I and group II celluloses, more than 50 wt% of hydrolyzed products were obtained as compared with degraded products. It was reported that about 31.2, 28.1 and 20.5 wt% of hydrolyzed products obtained from the cellulose of Japanese cedar, Japanese beech and Nipa frond, respectively (Phaiboonsilpa and Saka 2012). However, there were no results for DP of the cellulose from this study that it can be compared with. The higher yield in WS

portions observed in this present work could probably due to the shorter DP celluloses used for the starting materials.

According to Fig. 4-3, the hydrolyzed products were produced at the early stage of cellulose decomposition pathway. This could signify that these celluloses have resistance against decomposition. The total hydrolyzed products for cell I and cell III_I is similar but much lesser than cell IV_I, whereas the highest hydrolyzed products obtained in group II is from cell III_{II}, followed by cell IV_{II} and cell II. Overall, celluloses in group II have resulted more hydrolyzed products than those in group I. The observation is similar for the degraded products.

Figures 4-4 and 4-5, respectively, illustrated how the hydrolyzed and degraded products were obtained at every 5 min intervals at 270 ˚C/10 MPa/15 min. In Fig. 4-4, only the yields of cello-oligosaccharides, glucose and fructose were shown. These yields are comparable with the results in the literatures (Lu et al. 2009; Phaiboonsilpa et al. 2010; 2011). Based on these results, the cellulose has been cleaved into cello-oligosaccharides at the early stage of the treatment time and the production of glucose and fructose was seen to occur simultaneously. Celluloses in both group I and group II have similar behaviors; however, more products were seen from group II celluloses. The cello-oligosaccharides and glucose were recovered from the treatment time of 35 min. The crystalline structure of cellulose remained unchanged at temperatures around 230 ˚C (Phaiboonsilpa et al. 2009), thus, the WS portions emerged from the time-up (0-20 min treatment time) could be from paracrystalline cellulose, and the time at (20-35 min treatment time) was from cellulose.

Generally, these monosaccharides are further degraded by dehydration or fragmentation process (Kruse and Dinjus 2007; Lu et al. 2009; Kumar et al. 2010; Xiao et al. 2011). Figure 4-5 illustrated more dehydrated products were obtained than fragmented products and organic acids. During the treatments, it can be seen that the degraded products were generated at almost similar time as the hydrolyzed products (Fig. 4-4). Moreover, the productions of dehydrated and fragmented products as well as organic acids were generated concurrently.

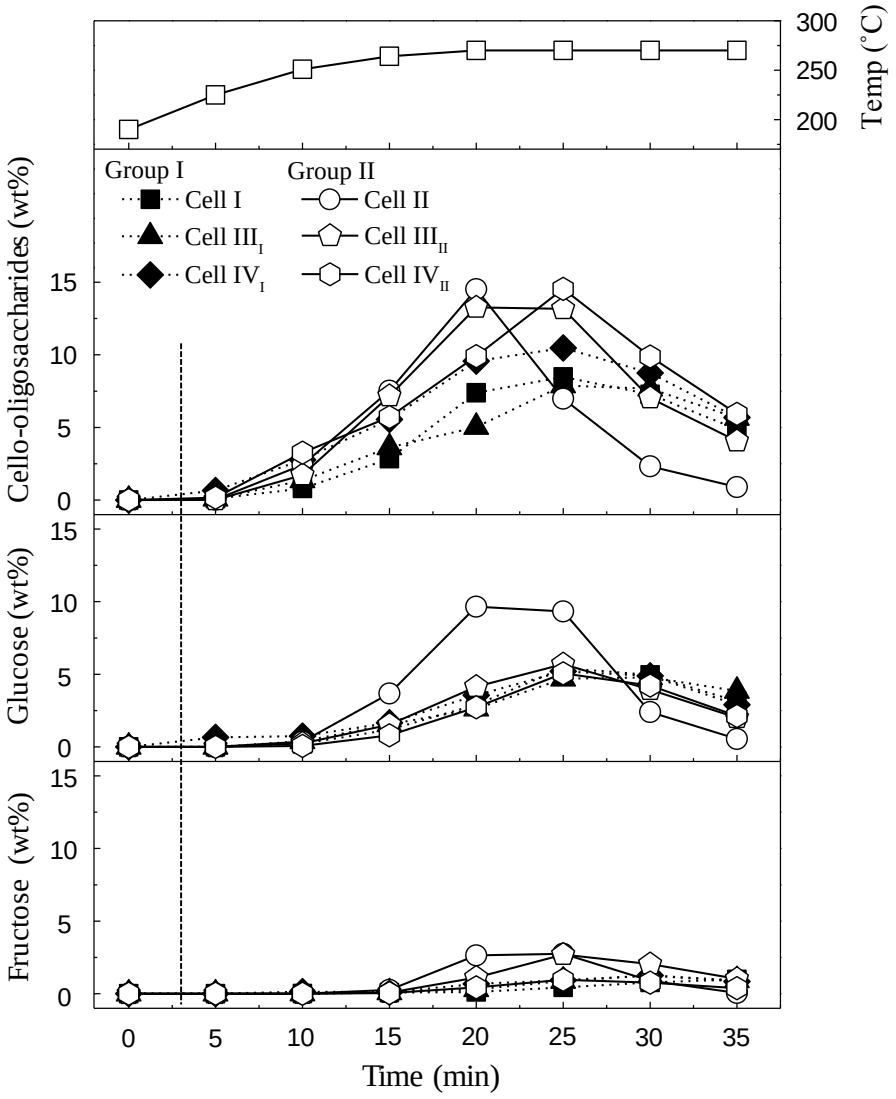

Fig. 4-4 The hydrolyzed products of cello-oligosaccharides, glucose and fructose in the WS portions from the celluloses as treated by semi-flow HCW at 270 ˚C/10 MPa/15 min. Top figure corresponds to treatment temperature (open squares)

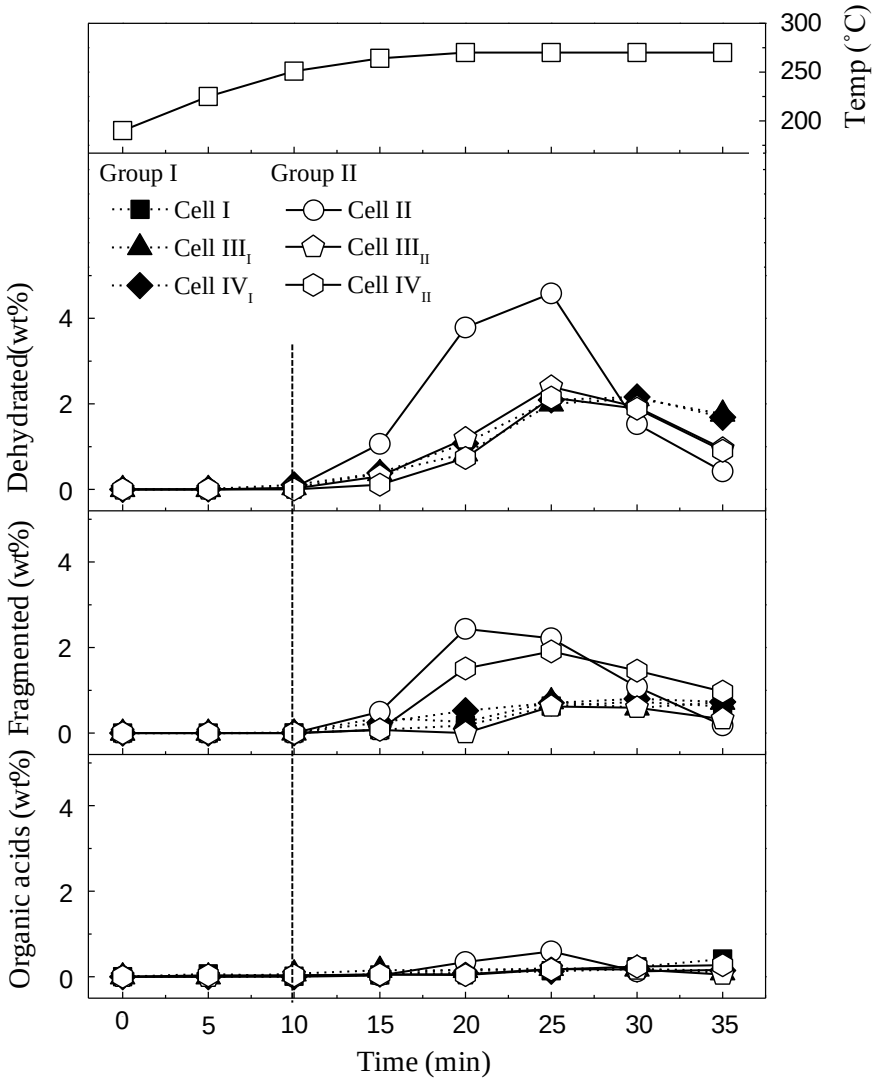

Fig. 4-5 The degraded products of dehydrated, fragmented and organic acids products in the WS portions from the celluloses as treated by semi-flow HCW at 270 ˚C/10 MPa/15 min. Top figure corresponds to treatment temperature (open squares)

Both group I and group II celluloses in Fig. 4-5 have the same trends as in Fig. 4-4, i.e., more products resulted from group II celluloses. The generation of hydrolyzed products started to be noticeable from around 3 min (Fig. 4-4) and followed by degraded products (Fig. 4-5) about 10 min later. This sequence is parallel with that shown in Fig. 4-3 at which the hydrolyzed products were produced earlier in the decomposition pathway, and later on followed by the by the production of degraded products.

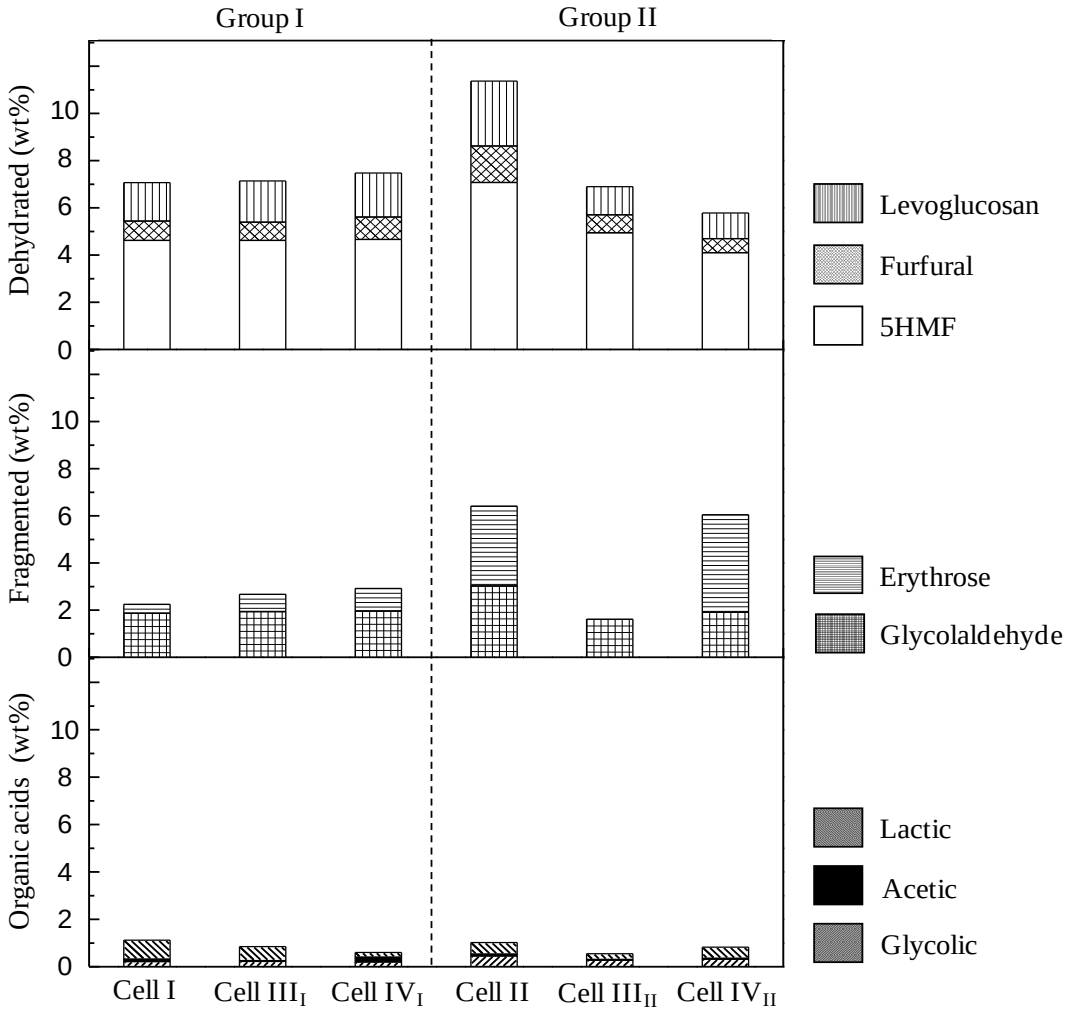

Fig. 4-6 The degraded products in WS portions from the celluloses as treated by semi-flow HCW at 270 ˚C/10 MPa/15 min

Figure 4-6 shows the yield in wt% for the individual degraded products in the WS portions for both group I and group II celluloses as treated by semi-flow HCW at 270 ˚C/10 MPa/15 min. The dehydrated products detected were consisted of levoglucosan, furfural and 5HMF, whereas fragmented products such as erythrose, glycolaldehyde and methylglyoxal. While for organic acids; lactic, acetic, glycolic and formic acids were identified. The furfural in Fig. 3-6 can not only be produced from pentose but also from hexose such as glucose. This means that the formation of furfural is possible without pentose via five-carbon ketoses pathway as proposed in the literature (Kallury et al. 1986).

Glycolaldehyde and erythrose were formed via retro-aldol condensation in glycolaldehyde/erythrose pathway (Kabyemela et al. 1999; Sasaki et al. 2002), while methylglyoxal was produced via glyceraldehyde/dihdroxyacetone pathway in hexose fragmentation. Nevertheless, the production of methylglyoxal in this case was too minute that it was excluded from Fig. 4-6. The production of furfural and 5HMF was significant as compared with other degraded products. The organic acids produced are the results of further degradation of dehydrated and fragmented products (Kabyemela et al. 1999; Yoshida et al. 2005). Formic acid production was only a trace to be included in Fig. 4-6. All the sequences of degradation reactions and productions are agreeable with Fig. 4-3.

Based on those results above, it can be seen that group II celluloses dominated both the hydrolyzed and degraded products as compared with group I celluloses. The result on the WS portions at 270 ˚C/10 MPa/15 min revealed that the degree of difficulty for decomposition is greater for celluloses in group I than those in group II.

4.4 Concluding Remarks

This study shows the essential effects of various crystalline celluloses on their hydrothermal decomposition and its kinetic behaviors as treated by semi-flow HCW. Both decomposition rate and E_a are helpful in defining the degree of difficulty for decomposition of the celluloses, however, the E_a obtained were merely based on empirical relationships of Arrhenius equation. Consequently, the direct

method is more preferable than the latter. Nevertheless, this study showed the new kinetic data as there was no previous data on these specific reaction systems.

These treatments can be used as viable decomposition media for celluloses at which under the given treatment conditions, cellulose is more readily hydrolyzed with less degraded products. Group I celluloses (cell I, cell III_I, cell IV_I) have shown to have more resistance to decompose than group II celluloses (cell II, cell III_{II}, cell IV_{II}). Based on this evidence, it was clear that the decomposition behaviors are due to the different crystalline forms of celluloses. These presented data are useful for understanding how the celluloses are hydrothermally decomposed, providing useful insights to efficient utilization of lignocelluloses for biofuels and biochemicals.

CHAPTER 5

Conversion of Cellulose III to Its Parent Cellulose in Hydrothermal Treatment

5.1 Introduction

In previous chapters, the decomposition behaviors of various crystalline celluloses by semi-flow hot-compressed water (HCW) and enzymatic treatment were carefully discussed. Both treatment conditions resulted in similar decomposition behaviors. The treatment with enzyme at 50 ˚C/0.1MPa for ~14 days showed better hydrolysis for celluloses in group II and cell III_I, and simultaneously, interconversion of celluloses occurred. Meanwhile, the treatment with semi-flow HCW at 230-270 ˚C/10 MPa/15 min illustrated that celluloses in group II hydrolyzed better, despite the occurrence of cellulose interconversion.

Amongst the prepared celluloses, cellulose (cell III) has shown a peculiar behavior. Since cell III is the basis for composite cellulose, it is considered as an important cellulose allomorph. As mentioned previously in section 1.3.3.3 of *Chapter* 1, cell III can be further classified into two polymorphs, cell III_I and cell III_{II}. Their unit cells are found to be very similar, with some differences in intensities of the meridional reflections only (Sarko et al. 1976; Wada et al. 2004b). Even so, one cannot use the crystal model of cell III_I for cell III_{II} and *vice versa*. The model for crystalline structure of cell III_I (details in *Chapter* 6) could be constructed from the work of Wada et al. (2004b), while, for cell III_{II}, its structure has yet to be solved (Zugenmaier 2008). Thus, cell III_{II} are not very commonly discussed in literatures and most findings or studies usually are focussing on cell III_I.

Despite of the reasons mentioned above, investigation on the conversion behavior of cell III under different temperature and pressure conditions in hydrothermal treatment would be interesting. Hence, this chapter describes a concise report to clarify the behavior of cell III qualitatively, in various treatment conditions as treated by semi-flow HCW.

The original publication is available at Springer via http://link.springer.com/book/10.1007/978-4-431-54264-3

5.2 Materials and Methods

5.2.1 Preparation of cellulose III

Both cell I and cell II were, respectively, converted into cell III_I and cell III_{II} by ethylenediamine (EDA) treatment as described previously. After drying process, the prepared cellulose samples were stored in desiccators over silicon pellets until further usage.

5.2.2 Semi-flow hot-compressed water treatment and cellulose residues analyses

The semi-flow HCW system and its operational procedures as carried out in earlier chapters were used in this study. Here, the cellulose samples were treated at temperatures between 100 to 270 ˚C under 4, 6 and 10 MPa for 5-15 min. The insoluble residues left in the reaction cell after treatment were collected, oven-dried and analyzed independently.

X-ray diffraction (XRD) diagrams of the untreated samples and residues after the treatment were recorded using an imaging plate (IP) of 80 x 100 mm, mounted on the X-ray box of Rigaku RINT 2200V. Ni-filtered Cu-K_α radiation (λ=0.15418nm) generated at 40 kV and 30 mA was used. The samples were irradiated using an incident X-ray beam that was collimated in the box. The IP was then converted to XRD diagrams via high sensitivity IP reader RAXIA-Di. In addition, the XRD pattern was also obtained using X-ray diffractometry and its crystallinity was measured accordingly.

5.3 Results and Discussion

5.3.1 The X-ray diffraction diagrams of celluloses III_I and III_{II}

Figure 5-1 showed the XRD diagrams of cell III_I before (*left*) and after (*right*) the HCW treatment at 270 ˚C/10 MPa/15 min. The diagram of cell III_I (*left*) has a strong reflections indexed 010 and $1\bar{1}0$ located at the equator at *d*= 0.76 and 0.43 nm (Wada et al. 2001), respectively. Figure 5-1 (*right*) illustrated the XRD diagram of the converted cell III_I to cell I at 270 ˚C/10 MPa/15 min. The reflections indexed $1\bar{1}0$, 110 and 200 occurred on the equator at *d*= 0.62, 0.55 and 0.40 nm, respectively.

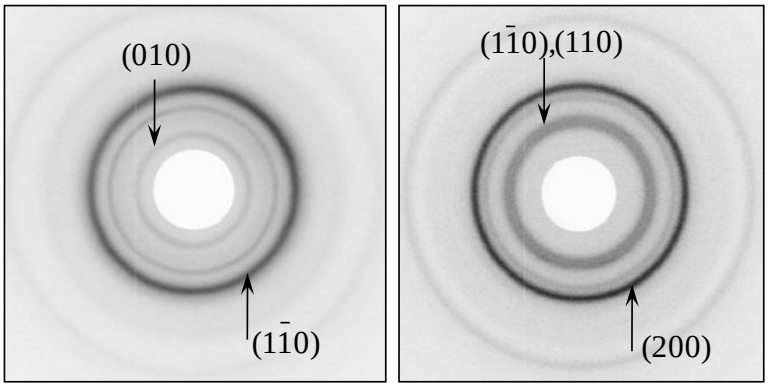

Fig. 5-1 The XRD diagrams of cell III_I before (*left*) and after (*right*) the HCW treatment at 270 ˚C/10 MPa/15 min

All reflection indices in the diagram of Fig. 5-1 (*right*) closely resembles that of the I_β monoclinic unit cell (Woodcock et al. 1980; Sugiyama et al. 1991b), which indicated that cell III_I fully converted into cell I (I_β phase) by the HCW treatment at 270 ˚C/10 MPa/15 min. The XRD diagrams to demonstrate the fully converted cell III_I to cell I at lower temperatures and pressures for 15 min, were not shown here, which however found to be similar. By using the same treatment time, cell III_I was shown to convert into cell I at 180 and 230 ˚C under the pressures of 4 and 6 MPa, respectively.

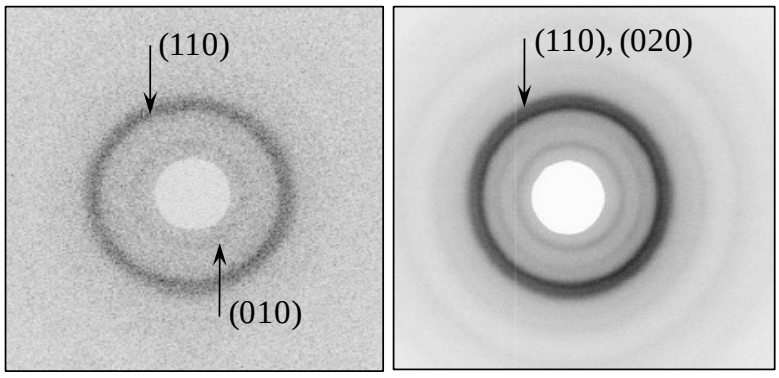

Fig. 5-2 The XRD diagrams of cell III_{II} before (*left*) and after (*right*) the HCW treatment at 230 ˚C/10 MPa/15 min

As for cell III_{II}, in general, the full conversion to cell II occurred at lower temperatures as compared with that of cell III_I. Figure 5-2 illustrated the XRD

diagrams of cell III_{II} before (*left*) and after (*right*) the HCW treatment at 230 ˚C/10 MPa/15 min. In Fig. 5-2 (*left*), the reflection of cell III_{II} indexed 010 and $1\bar{1}0$ located at the equator at *d*= 0.74 and 0.44 nm, respectively. As shown in Fig. 5-2 (*right*) after the HCW treatment, the reflections were then changed to 110 and 020, which occurring on the equator at *d*=0.46 and 0.41 nm, respectively. These reflections are the characteristic of cell II, which took place at 230 ˚C/10 MPa/15 min.

The XRD diagrams for the conversion of cell III_{II} to cell II at other treatment conditions (at 4, 6 MPa/15 min) were found to be similar. For 5 min treatment time at 190 ˚C/4 MPa and 200 ˚C/6 MPa, the conversions of cell III_{II} to cell II were already seen to occur.

5.3.2 The X-ray diffraction patterns of celluloses III_I and cell III_{II}

In Fig. 5-3, the XRD patterns were plotted over various temperatures in order to observe the full conversion of cell III_I to cell I, at constant pressure. For 10 MPa at 15 min treatment time, the full conversion occurred at 270 ˚C. Two equatorial reflections of cell III_I, labelled as 1 and 2 indexed at 010 and $1\bar{1}0$, respectively, were observed for the cell III_I (before treatment). As soon as cell III_I treated at lower temperature at 10 MPa/15 min, a peak 2 shifted noticeably to the smaller angles because of thermal expansion, in accordance with the peak 1 being smaller.

When the temperature is at 100 ˚C, the peak 1 slowly disappeared and peak 2 became smaller at 150 ˚C and diminished. Whereas peaks 3, 4 and 5 that correspond to cell I appeared markedly. Consequently, at 200 ˚C, cell III_I was almost completely converted into cell I_β phase, with a full transformation at 270 ˚C. The XRD peaks showed that the $1\bar{1}0$ lattice diffraction angles for treated crystalline cell III_I were shifted to around 22.5 ˚ from about 20.8 ˚. The XRD pattern obtained at 270 ˚C showed that cell I has a cell I_β pattern. The XRD patterns under 4 and 6 MPa at various temperatures for 15 min (data not presented) followed a similar pattern as in Fig. 5-3. The same results were also obtained under wet condition.

Earlier in section 2.3.1 of *Chapter* 2, it was stated that the conversion of cell III_I to cell I at lower temperature (230 ˚C/10 MPa) has already started at an early

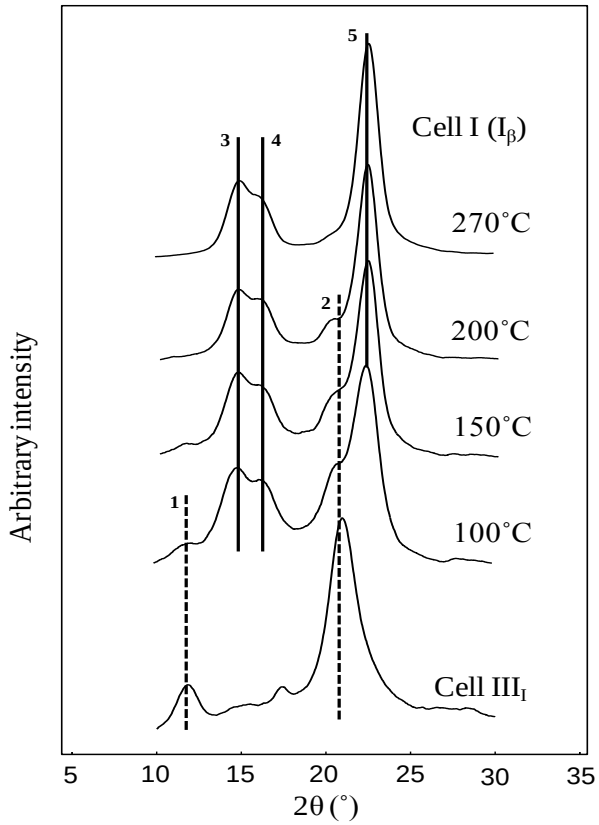

Fig. 5-3 The XRD patterns for cell III_I, converting to cell I (cell I_β) as treated by HCW at various temperatures under 10MPa/15min. Peaks 1, 2 and peaks 3, 4, 5 are diffraction angles of cell III_I and cell I, respectively

stage of the HCW treatment. The peaks indexed $1\bar{1}0$ for cell III_I disappeared even after 2 min treatment. However, at lower temperature and pressure treatment conditions, 180 ˚C/4 MPa and 230 ˚C/6 MPa at shorter treatment time, 5 min, the full XRD pattern for cell I was not obtained, as in Fig. 5-4. Here, it can be seen that peaks 3, 4 and 5 have not yet completely shifted to cell I index planes.

In the case of Fig. 5-5, the XRD patterns for cell III_{II} are shown to convert to cell II when treated by HCW at various temperatures under 10 MPa at 15 min. For 10 MPa/15 min, the full conversion to cell II occurred at 230 ˚C. The equatorial reflections of cell III_{II}, labelled as 1 which indexed $1\bar{1}0$, totally disappeared and replaced by the characteristic peaks of cell II; peaks 2 and 3. The behavior is very similar for treatment at lower pressures (4 and 6 MPa) for 15 min treatment time, thus, the data are not presented.

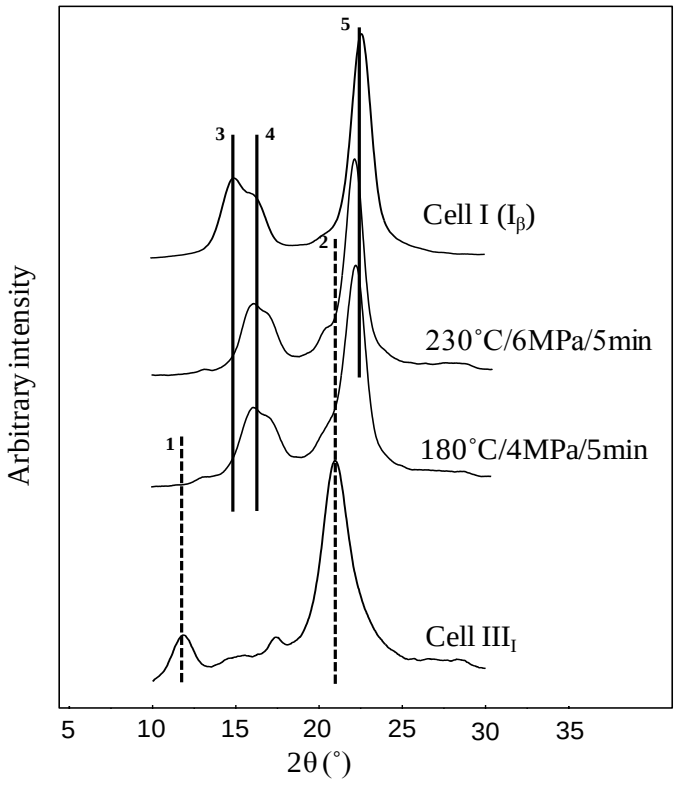

Fig. 5-4 The XRD patterns for the residues from cell III_I after treated by semi-flow HCW at 180 ˚C/4 MPa and 230 ˚C/6 MPa at 5 min. Peaks 1, 2 and peaks 3, 4, 5 are diffraction angles of cell III_I and cell I, respectively

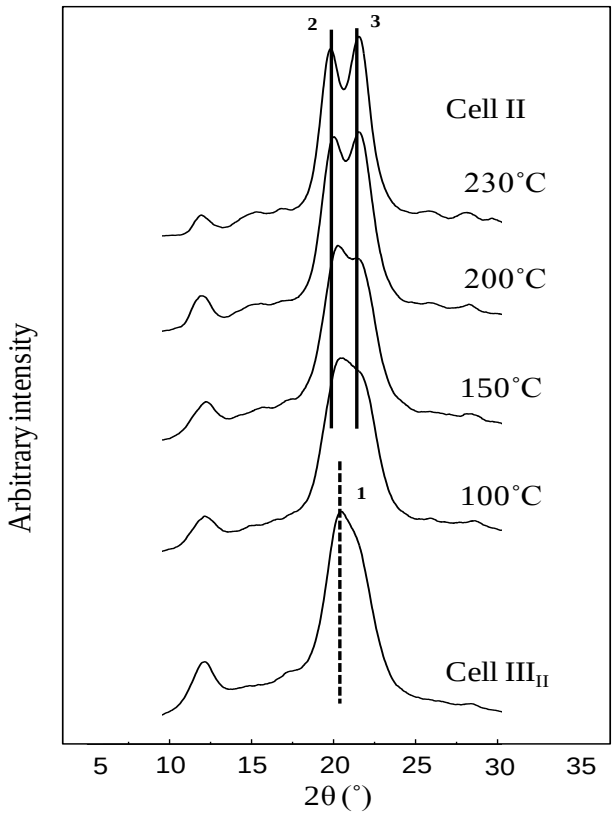

Fig. 5-5 The XRD patterns for cell III_{II}, converting to cell II as treated by HCW at various temperatures under 10MPa/15min. Peak 1 and peaks 2, 3 are diffraction angles of cell III_{II} and cell II, respectively

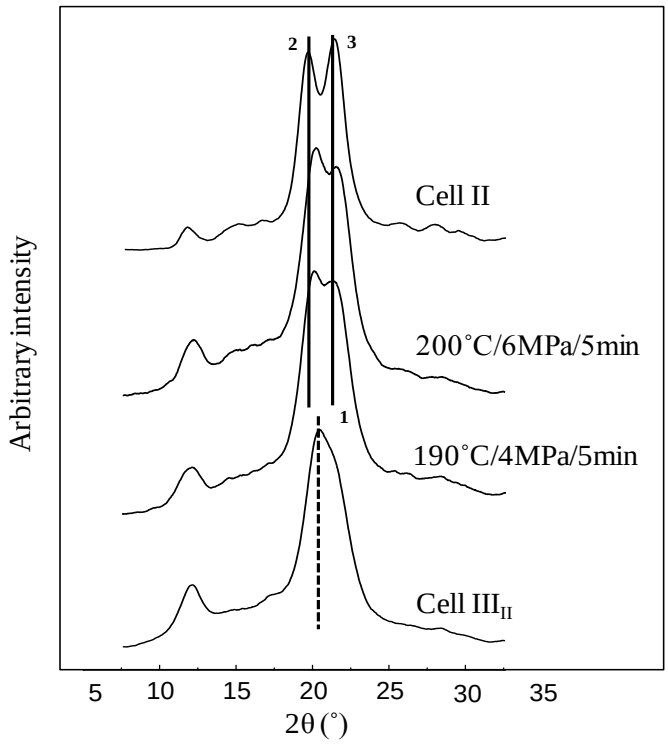

Fig. 5-6 The XRD patterns for the residues from cell III_{II} after treated by semi-flow HCW at 190 ˚C/4 MPa and 200 ˚C/6 MPa at 5 min Peak 1 and peaks 2, 3 are diffraction angles of cell III_{II} and cell II, respectively

Figure 5-6 shows the XRD pattern for conversion of cell III_{II} to cell II at 190 ˚C/4 MPa and 200 ˚C/6 MPa for shorter treatment time, 5 min. It can be noticed that the peaks 2 and 3 are readily shown, however, not as sharp as in cell II. Cell III_{II} converted to its parent cellulose much faster, as compared with the conversion of cell III_I to cell I, in such treatment conditions.

As for the overall crystallinity of residues, from cell III_I (i.e. cell I) and cell III_{II} (i.e. cell II) after HCW treatments they have not change tremendously and remained almost constant. The results have no significant difference when they are treated under different pressure conditions.

5.4 Concluding Remarks

This short experiment has shown how the polymorphs of cell III behave in lower temperature, pressure and treatment time, within the limits of HCW conditions.

It can be seen that the conversion of cell III to its parent cellulose are dependent on pressure and temperature in HCW treatments. The semi-flow HCW treatment conditions at a range of temperatures between 100-270 ˚C under 4-10 MPa for 5-15 min resulted a slower conversion of cell III_I and cell III_{II} to their parent celluloses. The results are useful additional information to the earlier discussed studies. Nevertheless, further qualitative and quantitative investigation would be needed in the future for more in details to reason why such behaviors are occurring in the HCW conditions.

CHAPTER 6

Molecular Dynamics Simulation on Decomposition Behaviors of the Celluloses

6.1 Introduction

In *Chapters* 2 and *4*, the decomposition behaviors of various crystalline celluloses by hydrothermal treatment i.e., semi-flow hot-compressed water (HCW) treatments at 230-270 ˚C/10 MPa/15 min have been discussed and shown that the degree of difficulty for decomposition was dependent on the crystalline structure of the starting celluloses (Abdullah et al. 2013; 2014). It was concluded that the cell I, cell III_I and cell IV_I (i.e. group I) have more resistance to be decomposed than cell II, cell III_{II} and cell IV_{II} (i.e. group II). Furthermore, observable crystallographic changes have occurred for cell III_I, cell IV_I and cell III_{II} during the HCW treatment.

The results above, nevertheless, were not succeeded in explaining the mechanism that occurred during the HCW treatment. The knowledge on the interaction process between the water molecules and the celluloses in the HCW condition would give a better understanding on the decomposition process. Hence, it is necessary to study the reaction process that takes place during the treatments. The relationship between cellulose decomposition and various cellulose crystalline structures is made possible by using computer simulation techniques.

There have been many studies done on molecular dynamics (MD) simulations for the investigation of crystalline cellulose structures (Bellesia et al. 2010). Some of them involved the behaviors of cellulose at high temperature conditions. Shen et al. (2009) performed replica exchange MD simulation at the temperature regions from ~2 to 284˚C by using oligomer model of cellulose. It was demonstrated that the increment on the flexibility of the glucosidic torsion angles (φ=O5'-C1'-O4-C4; ψ=C1'-O4-C4-C5), which fluctuated from the global minimum of (-75˚, -120˚) to the neighbor energy minima at (60 ˚, -120 ˚) and (-80 ˚, 70 ˚), followed according to the

The original publication is available at Springer via http://dx.doi.org/ 10.1007/s10570-014-0343-y

increment of the temperatures. Queyroy et al. (2004) studied the MD simulation of tetraose and octaose of cellulose and observed that most of the glucopyranose rings assumed a puckered un-chaired conformation at ~527 ˚C. As the decomposition of cellulose was considered to relate to the ring conformation change, the evaluation of the conformational changes would be important (Hosoya et al. 2009).

It is common to use mini crystalline cellulose structure for MD simulation studies at high temperature regions. The MD simulation of cellulose chains at high temperature suggested the possibility of the folding of cellulose in its chain conformation (Tanaka and Fukui 2004). Subsequently, Bergenstråhle et al. (2007) reported the conformational behavior of cellulose I_β (cell I_β) under the high temperature condition using GROMOS 45a4 force field. They observed that most of the orientation of hydroxyl group changed from *tg* to *gt* conformation and the intra-molecular hydrogen bond between O2-H and O6 disappeared at high temperature. Moreover, the unit cell dimension of the crystalline structure shrunk 0.5 % along to *c*-axis and elongated 7.4 and 6.0 % along to *a*- and *b*- axes, respectively. The value of γ angle at ~227 ˚C became 2.9 % smaller than that of room temperature.

Another MD simulation by Zhang et al. (2011) indicated the existence of the phase transition temperature of cell I_β at ~200 to 227 ˚C. Matthew et al. (2011) used two different force fields of CHARMM35 and GLYCAM06 to perform a detail investigation on the temperature effect on cell I_β. They observed the change of the side chain orientation from *tg* to *gt* in the 'origin' chain and *tg* to *gg* in the 'center' chain, respectively.

Crystalline cellulose I_α (cell I_α) converts to cell I_β (Horii et al. 1987; Yamamoto et al. 1989; Debzi et al. 1991) and cell III_I to cell I_β (Roche and Chanzy 1981; Yatsu et al. 1986; Wada 2001) under high temperature region treatments. The MD simulation on the conversion cell I_α to cell I_β was reported by Matthews et al. (2012) and the existence of the intermediate state between cell I_α and cell I_β is suggested in their works. Whereas, the conversion from cell III_I to cell I_β by using MD simulation were studied by Yui and Hayashi (2007; 2009), Yui (2012) and Uto et al. (2013). Although the above works discussed the transition behavior of the crystalline cellulose in details, the decomposition behavior at high temperature and

pressure have not been explored fully, except, the investigation on the behavior of cell I_β structure in supercritical water (Ito et al. 2002).

This chapter is, therefore, examined the relationship between the crystalline structures of cellulose and cellulose decomposition in HCW by using MD simulation by using mini crystalline models of various celluloses. This methodology also provides the information about the interaction of hydrogen bonds of the models in HCW conditions, as well as hints in solving the decomposition mechanism.

6.2 Computational Procedures

The MD simulations were carried out with the Gromacs 4.5.5 (Berendsen et al. 1995; Lindahl et al. 2001; Van Der Spoel et al. 2005; Hess et al. 2008), utilizing the CHARMM 35 force field for mini crystalline cellulose (Guvench et al. 2008; 2009) and TIP3P for water models (Jorgensen et al. 1983; Durell et al. 1994). The initial cellulose models used in this study were constructed from the crystalline coordinates of cell I_β (Nishiyama et al. 2002) – cotton linter mainly consisted of I_β phase, cell II (Langan et al. 2001), cell III_I (Wada et al. 2004b), and cell IV_I (Gardiner and Sarko 1985), respectively. The initial structures of these four crystalline celluloses are shown in Fig. 6-1. Each model of mini crystalline cellulose consists of 36 chains with degree of polymerization 10. The mini crystalline surfaces of the cell I_β used in our model are (110) and $(1\bar{1}0)$, which are known as a lattice imaging of cotton microfibrils (Abdullah et al. 2013).

Other simulation models with cellulose polymorphs of cell II, cell III_I, and cell IV_I are also constructed to have the same number and the same length of chains with the model of cell I_β. The mini crystalline surfaces of the simulation models of cell II and cell IV_I are (110) and $(1\bar{1}0)$, which is generally expected as the surface of these microcrystallites.

Yui and Hayashi (2007; 2009) and Yui (2012) discussed the structure of the simulation model to investigate the crystalline transformation from cell III_I to cell I. They reported that the *a*- and *b*- planes are very critical for the change of the hydrogen bonding system when the cell III_I model is simulated at high temperature

~97 ˚C. From their results, the mini crystalline with planar (100) and (010) surfaces was used in our simulation model of cell III_I.

Each crystalline model was placed in an equilibrated cubic box of water molecules with 8 nm length. All those water molecules that overlapped with the carbohydrate heavy atoms were deleted. The system first minimized on the water molecules, while the cellulose chains were fixed at their initial position during 500 ps with 1.0 fs time step in an NPT ensemble. A Leap-frog algorithm was applied to integrate the equations of motion in the MD simulations (Hockney 1970). Van der Waals interactions were smoothly truncated on an atom-by-atom basis using switching functions from 1.2 to 1.35 nm. Electrostatic interactions were treated using the particle-mesh Ewald method (Darden et al, 1993; Essmann et al. 1995) with a real space cut-off of 1.35 nm.

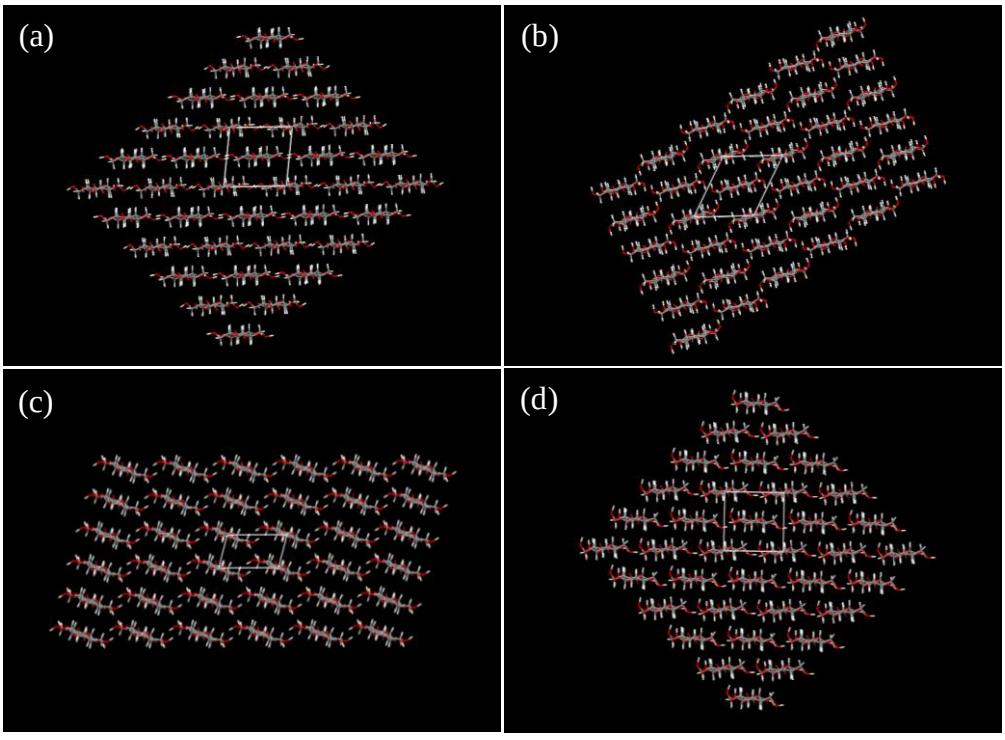

Fig. 6-1 Projection of the initial mini crystalline structures: (a) cell I_β, (b) cell II, (c) cell III_I and (d) cell IV_I. C, O, and H are represented as gray, red, and white line, respectively

The simulation was run at a constant temperature of 230 ˚C and a constant pressure of 10 MPa, maintained using a constant Nose-Hoover temperature (Nose 1984; Hoover 1985) and Parrinello-Rahman pressure algorithm (Parrinello and Rahman 1981). The trajectories were run for 10 ns with a step size of 1 fs using full periodic boundary conditions. For comparison purposes, the systems were also run at 27 ˚C and 0.1 MPa for 10 ns. Molecular graphics were generated with the Visual Molecular Dynamics (VMD1.9) program (Humphrey et al. 1996).

6.3 Results and Discussion

6.3.1 Dynamics behaviors of the celluloses

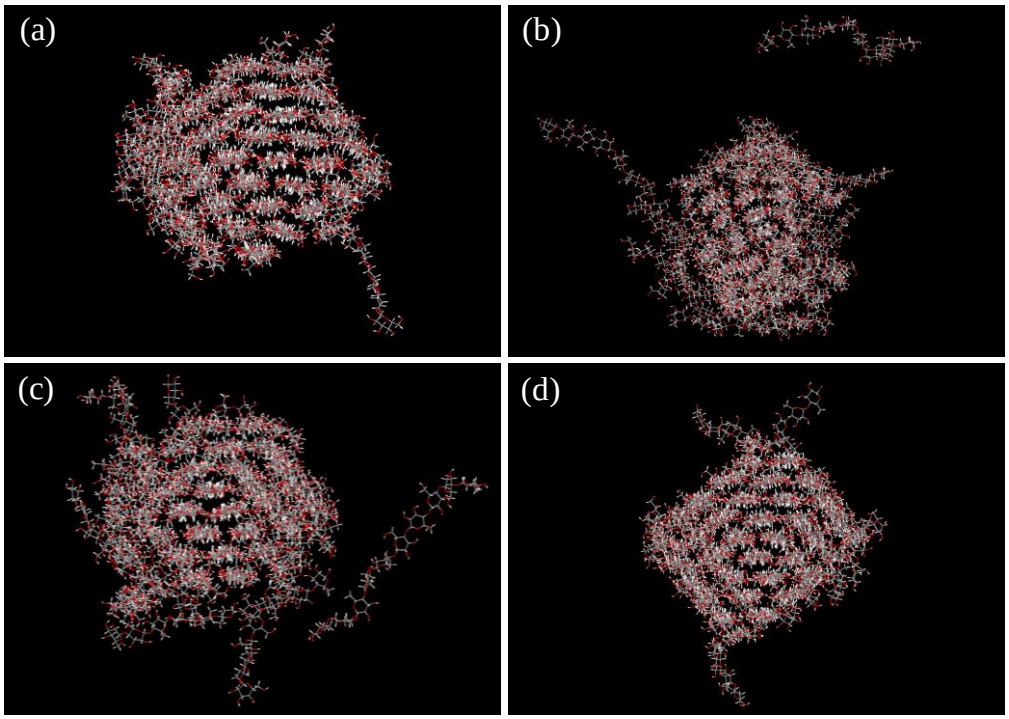

Fig. 6-2 Snapshots of cellulose mini crystalline structure after 10 ns MD simulations at 230 ˚C/10 MPa: (a) cell I_β, (b) cell II, (c) cell III_I and (d) cell IV_I. Solvent water molecules are not shown in the figures for simplicity

Figure 6-2 shows the snapshots of the final structures on mini crystalline celluloses at 230 ˚C/10 MPa after the 10 ns dynamics run. In each model, the disordering of the crystalline structures and the decomposition of a few chains from

the mini crystalline structures were observed. It can be seen that the behavior of the disordering were dependent on the types of the crystalline structures i.e., cell II and cell III_I degrade earlier than those of cell I_β and cell IV_I.

To investigate the disordering behavior on these crystalline structures in more detail, time dependence of the interaction energies during the simulation were analyzed and the results are shown in Fig. 6-3. The interaction energies among the cellulose chains in the crystalline structures are shown in Fig. 6-3 (a), whereas, the interaction energies between cellulose chains and the surrounding water molecules are illustrated in Fig. 6-3 (b). The interaction energies of cell I_β among the cellulose chains decreased at the beginning stage of the simulation time. However, they keep almost at constant values most the simulation time. This behavior is very similar to cell IV_I.

These behaviors are well explained from the snapshot conformation in Fig. 6-2 (a) and (d), that some of the chains existed at the surface area of the mini crystalline structures decomposed into the water, but the core part of the mini crystalline structures keep their original arrangement in both cell I_β and cell IV_I. It is also observed that no water molecules penetrate into the core part of both crystalline structures.

Although the chains at the surface area are affected by the high temperature and high pressure conditions, the core part of the crystalline structure remained, which are observed as the constant interaction energies in the simulation for both mini crystalline cell I_β and cell IV_I. The similarity on the properties between cell I_β and cell IV_I has been discussed experimentally as a transition of the crystalline structure from cell IV_I to cell I_β. We also reported that cell IV_I is easily converted to cell I as treated by HCW experiment over 250 ˚C (Abdullah et al. 2013). Wada et al. (2004a) mentioned that the crystalline structure of cell IV_I is essentially the same with cell I_β but it contains lateral disorder in the structure. The results of our simulation also show that the mini crystalline cell I_β and cell IV_I behave almost the

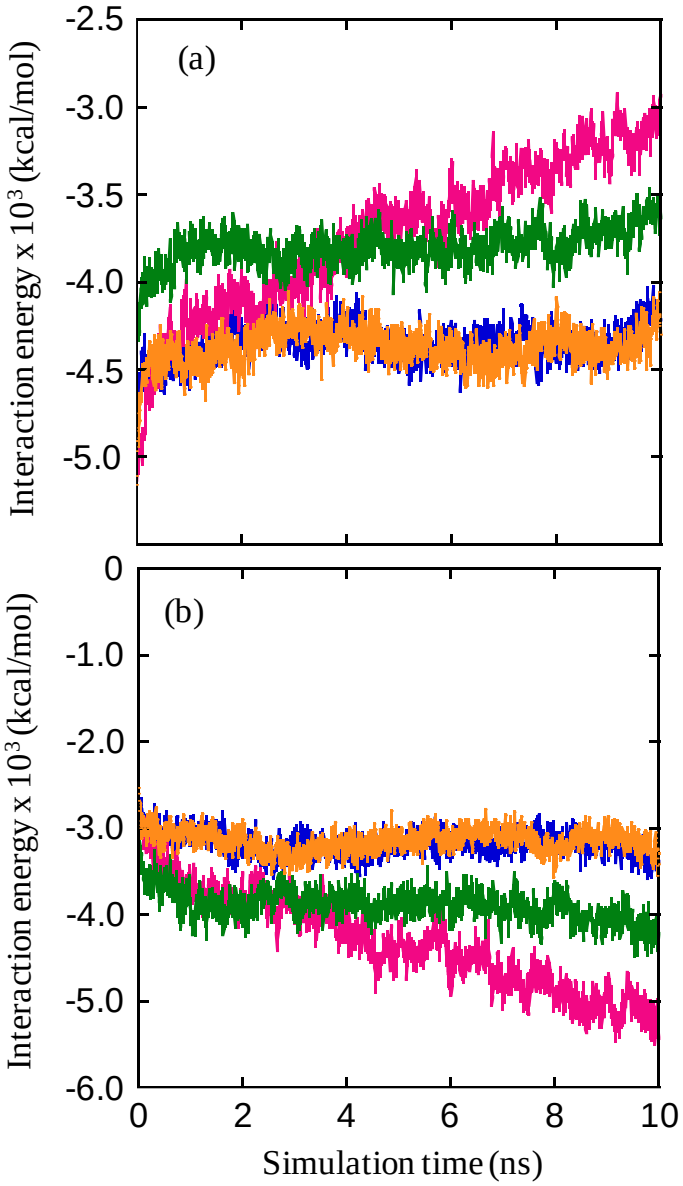

Fig. 6-3 Time courses of the interaction energy at 230 ˚C: (a) between cellulose chains, and (b) between cellulose and water molecules. Blue: cell I_{β}, pink: cell II, green: cell III_I, orange: cell IV_I

same under the HCW conditions which implies the occurrence of the transformation from cell IV_I to cell I in an early stage of the simulation.

On the other hand, Fig. 6-3 (a) and (b), respectively, showed the interaction energy between cellulose chains for cell II increases proportionally with the simulation time, and, the interaction energy between the cellulose and water molecules decreases with the simulation time. This indicates that the disordering of mini crystalline cell II and decomposition of chains progress proportionally according to the simulation time. In contrast, the interaction energies of cell III_I is observed to decrease until around 2 ns and then becoming constant until the end of the simulation time. This behavior is well explained by the snapshot obtained for cell III_I, Fig. 6-2(c), where two types of behaviors can be observed i.e., on the cellulose chains at the surface and also at the core regions.

The core part of the cell III_I should be considered to be transformed to the crystalline structure of cell I (the details will be discussed in the following section). The transformation of the crystalline structure of cell III_I to cell I have been reported experimentally and theoretically by some researchers (Wada 2001; Yui and Hayashi 2007; 2009; Yui 2012).

In our experimental report, we observed that the X-ray peak at $2\theta \approx 11.7^{o}$ from cell III_I totally disappeared after the HCW treatments at 230-270 ˚C/10 MPa/15 min and instead, the peaks of cell I appeared at $2\theta \approx 14.4$, 16.3 and 22.5 ˚ (Abdullah et al. 2013). Our simulation results could explain the experimental results from the atomistic scale point of view that the conversion from cell III_I to cell I occurs at the core part of the mini crystalline structure. From the observation of the MD simulation, the general behavior of these four crystalline structures can be summarized in the order of stability under high temperature and pressure conditions: cell II < cell III_I < cell $IV_I \approx$ cell I_β. The decomposition processes of these crystalline structures are discussed in the next sections.

6.3.2 Decomposition processes of celluloses I_β and IV_I

As stated in the previous section, the behavior of cell IV_I is very similar to that of cell I_β. This similarity is probably due to the transformation of the crystalline structure from cell IV_I to cell I_β at an early stage of the simulation. This is confirmed

by the analyses of the hydrogen bonding networks and the side chain conformation of cellulose as describe below.

It is known that the major intra-molecular hydrogen bonds of cell I_β exist at O3–H…O5 and O6–H…O2 (Nishiyama et al. 2002), and the minor hydrogen bonds exits at O2-H…O6 and O6-H…O4 (Nishiyama et al. 2002). As the hydrogen should exchange its position between donor and acceptor atoms during the dynamics run in the hydrogen bond formation because of the thermal fluctuation, the occupancy ratios of the hydrogen bonds between the donor and acceptor atoms are calculated and shown in Table 6-1. As an example, the occupancy ratio of the O3…O5 shows the addition of the results separately calculated on the O3-H…O5 and O3…H-O5. The occupancy ratio of the intra-molecular hydrogen bonds of O3…O5 is 0.62. The occupancy ratio for O6…O2 is also shown in the same table as 0.28. On the other hand, those in cell IV_I are found to be 0.62 and 0.30.

Table 6-1 The occupancy ratio of the hydrogen bond of cell I_β and cell IV_I during the MD simulation. Only hydrogen bonds with an occurrence above 0.09 are shown.

Cellulose	Intra-molecular hydrogen bonds		Inter-molecular hydrogen bond	
	O3…O5	O6…O2	O6…O3	O6…O2
Cell I_β	0.62	0.28	0.09	0.62
Cell IV_I	0.62	0.30	0.09	0.63

The criteria used for the hydrogen bonds are A-H distance is less than 2.8 Å and the D-H-A angle is greater than 110˚, where A and D represent acceptor and donor atoms, respectively.

It can be seen that the occupancy ratios of the intra-molecular hydrogen bonds of cell IV_I are very similar to those of cell I_β. This indicates the occurrence on the

transition of crystalline cell IV_I to cell I_β during the simulation under high pressure and temperature conditions in the earlier stage of the simulation.

Nishiyama et al. (2002) reported that the inter-molecular hydrogen bonds of cell I_β exist between O6–H…O3 of the 'origin' (the notations are shown in the paper) chains and between O6–H…O3, O6–H…O2, and O2–H…O6 of the 'center' chains. However, the analysis shows that the inter-molecular hydrogen bonds between O6…O3 are almost disappeared in our simulation as listed in table 6-1.

On the other hand, inter-molecular hydrogen bonds of O6…O2 remains. The same analysis was performed to the mini crystalline structure of cell IV_I and the results are shown in the same table. The behavior of cell IV_I is almost similar to the case of cell I_β, which again indicates the occurrence of the transition from crystalline structure of cell IV_I to cell I_β. There are various studies on the hydrogen bonding systems at high temperature conditions by MD simulation. Those studies mentioned that the O6…O2 inter-molecular hydrogen bond appeared during the simulations of cell IV_I (Bergenstråhle et al. 2007; Zhang et al. 2011; Agarwal *et al*. 2011), which we observed the same behavior.

The torsion angle distributions of the hydroxymethyl side group (O5–C5–C6–O6) are analyzed for two mini crystalline structures of cell I_β and cell IV_I. It has three low-energy conformations of *gg*, *gt* and *tg*. The ratios of these conformers are calculated to be 0.35, 0.26 and 0.39 for the both cases of cell I_β and cell IV_I, respectively. This result agrees well with the results obtained by other researchers (Bergenstråhle et al. 2007; Zhang et al. 2011; Matthews et al. 2011). As a summary, all these results indicate that the structure of cell IV_I is transformed into cell I_β in an earlier stage of the simulation.

6.3.3 Decomposition process of cellulose II

Previously, we observed that the mini crystalline structures of cell II and cell III_I decomposed more easily than those of cell I_β and cell IV_I. In this section, the decomposition process of cell II is discussed in more detail. Figure 6-4 shows some snapshots of the decomposition behavior of cell II during the 10 ns simulation. Here,

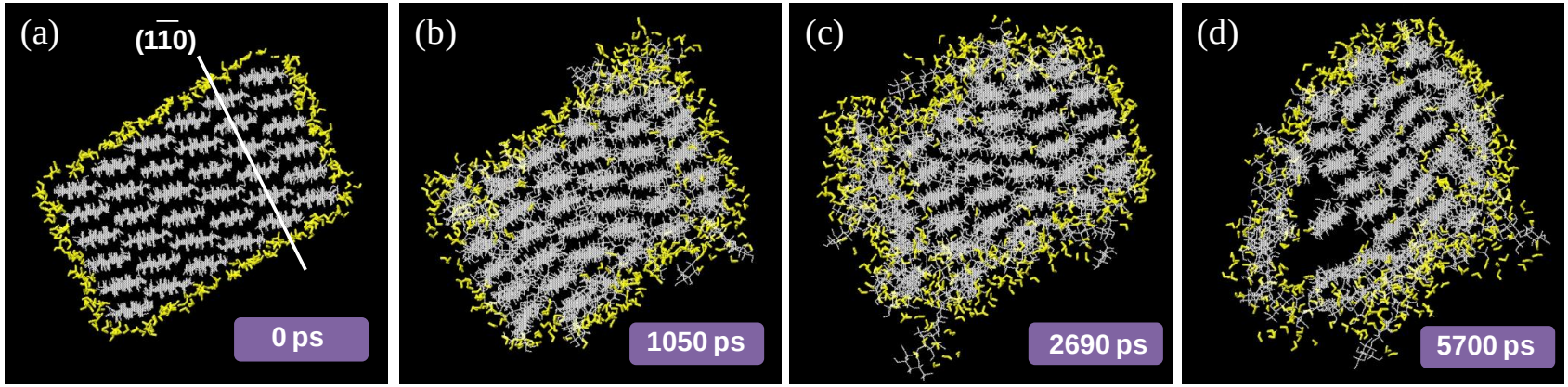

Fig. 6-4 The snapshots of decomposition process of cell II during the MD simulation. The water molecules (yellow) were shown only when they were placed within 3.0 Å from cellulose molecules

the water molecules are shown only when they are located within 3.0 Å from the cellulose chains. It can be observed that the water molecules began to enter the inside of crystalline cell II according to the progress of the simulation time. After 1 ns dynamics run, the cellulose chains located at the edge of the mini crystalline structures are found to be surrounded by the water molecules. Then, these chains decomposed into the water environment as shown in Fig. 6-4 (c).

Another interesting feature is that some waters are entering the crystalline structure not only to surround the chains at the edge region but also to enter between the chains along to the $(1\bar{1}0)$ crystalline plane. Even after 1 ns simulation, some water molecules can be observed at the inter-space between the chains along to the $(1\ \bar{1}0)$ crystalline plane as shown in Fig.6-4 (b).

It is well known that the cellulose molecules have intrinsically structural anisotropy (Yamane et al. 2006). i.e., the equatorial direction of the glucopyranose ring is hydrophilic due to the three hydroxyl groups on the glucopyranose ring. In contrast, the axial direction of the ring is hydrophobic because of the CH groups that are located on the axial positions of the ring. Because of this hydrophobic properties of the glucopyranose plane, the cellulose chains along to the $(1\bar{1}0)$ direction can stack with each other by hydrophobic interactions and forms a sheet like structure.

As a result, the surface of this sheet structure should be surrounded by the hydroxyl groups with high density, which makes the surface of this sheet hydrophilic. It is reasonable to say that the water molecules should enter the crystalline structure of cell II along the $(1\bar{1}0)$ surface because the water molecules can make hydrogen bond with the hydroxyl groups on the $(1\bar{1}0)$ surface. Figure 6-4 (c) shows that the whole sheet like structure along to the $(1\bar{1}0)$ surface is completely surrounded by the water molecules. Then the whole sheet like structure is observed to be dissociated into the water.

To investigate the breakage of the hydrogen bonds between the chains in the mini crystalline structure of cell II, the time courses of the occupancy ratio of the inter-molecular hydrogen bonds in the cell II were analyzed and the results are

shown in Fig. 6-5. Langan *et al*. (1999) investigated the inter-molecular hydrogen bonds in the crystalline structure of cell II and reported the patterns of them as follows: O6-H…O2 for center–center chains, O2-H…O6 for origin–origin chains, and O6…O3, O2-H…O2 and O6-H…O6 for origin–center chains. Note that, all these inter-molecular hydrogen bonds of cell II are formed between the cellulose chains are along to the $(1\bar{1}0)$ crystalline plane.

Among the above hydrogen bonds, we analyzed the inter-molecular hydrogen bonds that were formed between O2…O2, O6…O6 and O6…O2, and the results are shown in Fig. 6-5. The criteria of the hydrogen bonds are the A–H distance is less than 2.8 Å and the D–H–A angle is greater than 110°, where A and D are acceptor and donor atoms, respectively. Occupancy ratio is the percentage of the formation of hydrogen bond in whole. It can be seen that the occupancy ratio of these hydrogen bonds monotonically decreases with the progress of the simulation time. These results suggest that water molecules gradually enter the crystalline structure along the $(1\bar{1}0)$ plane by breaking the inter-molecular hydrogen bonds between cellulose chains and instead forming the hydrogen bonds between water and cellulose chains. Hayashi et al. (1974) and Hermans (1949) experimentally identified the existence of the molecular sheet structures in regenerated cellulose although they called this structure as plane lattice structures and sheet-like structures, respectively.

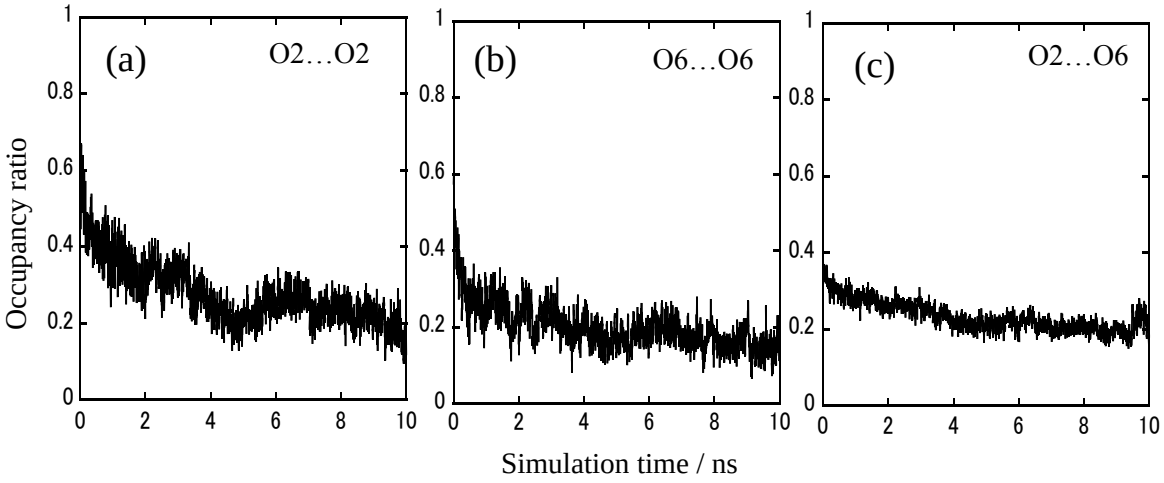

Fig. 6-5 Time courses of the occupancy ratio of the inter-molecular hydrogen bonds in the cell II: (a) O2…O2, (b) O6…O6 and (c) O2…O6

We previously proposed a structural formation for regenerated cellulose from a cellulose/aqueous system using MD simulations (Miyamoto et al. 2009). From the study, a mechanism of the initial step of the formation of crystalline structure from the solution was proposed: (i) glucopyranose rings are first stacked with each other by a hydrophobic interaction and form molecular sheets; (ii) the randomly dispersed sheet like structures in solution associate by hydrogen bonds with each other to form three-dimensional structures.

In the case of the structural decomposition mechanism like hydrolysis, the process might take place with a reverse way of the structural formation mechanism as follows: (i) water molecules enter the cell II crystalline structures along the $(1\bar{1}0)$ surface, and then the inter-molecular hydrogen bonds between the cellulose sheets are broken and substituted by the hydrogen bond with water molecules; (ii) molecular sheets formed by hydrophobic interactions are dissociated from the remaining mini crystalline structure (see Fig. 6-4 (d)); (iii) the molecular sheets are dispersed into individual chains, and then each chain is hydrolyzed. These processes are clearly observed in Fig. 6-4, except the hydrolysis process which cannot be observed in the MD simulation.

6.3.4 Decomposition process of cellulose III_I

Figure 6-6 shows some snapshots of the decomposition process of mini crystalline structure of cell III_I during the MD simulation. Water molecules are again shown when they locate within 3.0 Å from the cellulose molecules. It is observed that the water molecules enter in between the cellulose chains at an early stage of the simulation and the disruption of the crystalline arrangement of the chains occurs at the surface area of the mini crystalline structure. However, it is also observed that the core part of the crystalline structure still keep its ordered structure even after the 5 ns simulations run (Fig. 6-6(d)). To investigate the structure change at the core part of cell III_I during the simulation, the time dependence of the inter-molecular hydrogen bonds, which is formed between the chains in the cell III_I, were analyzed.

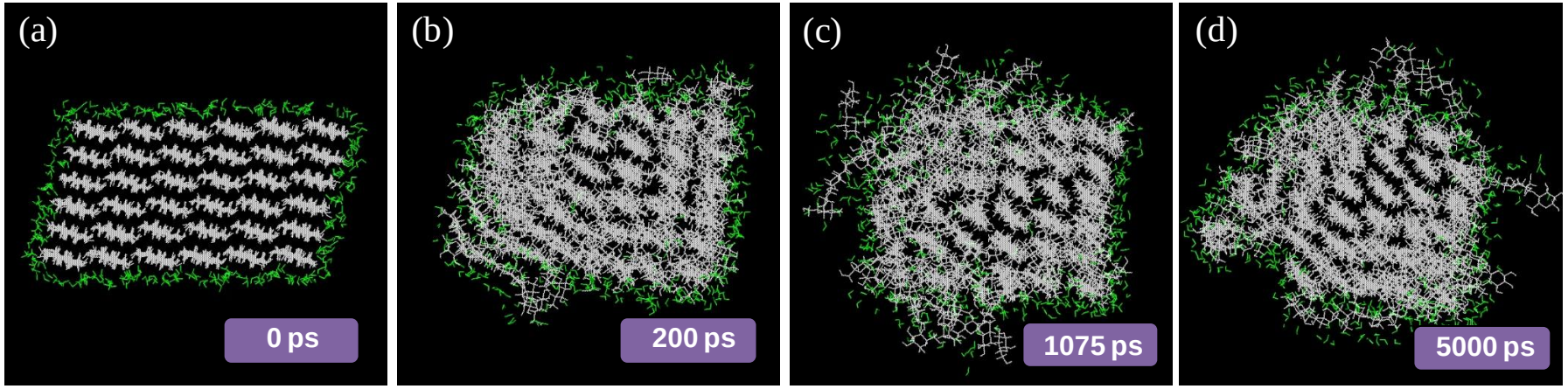

Fig.6-6 Snapshots of decomposition process of cell III_I during the MD simulation. The water molecules (green) were shown only when they were placed within 3.0 Å from cellulose molecule.

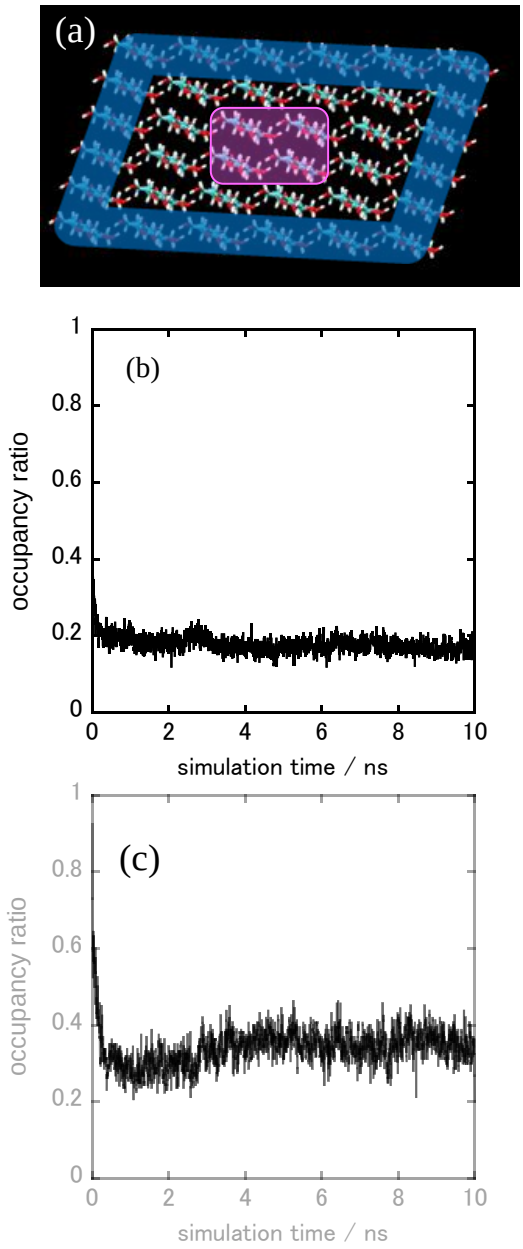

Fig. 6-7 Time dependence of the occupancy ratio of the inter-molecular hydrogen bonds O6…O2 in cell III_I performed at two separate regions; the surface area (blue) and the core area (pink), as in (a). The time courses of the occupancy ratio of these inter-molecular hydrogen bonds are shown in (b) and (c), respectively.

Wada et al. (2004b) investigated the crystalline structure of cell III_I by using X-ray diffraction experiment and reported that the inter-molecular hydrogen bonds exist between O2-H…O6 and O6-H…O2 in the crystalline structure. According to their results, the formation of the inter-molecular hydrogen bonds in the mini crystalline structure was investigated. The analyses were separately performed in two regions, one is the surface area (blue) and the other is the core area (pink), as are shown in Fig.6-7(a). Its time courses of the occupancy ratio of the inter-molecular hydrogen bonds are shown in Fig.6-7(b) and (c), respectively.

It is seen that the inter-molecular hydrogen bonds at the surface area of cell III_I decreases rapidly at an early stage of the simulation. However, in the core part, the O2…O6 inter-molecular hydrogen bonds decreases but still keep about 40% of the formation. This result can well be explained when we assume the transformation of the crystalline structure from cell III_I to cell I as is discussed with Fig.6-8.

.

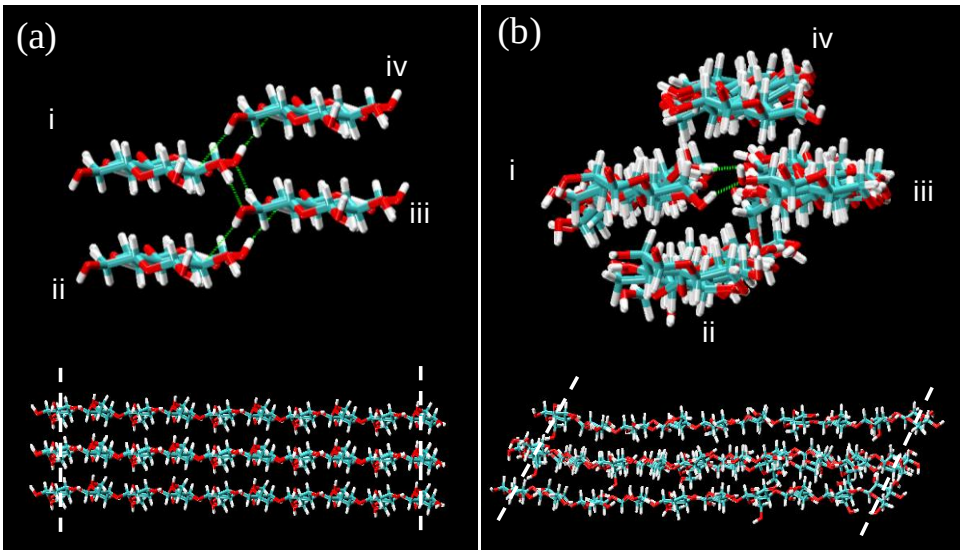

Fig. 6-8 The transition behaviors of four core chains in cell III_I mini crystalline structure located at the center in Fig. 6-7 (a) and coloured by pink, are shown for (a) initial and (b) after 2 ns simulation. Dotted green lines indicate the inter-molecular hydrogen bonds between O2…O6. Views along to the molecular axis before and after 2 ns simulation are shown in the lower part of the figures. *C*-axis is staggered by ± c/4 along to the *c*-axis after 2 ns

Figure 6-8 shows four chains in the core region of cell III_I model before and after 2 ns dynamics run. At the beginning of the simulation, inter-molecular hydrogen bonds of O2…O6 formed between chains i and iii, and between ii and iv, respectively. These two hydrogen bonds indicate the typical characteristic feature of the cell III_I crystalline structure

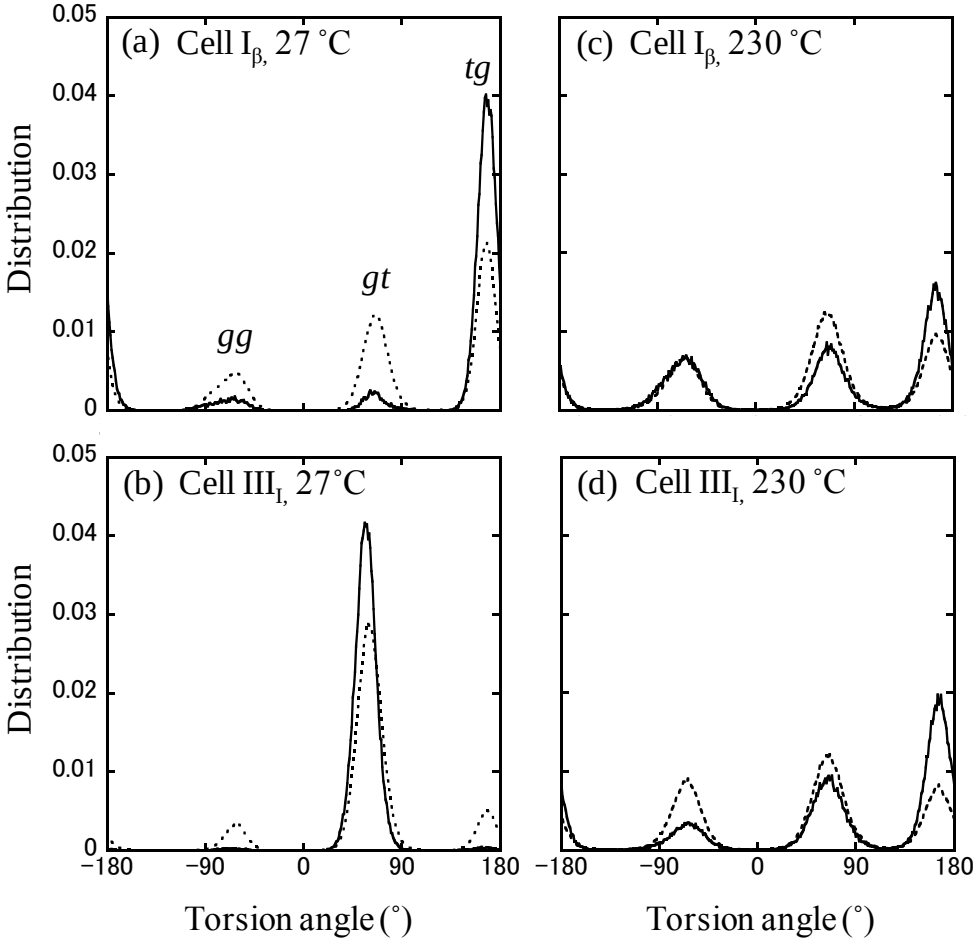

Fig. 6-9 Distribution of the torsion angle of O5–C5–C6–O6. Solid lines analyzed for four core chains (pink in Fig. 6-7 (a)) and the dotted lines analyzed for twenty outer chains (blue in Fig.6-7 (a)). (a) cell I_β at 27 ˚C/0.1 MPa, (b) cell III_I at 27 ˚C/0.1 MPa, (c) cell I_β at 230 ˚C/10 MPa and (d) cell III_I at 230 ˚C/10 MPa, respectively

On the other hand, the arrangements of these four chains changes after the 2 ns simulation. The inter-molecular hydrogen bonds can be observed between chain i and iii, where a hydrogen bond formed between O2…O6. However, the hydrogen bond between the chain i and iv disappeared after the transition. This transition

should reduce the number of the hydrogen bond to the half of cell III_I as was observed in Fig. 6-7.

The arrangement of the chains and the hydrogen bond pattern in Fig. 6-8(b) shows the characteristic feature of the crystalline structure of cell I. These results indicate the occurrence of the transformation of the crystalline structure to cell I at the core part of the cell III_I under high temperature and pressure conditions.

Another characteristic feature of the transformation from cell III_I to cell I can be seen in the arrangement of the chains. The observed arrangements of the crystal along to the fiber axis are shown at the bottom of each Fig. 6-8(a) and (b), respectively. The slide of chain arrangement along to the *c*-axis by c/4 can be observed after 2 ns simulation, which is another characteristic feature of cell I crystal.

The similarity between cell I and core part of cell III_I after 2 ns simulation is also found in the conformation of the torsion angle at 6 position of glucopyranose ring. Figure 6-9(c) and (d) shows the torsion angle distribution of O5–C5–C6–O6 for cell I and cell III_I at 230 ˚C. As a comparison, MD simulations at 27 ˚C were also performed and the results of the torsion angle distribution are shown in the same Fig. 6-9(a) and (b), respectively.

In cell I_β, the well known *tg* conformation appeared at 27 ˚C. However, at 230 ˚C, the proportion of *tg* conformer decreased because of the thermal fluctuation of the side chain even in the cell I_β structure (Fig. 6-9 (a) and (c)). In contrast, the torsion angle distribution of cell III_I had almost no *tg* conformation at 27˚C. However, *tg* conformation increases at high temperature, 230 ˚C. Moreover, torsion angle distribution of cell III_I at 230 ˚C is similar to that of cell I_β (Fig.6-9 (c) and (d)). This supports that the core chains of cell III_I were transformed into cell I.

It is concluded that the process of the decomposition mechanism of cell III_I crystalline structure is as follows: under high temperature and pressure, cell III_I transforms to cell I. During the transition process, half number of the inter-molecular hydrogen bonds is broken and therefore, the cellulose chains at the surface of the crystal should make hydrogen bonds with water molecules, instead. The surface chains which are fully solvated by hydrogen bonds with surrounding waters are then decomposed into the water region. On the other hand, the cellulose chains at the core

part of the crystalline structure should resist the decomposition because the structure is transformed to the cell I structure.

6.4 Concluding Remarks

The decomposition behaviors of the cell I_β, cell II, cell III_I and cell IV_I under the HCW condition were investigated using MD simulation. Since MD simulation is not able to calculate the hydrolysis, especially a bond cleavage reaction, the decomposition of the chains from the crystalline structure is regarded as an indication for an early stage of hydrolysis in this work. The order of the stability of four crystalline structures under high temperature and pressure was observed in the order of cell II < cell III_I < cell $IV_I \approx$ cell I_β.

Their decomposition mechanisms were discussed from the analysis of the simulation. The decomposition behavior of cell I_β is very similar to that of cell IV_I. This similarity is probably due to the transformation of the crystalline structure from cell IV_I to cell I_β in an early stage of the simulation. Cell I_β and cell IV_I are difficult to hydrolyze due to extremely tight networks of hydrogen bonds. As a result, only the decomposition of a few molecular chains from the surface of the mini crystalline structure was observed. This simulation results are in good agreement with our experimental data reported previously (Abdullah et al. 2013).

The process of the structural decomposition mechanism such as hydrolysis for cell II is proposed as follows: (i) water molecules enter the crystalline cell II along the $(1\bar{1}0)$ surface, and then the inter-molecular hydrogen bonds are broken; (ii) molecular sheets formed by hydrophobic interactions are decomposed from the mini crystalline structure; (iii) the molecular sheets are separated into various chains, and then each chain is dissociated.

Whereas, the mechanism for cell III_I is proposed as follows: (i) cell III_I starts to transform into cell I under high temperature and pressure; (ii) when the structure are transformed, half of the inter-molecular hydrogen bonds are broken, and the chains at the surface area should make hydrogen bonds with water molecules; (iii) the surface chains are then decomposed in the water but the core chains transform into cell I which resist to the decomposition by the water molecules.

It has been shown that all the mechanisms above can well explain the observed phenomena found in the experiments. It is hoped that these findings will be able to assist further development of the new methods in the dissolution and the decomposition of the cellulosic materials.

CHAPTER 7

Concluding Remarks

7.1 Conclusions

The knowledge on lignocellulosic decomposition in various decomposition systems is very useful for better and efficient exploitation of wood cellulose. One of the common current issues is that almost all ethanol from renewable carbon is obtained from food-based sources. Therefore, such information as above would certainly affect and possibly reduce the topic of food versus fuel, plus increasing cellulose utilization in biorefinery. Though a lot of conventional methods have been proven to utilize lignocelluloses for biofuel and biorefinery; more efficient processes, techniques as well as products are still in need.

In this dissertation, wood celluloses from cotton linter in various crystalline forms, as the feedstocks, have been used for hydrothermal treatment by means of a semi-flow hot-compressed water (HCW) system. This treatment has proven to be effective in providing hydrolyzed and degraded products as separate product streams. The physical and hydrothermal conversions of these celluloses treated in HCW conditions have been discussed in Chapters 2 and 4.

In the HCW treatment condition, at 230˚C/10MPa/15min, the paracrystalline part of cellulose, whose crystalline structure is somewhat disordered, is readily decomposed. Furthermore, 270˚C/10MPa/15min is still an optimum condition for the decomposition of cellulose into glucose and various other cello-oligosaccharides products. In addition, minimal amounts of degraded products consisted of dehydrated, fragmented compounds as well as organic acids were also recovered.

The crystallinity is still one of the limiting factors for hydrolysis of cellulose. It remained unaffected even at a severe treatment condition of 270˚C/10MPa/15min. The degree of polymerization (DP) is a good parameter to be observed for direct comparison between various crystalline celluloses. Here, the DP decreased with treatment temperatures. The crystalline celluloses, which are grouped into group I (cell I, cell III_I, cell IV_I) and group II (cell II, cell III_{II}, cell IV_{II}), showed similar

behaviors according to their groups. Group I has higher resistance to be decomposed than group II and the decomposition behaviors were dependent on the different crystalline forms of the starting celluloses. The decomposition behaviors of these celluloses were found to follow the native cellulose decomposition pathway under HCW condition, as reported in literature.

The HCW treatment was also compared with the low temperature/pressure enzymatic treatment. The modification on the crystalline cell I into other crystalline structures has someway assisted the enzyme to perform better during hydrolysis reaction. Among all celluloses, it is shown that enzymatic hydrolysis treatment is better with cell III_I, and equivalent to group II celluloses, than cell I. Here, the crystallinity was observed to reduce. This is believed to occur due to the enzyme. The observation on the DP was similar as in that of HCW treatment. From the results presented in *Chapter* 3, it can be said that, the prepared various crystalline celluloses have assisted the hydrolysis and decomposition process in enzymatic treatments.

In Chapter 5, further investigation was done to observe the physical behaviors of cell III at lower pressures in HCW environment. During the HCW treatment at a temperature range between 20-270 ˚C under 4-10 MPa for 5-15 min, it was found that cell III_I and cell III_{II} were reconverted into their respective parent celluloses. The transformation is observed to be slower at lower temperature and pressures. For that reason, the physical behaviors of the polymorphs in HCW are dependent on pressure and temperature within the limit of HCW condition.

The work for this dissertation would not be complete without understanding the interaction process between the water molecules and the celluloses during the HCW treatment. Hence, in *Chapter* 6, a detail investigation by using MD simulation was performed in order to understand the decomposition behaviors of the crystalline cellulose structures of cell I_β, cell II, cell III_I and cell IV_I under the HCW condition. Since MD simulation is not able to calculate hydrolysis, especially a bond cleavage reaction, the decomposition of the chains from the crystal is then defined as an indication for an early stage of hydrolysis.

Their decomposition mechanisms were discussed from the analysis of the simulation. It was found that the decomposition behavior of cell I_β is very similar to cell IV_I, which probably due to the conversion of cell IV_I to cell I_β in an early stage

of the simulation. Both celluloses are more difficult to hydrolyze than cell II and cell III_I because of the extremely tight networks of hydrogen bonds. As a result, only the decomposition of few molecular chains from surface of the mini crystal was observed, agreeable with the experimental data of HCW treatments in *Chapter* 2. From the MD simulation analysis, the process of the structural decomposition mechanism, such as hydrolysis, for cell II and cell III_I are proposed. All the mechanisms described above can well explain what have been observed experimentally.

The information discovered from this comprehensive study may lead to a better way to learn and assist further development of the newer methods in the liquefaction or decomposition of the cellulosic materials. Not only for bioethanol productions, the variety of products from celluloses can suggest a great prospect for their application in many purposes.

7.2 Prospects for Future Researches

This dissertation has successfully demonstrated that hydrothermal technology, such as non-catalytic HCW, can play important roles in decomposition of cellulosic materials by producing various bio-products. Though it features many similar trends with the established non-catalytic sub/supercritical methods of lignocelluloses, yet, it offers a new alternative process for bioethanol productions. The present research has opened up few avenues for continuing the development research works on biofuels or biorefineries. The following research topics may be further explored to acquire a more inclusive representation of this work: (1) Thorough kinetic studies on the decomposition of model compounds in both HCW and enzymatic treatments. This would be useful for reactor design. The enzymatic treatment may proceed better if potential additives are also included. (2) Developing a suitable catalyst to enhance and facilitate the decomposition process at a much lower temperature/pressure in HCW system, thus, higher hydrolysis reactions and lesser production of degraded products may be achieved. (3) Details investigation of cell IV by high temperature hydrothermal treatment.

References

Abdullah R, Ueda K, Saka S (2013) Decomposition behaviors of various crystalline celluloses as treated by semi-flow hot-compressed water. Cellulose 20:2321-2333

Abdullah R, Ueda K, Saka S (2014) Hydrothermal decomposition various crystalline celluloses as treated by semi-flow hot-compressed water. J. Wood Sci. 60:278-286

Aden A, Ruth M, Ibsen K, Jechura J, Neeves K, Sheehan J, Wallace B, Montague L, Slayton A, Lukas J (2002) Lignocellulosic biomass to ethanol process design and economics utilizing co-current dilute acid prehydrolysis and enzymatic hydrolysis for corn stover. Colorado, US, NREL/TP-510-32438

Adschiri T, Hirose S, Malaluan RM, Arai K (1993) Non-catalytic conversion of cellulose in supercritical and subcritical water. J. Chem. Eng. Jpn. 26:676-680

Agarwal V, Huber GW, Curtis Conner W Jr, Auerbach SM (2011) Simulating infrared spectra and hydrogen bonding in cellulose I_β at elevated temperatures. J Chem. Phys. 135:134506-1–134506-13

Aida TM, Sato Y, Watanabe M, Tajima K, Nonaka T, Hattori H, Arai K (2007) Dehydration of D-glucose in high temperature water at pressures up to 80 MPa. J. Supercrit. Fluids 40:381-388

Ando H, Sakaki T, Kokusho T, Shibata M, Uemura Y, Hatate Y (2000) Decomposition behavior of plant biomass in hot-compressed water. Ind. Eng. Chem. Res. 39:3688-3693

Antal MJ, Mok WSL (1990a) Four-carbon model compounds for the reactions of sugars in water at high temperature. Carbohydr. Res. 199:111-115

Antal MJ, Mok WSL (1990b) Mechanism of formation of 5-(hydroxymethyl)-2-furaldehyde from D-fructose and sucrose. Carbohydr. Res. 199:91-109

Ashby MF, Gibson LJ, Wegst U, Olive R (1995) The mechanical properties of natural materials. I. Material property charts. Proceedings: Mathematical and Physical Sciences 450:123-140

Atalla RH, VanderHart DL (1984) Native cellulose: a composite of two distinct crystalline forms. Science 223:283-285

Beckham GT, Matthews JF, Peters B, Bomble YJ, Himmel ME, Crowley MF (2011) Molecular-level origins of biomass recalcitrance: Decrystallization free energies for four common cellulose polymorphs. J. Phys. Chem. B 115:4118-4127

Bellesia G, Asztalos A, Shen T, Langan P, Redondo A, Ganakaran S (2010) In silico studies of crystalline cellulose and its degradation by enzymes. Acta Cryst. D66:1184–1188

Berendsen HJC, Van der Spoel D, Van Drunen R (1995) GROMACS: A message-passing parallel molecular dynamics implementation. Comput. Phys. Commun. 91:43-56

Bergenstråhle M, Berglund LA, Mazeau K (2007) Thermal response in crystalline I_β cellulose: a molecular dynamics study. J. Phys. Chem. B. 111:9138-9145

Béguin P, Aubert JP (1994) The biological degradation of cellulose. FEMS Microbial. Rev. 13:25-58

Bisaria VS (1991) Bioprocessing of agro-residues to glucose and chemicals. In: Martin AM (ed) Bioconversion of waste materials to industrial products, Elsevier, London, p210-213

Bjeree AB, Olesen AB, Fernqvist T (1996) Pretreatment of wheat straw using combined wet oxidation and alkaline hydrolysis resulting in convertible cellulose and hemicellulose. Biotechnol. Bioeng. 49:568-577

Bobleter O, Niesner R, Rohr M (1976) The hydrothermal degradation of cellulosic matter to sugars and their fermentative conversion to protein. J. Appl. Polym. Sci. 20:2083-2093

Bobleter O, Bonn G, Concin R (1983) Hydrothermalysis of biomass-production of raw material for alcohol fermentation and other motor fuels. Alternative En. Sourc. 3:323-332

Bommarius A, Katona A, Cheben SE, Patel AS, Ragauskas AJ, Knudson K, Pu Y (2008) Cellulase kinetics as a function of cellulose pretreatment. Metab. Eng. 10:370-381

Bracmort K (2013) Algae's potential as transportation biofuel. Washington DC, US, CRS/R42122

Camacho F, González-Tello P, Jurado E, Robles A (1996) Microcrystalline cellulose hydrolysis with concentrated sulphuric acid. J. Chem. Tech. Biotechol. 67:350-356

Cao Y, Tan H (2002) Effects of cellulase on the modification of cellulose. Carbohydr. Res. 337:1291-1296

Cao Y, Tan H (2005) Study on crystal structures of enzyme-hydrolyzed cellulosic materials by X-ray diffraction. Enzyme Microb. Technol. 36:314-317

Cetinkol OP, Dibble DC, Cheng G, Kent MS, Knierim B, Auer M, Wemmer DE, Pelton JG, Melnichenko YB, Ralph J, Simmons BA, Holmes BM (2010) Understanding the impact of ionic liquid pretreatment on eucalyptus. Biofuels 1:33-36

Chanzy H, Imada K, Mollard A, Vuong R, Barnoud F (1979) Crystallographic aspects of sub-elementary cellulose fibrils occurring in the wall of rose cells cultured in vitro. Protoplasma 100:303-316

Chanzy H, Henrissat B, Noe P, Roche E, Smith P (1983) Subfibrillation of *Valonia* cellulose microfibrils. Tappi Proceedings Int. Dissolving and Speciality Pulps Tappi Press, Atlanta, p203-206

Chidambareswaran PK, Sreenivasan S, Patil NB (1982) Further studies on cellulose III polymorphs. Transformations to cellulose IV lattices and subsequent reactions. J. Appl. Polym. Sci. 27:709-730

Classen PAM, Sijtsma L, Stams AJM, De Vries SS, Weusthuis RA (1999) Utilization of biomass for the supply of energy carriers. Appl. Microbiol. Biotechnol. 52:741-755

Da Silva Perez D, Montanari S, Vignon MR (2003) TEMPO-mediated oxidation of cellulose III. Biomacromolecules 4:1417-1425

Dadi AP, Varanasi S, Schall CA (2006) Enhancement of cellulose saccharification kinetics using an ionic liquid pretreatment step. Biotechnol. Bioeng. 95:904-910

Darden T, York D, Pedersen L (1993) Particle mesh Ewald: An $N \cdot \log(N)$ method for Ewald sums in large systems. J. Chem. Phys. 98:10089-10092

Debzi EM, Chanzy H, Sugiyama J, Tekely P, Excoffier G (1991) The $I_\alpha \rightarrow I_\beta$ transformation of highly crystalline cellulose by annealing in various media. Macromolecules 24:6816-6822

Deguchi S, Tsujii K, Horikoshi K (2008) Crystalline-to-amorphous transformation of cellulose in hot and compressed water and its implications for hydrothermal conversion. Green Chem. 10:191-196

Dinjus E, Kruse A (2004) Hot-compressed water - a suitable and sustainable solvent and reaction medium? J. Phys.: Condens. Matter 16:S1161-S1169

Duff SJB, Murray WD (1996) Bioconversion of forest products industry waste cellulosics to fuel ethanol: a review. Bioresour. Technol. 55:1-33

Durell SR, Brooks BR, Ben-Naim A (1994) Solvent induced forces between two hydrophilic groups. J. Phys. Chem. 98:2198-2202

Ehara K, Saka S (2002) A comparative study on chemical conversion of cellulose between the batch-type and flow-type systems in supercritical water. Cellulose 9:301-311

Ehara K, Saka S, Kawamoto H (2002) Characterization of the lignin-derived products from wood as treated in supercritical water. J. Wood Sci. 48:320-325

Ehara K, Saka S (2005) Decomposition behavior of cellulose in supercritical water, subcritical water, and their combined treatments. J. Wood Sci. 51:148-153

Essmann U, Perera L, Berkowitz ML, Darden T, Lee H, Pedersen LG (1995) A smooth particle mesh Ewald potential. J. Chem. Phys. 103:8577-8592

Eriksson KE (1982) Degradation of cellulose. Experientia 38:156-159

Evans R, Wearne RH, Adrian FA (1989) Molecular weight distribution of cellulose as its tricarbanilate by high performance size exclusion chromatography. J. Appl. Polym. Sci. 37:3291-3303

Fan LT, Lee YH, Beardmore DH (1980) Mechanism of the enzymatic hydrolysis of cellulose: effect of major structural features of cellulose on enzymatic hydrolysis. Biotechnol. Bioeng. 23:177-199

Fan LT, Gharpuray MM, Lee YH (1987) Cellulose hydrolysis biotechnology monographs. Springer, Berlin, p57-59

Favier V, Chanzy H, Cavaille JY (1995) Polymer nanocomposites reinforced by cellulose whiskers. Macromolecules 28:6365-6367

Fávaro1 SL, Ganzerli TA, de Carvalho Neto AGV, Da Silva ORRF, Radovanovic E (2010) Chemical, morphological and mechanical analysis of sisal fiber-reinforced recycled high-density polyethylene composites. Express Polym. Lett. 4:465–473

Fischer G, Schrattenholzer L (2001) Global bioenergy potentials through 2050. Biomass Bioenerg. 20:151-159

Franck EU (1987) Fluids at high pressures and temperatures. Pure Appl. Chem. 59:25-34

French AD, Miller DP, Aabloo A (1993) Miniature crystal models of cellulose polymorphs and other carbohydrates. Int. J. Biol. Macromol. 15:30-36

French AD (2014) Idealized powder diffraction patterns for cellulose polymorphs. Cellulose 21:885-896

Fujita M, Harada H (2001) Ultrastructure and formation of wood cell wall. In: Hon DN-S, Shiraishi N (eds) Wood and Cellulosic Chemistry. 2nd ed., New York, Marcel Dekker, p1-5

Gardiner ES, Sarko A (1985) Packing analysis of carbohydrates and polysaccharides. 16. The crystal structures of cellulose IV_I and IV_{II}. Can. J. Chem. 63:173-180

Gardner KH, Blackwell J (1974) The structure of native cellulose. Biopolym. 13:1975-2001

Gray KA, Zhao L, Emptage M (2006) Bioethanol. Cur. Opin. Chem. Biol. 10:141-146

Guvench O, Greene SN, Kamath G, Brady JW, Venable RM, Pastor RW, Mackerell AD (2008) Additive empirical force field for hexopyranose monosaccharides. J. Comput. Chem. 29:2543-2564

Guvench O, Hatcher E, Venable RM, Pastor RW, Mackerell AD (2009) CHARMM additive all-atom force field for glycosidic linkages between hexopyranoses. J. Chem. Theory Comput. 5:2353-2370

Hall M, Bansal P, Lee JH, Realff MJ, Bommarius AS (2010) Cellulose crystallinity - a key predictor of the enzymatic hydrolysis rate. J. FEBS 277:1571-1582

Harris EE, Beglinger E (1946) Madison wood sugar process. Indus. Eng. Chem. 38:890-895

Hayashi J, Masuda S, Watanabe S (1974) Plane lattice structure in amorphous region of cellulose fibers. Nippon Kagaku Kaishi 5:948-954

Hayashi J, Sufoka A, Ohkita J, Watanabe S (1975) The confirmation of existences of celluloses III_I, III_{II}, IV_I and IV_{II} by the X-ray method. Polym. Lett. Ed. 13:23-27

Heinze T (1998) New ionic polymers by cellulose functionalization. Macromol. Chem. Phys. 199:2341-2364

Hermans PH (1949) Degree of lateral order in various rayons as deduced from X-ray measurements. J. Polym. Sci. 4:145-151

Hess B, Kutzner C, Van Der Spoel D, Lindahl E (2008) GROMACS 4: Algorithms for highly efficient, load-balanced, and scalable molecular simulation. J. Chem. Theory Comput. 4:435-447

Hockney RW (1970) The potential calculation and some applications. Methods Comput. Phys. 9:135-211

Hon DNS (1994). Cellulose: a random walk along its historical path. Cellulose 1:1-25

Hon DNS (1996) Functional polymers: a new dimensional creativity in lignocellulosic chemistry. In: Hon DNS (ed) Chemical modification of lignocellulosic materials. Dekker, New York, p1-10

Hoover WG (1985) Canonical dynamics: Equilibrium phase-space distributions. Phys. Rev. A 31:1695-1697

Horii F, Yamamoto H, Kitamaru R, Tanahashi M, Higuchi T (1987) Transformation of native cellulose crystals induced by saturated steam at high-temperatures. Macromolecules 20:2946-2949

Horii F (2000) Structure of cellulose: recent developments in its characterization. In: Hon DN-S, Shiraishi N (eds) Wood and Cellulosic Chemistry. 2nd edition, New York, Marcel Dekker, p83-91

Hosoya T, Nakao Y, Sato H, Kawamoto H, Sakaki S (2009) Thermal degradation of methyl β-D-glucoside. A theoretical study of plausible reaction mechanisms. J. Org. Chem. 74:6891-6894

Hsu TA (1996) Pretreatment of biomass. In: Wyman CE (ed) Handbook on bioethanol: production and utilization. Taylor and Francis, Bristol, p179-195

Humphrey W, Dalke A, Schulten K (1996) VMD: visual molecular dynamics. J. Mol. Graphics 14:33-38

Igarashi K, Wada M, Samejima M (2007) Activation of crystalline cellulose to cellulose III_I results in efficient hydrolysis by cellobiohydrolase. FEBS J. 274:1785-1792

IEA, International Energy Agency (2012). IEA on renewable: An expert view. J. International Energy Agency, Issue 2, p11-13

IEA, International Energy Agency (2013). Retrieved June 2014: [http://www.iea.org/aboutus/faqs/renewableenergy/]

Isogai A, Usuda M, Kato T, Uryu T, Atalla RH (1989) Solid-state CP/MAS ^{13}C NMR study of cellulose polymorphs. Macromolecules 22:3168-3172

Isogai A (1994) Allomorphs of cellulose and other polysaccharides. In: Gilbert RD (ed) Cellulosic Polymers. Munich, Hanser, p1-24

Isogai A, Atalla RH (1998) Dissolution of cellulose in aqueous NaOH solutions. Cellulose 5:309-319

Ito T, Hirata Y, Sawa F, Shirakawa N (2002) Hydrogen bond and crystal deformation of cellulose in sub/super-critical water. Jpn. J. Appl. Phys., Part 141:5809-5814

Jollet V, Chambon F, Rataboul F, Cabiac A, Pinel C, Guillon E, Essayem N (2009) Non-catalyzed and Pt/γ-Al_2O_3-catalyzed hydrothermal cellulose dissolution-conversion: influence of the reaction parameters and analysis of the unreacted cellulose. Green Chem. 11:2052-2060

Jones JL, Semrau KT (1984) Wood hydrolysis for ethanol production - previous experience and the economics of selected processes. Biomass 5:109-135

Jorgensen WL, Chandrasekhar J, Madura JD, Impey RW, Klein ML (1983) Comparison of simple potential functions for simulating liquid water. J. Chem. Phys. 79:926-935

Jörgensen L (1950) Swelling and heterogeneous hydrolysis of cotton linters and wood pulp fibers related to their fine structure. Acta Chem. Scand. 4:185-199

Kabyemela BM, Adschiri T, Malaluan RM, Arai K (1999) Glucose and fructose decomposition in subcritical and supercritical water: detailed reaction pathway, mechanisms and kinetics. Ind. Eng. Chem. Res. 8:2888-2895

Kadam KL, Rydholm EC, McMillan JD (2004) Development and validation of a kinetic model for enzymatic saccharification of lignocellulosic. Biotechnol. Progr. 20:698-705

Kalinichev AG, Churakov SV (1999) Size and topology of molecular clusters in supercritical water: a molecular dynamics simulation. Chem. Phys. Letters, 302:411-417 ISSN 2091-2730

Kalita BB, Gogoi N, Kalita S (2013) Properties of ramie and its blends. Int. J. Eng. Res. Gen. Sci. 1:1-6

Kallury RKMR, Ambidge C, Tidwell TT, Boocock DGB, Anglevor FA, Steward DJ (1986) Rapid hydrothermolysis of cellulose and related carbohydrate. Carbohydr. Res. 158:253-261

Kamio E, Takahashi S, Noda H, Fukuhara C, Okamura T (2006) Liquefaction of cellulose in hot-compressed water under variable temperatures. Ind. Eng. Chem. Res. 45:4944-4953

Karr WE, Holzapple MT (2000) Using lime pretreatment to facilitate the enzymatic hydrolysis of corn stover. Biomass Bioenerg. 18:189-199

Kheshgi HS, Prince RC, Marland G (2000) The potential of biomass fuels in the context of global climate change: Focus in transportation fuels. Annu. Rev. Energy Environ. 25:199-244

Klemm D, Heublein B, Fink HP, Bohn A (2005) Cellulose: fascinating biopolymer and sustainable raw material. Angew. Chem. Int. Ed. 44:3358-3393

Kokot S, Czarnik-Matusewicz B, Ozaki Y (2002) Two-dimensional correlation spectroscopy and principal component analysis studies of temperature-dependent IR spectra of cotton-cellulose. Biopolymers (Biospectroscopy), 67:456-469

Kolpak FJ, Weih M, Blackwell J (1978) Mercerization of cellulose: 1. Determination of the structure of mercerized cotton. Polymer 19:123-131

Kroon-Batenburg LMJ, Bouma B, Kroon J (1996) Stability of cellulose structures studied by MD simulations. Could mercerized cellulose II be parallel? Macromolecules 29:5695-5699

Kruse A, Gawlik A(2003) Biomass conversion in water at 330-410 ˚C and 30-50 MPa. Identification of key compounds for indicating different chemical reaction pathways. Ind. Eng. Chem. Res. 42:267-279

Kruse A, Dinjus E (2007) Hot-compressed water as reaction medium and reactant. Properties and synthesis reactions. J. Supercrit. Fluids 39:362-380

Kulshreshtha AK (1979) A review of the literature on the formation of cellulose IV, its structure, and its significance in the technology of rayon manufacture. J. Textile Inst. 70:13-18

Kumar S, Gupta RB (2008) Hydrolysis of microcrystalline cellulose in subcritical and supercritical water in a continuous flow reactor. Ind. Eng. Chem. Res. 47:9321-9329

Kumar S, Gupta R, Lee YY, Gupta RB (2010) Cellulose pretreatment in subcritical water; effect of temperature on molecular structure and enzymatic reactivity. Biores. Technol. 101:1337-1347

Kusdiana D, Minami E, Ehara K, Saka S (2002) Development of the batch-type and flow-type supercritical fluid biomass conversion systems. In: Proceedings of the 12th European Conference and Technology Exhibition on Biomass for Energy, Industry and Climate Protection, Amsterdam, Germany, p789-792

Langan P, Nishiyama Y, Chanzy H (1999) A revised structure and hydrogen-bonding system in cellulose II from a neutron fiber diffraction analysis, J. Am. Chem. Soc. 121:9940-9946

Langan P, Nishiyama Y, Chanzy H (2001) X-ray structure of mercerized cellulose II at 1Å Resolution. Biomacromolecules 2:410-416

Lee SB, Kim IH, Ryu DDY, Taguchi H (1983) Structural properties of cellulose and cellulase reaction mechanism. Biotechnol. Bioeng. 25:33-51

Lee SH, Doherty TV, Linhardt RJ, Dordick JS (2009) Ionic liquid-mediated selective extraction of lignin from wood leading to enhanced enzymatic cellulose hydrolysis. Biotechnol. Bioeng. 102:1368-1376

Lindahl E, Hess B, Van Der Spoel D (2001) GROMACS 3.0: A package for molecular simulation and trajectory analysis. J. Mol. Model. 7:306-317

Liu C, Wyman CE (2003) The effect of flow rate of compressed-hot water on xylan, lignin, and total mass removal from corn stover. Indus. Eng. Chem. Res. 42:5409-5416

Liu C, Wyman CE (2005) Partial flow of compressed-hot water through corn stover to enhance hemicelluloses sugar recovery and enzymatic digestibility of cellulose. Bioresour. Technol. 96:1978-1985

Loeb L, Segal L (1955) Studies of the ethylenediamine-cellulose complex. I. Decomposition of the complex by solvents. J. Polym. Sci. 15:343-354

Lu X, Yamauchi K, Phaiboonsilpa N, Saka S (2009) Two-step hydrolysis of Japanese beech as treated by semi-flow hot-compressed water. J. Wood Sci. 55:367-375

Lynd LR, Cushman JH, Nichols RJ, Wyman CE (1991) Fuel ethanol from cellulosic biomass. Science 251:1318-1323

Marchessault RH, Liang CY (1960) Infrared spectra of crystalline polysaccharides. III. Mercerized cellulose. J. Polym. Sci. 43:71-84

Marcus Y (1999) On transport properties of hot liquid and supercritical water and their relationship to the hydrogen bonding. Fluid Phase Equilib. 164:131-142

Marshall WL, Franck EU (1981) Ion product of water substance, 0-1000 ˚C, 1-10000 bars new international formulation and its background. J. Phys. Chem. Ref. Data. 10:295-304

Marrinan HJ, Mann J (1956) Infrared spectra of crystalline modifications of cellulose. J. Polym. Sci. 21:301-311

Matsuoka S, Kawamoto H, Saka S (2011) Thermal glycosylation and degradation reactions occurring at the reducing ends of cellulose during low-temperature pyrolysis. Carbohydr. Res. 346:272–279

Matthews JF, Bergenstråhle M, Beckham GT, Himmel ME, Nimlos MR, Brady JW, Crowly MF (2011) High-temperature behavior of cellulose I. J. Phys. Chem. B. 115:2155-2166

Matthews JF, Himmel ME, Crowly MF (2012) Conversion of cellulose I_α to I_β via a high temperature intermediate (I-HT) and other cellulose phase transformations. Cellulose 19:297-306

McMillan JD (1994) Pretreatment of lignocellulosic biomass. In: Himmel ME, Baker JO, Overend RP (eds) Enzymatic conversion of biomass for fuels production. American Chemical Society, Washington DC, p292-324

Meyer KH, Misch L (1937) Positions des atomes dans le nouveau modéle spacial de la cellulose. Helv. Chim. Acta. 20:232-244

Minowa T, Zhen F, Ogi T, Va´rhegyi G, (1998) Decomposition of cellulose and glucose in hot-compressed water under catalyst-free conditions. J. Chem. Eng. Jpn. 31:131-134

Mittal A, Katahira R, Himmel ME, Johnson DK (2011) Effects of alkaline or liquid-ammonia treatment on crystalline cellulose: changes in crystalline structure and effects on enzymatic digestibility. Biotechnology for Biofuels 4:1-16

Miyafuji H, Miyata K, Saka S, Ueda F, Mori M (2009) Reaction behavior of wood in an ionic liquid, 1-ethyl-3-methylimidazolium chloride. J. Wood Sci. 55:215-219

Miyamoto H, Umemura M, Aoyagi T, Yamane C, Ueda K, Takahashi K (2009) Structural reorganization of molecular sheets derived from cellulose II by molecular dynamics simulations. Carbohydr. Res. 344:1085-1094

Mok WS, Antal MJ Jr (1992) Uncatalyzed solvolysis of whole biomass hemicelluloses by hot-compressed liquid water. Ind. Eng. Chem. Res. 31:1157-1161

Mok WSL, Antal MJ, Varhegyi G (1992) Productive and parasitic pathways in dilute acid-catalyzed hydrolysis of cellulose. Ind. Eng. Chem. Res. 31:94-100

Mormann W, Michel U (2002) Improved synthesis of cellulose carbamates without by-products. Carbohydr. Polym. 50:201-208

Nakashima K, Yamada L, Satou Y, Azuma J, Satoh N (2004) The evolutionary origin of animal cellulose synthase. Dev. Genes Evol. 214:81-88

Newman RH (2008) Simulation of X-ray diffractograms relevant to the purported polymorphs cellulose IV_I and IV_{II}. Cellulose 15:769–778

Nishiyama Y, Langan P, Chanzy H (2002) Crystal structure and hydrogen-bonding system in cellulose I_β from synchrotron X-ray and neutron fiber diffraction. J. Am. Chem. Soc. 124:9074-9082

Nishiyama Y, Sugiyama J, Chanzy H, Langan P (2003) Crystal structure and hydrogen-bonding system in cellulose I_α from synchrotron X-ray and neutron fiber diffraction. J. Am. Chem. Soc. 125:14300-14306

Nose S (1984) A molecular dynamics method for simulations in the canonical ensemble. Mol. Phys. 52:255-268

Oilgae (2010) Cellulosic ethanol from algae - facts and status. Retrieved August 2014 [http://www.oilgae.com/blog/2010/09/cellulosic-ethanol-from-algae-%E2%80%93-facts-and-status.html]

Olanrewaju KB (2012) Reaction kinetics of cellulose hydrolysis in subcritical and supercritical water, Doctoral Dissertation, University of Iowa, United States. Retrieved August 2014 [http://ir.uiowa.edu/cgi/viewcontent.cgi?article=3101&context=etd]

O'Sullivan AC (1997) Cellulose: the structure slowly unravels. Cellulose 4:173–207

Palmqvist E, Hahn-Hägerdal B (2000) Fermentation of lignocellulosic hydrolysates. II: inhibitors and mechanisms of inhibition. Bioresour. Technol. 74:25-33

Park S, Baker JO, Himmel ME, Parilla PA, Johnson DK (2010) Cellulose crystallinity index: measurement techniques and their impact on interpreting cellulase performance. Biotechnology for Biofuels 3:1-10

Parrinello M, Rahman A (1981) Polymorphic transitions in single crystals: a new molecular dynamics method. J. Appl. Phys. 52:7182-7190

Pereira AN, Mobedshahi M, Ladisch MR (1988) Preparation of cellodextrin. Methods in Enzymol. 160:26-38

Peterson AA, Vogel F, Lachance RP, Froling M, Antal MJ Jr, Tester JW (2008) Thermochemical biofuel production in hydrothermal media: A review of sub- and supercritical water technologies. Energy Environ. Sci. 1:32-65

Phaiboonsilpa N, Lu X, Yamauchi K, Saka S (2009) Chemical conversion of lignocellulosics as treated by two-step semi-flow hot-compressed water. In: Proceedings of the World Renewable Energy Congress 2009—Asia, May 19–21, 2009, Bangkok, p 235–240

Phaiboonsilpa N (2010) Chemical conversion of lignocellulosics as treated by two-step semi-flow hot-compressed water, (Unpublished) Doctoral Dissertation, Kyoto University, Japan

Phaiboonsilpa N, Yamauchi K, Lu X, Saka S (2010) Two-step hydrolysis of Japanese cedar as treated by semi-flow hot-compressed water. J. Wood Sci. 56:331-338

Phaiboonsilpa N, Tamunaidu P, Saka S (2011) Two-step hydrolysis of nipa (*Nypa fruiticans*) frond as treated by semi-flow hot-compressed water. Holzforschung 65:659-666

Phaiboonsilpa N, Saka S (2012) Hydrolysis behaviors of lignocellulosics as treated by two-step semi-flow hot-compressed water. Proceedings of the 10th International Symposium on Supercritical Fluids (ISSF 2012), May 13-16, 2012, San Fransisco, California, USA. Retrieved June 2014 [http://issf2012.com/handouts/documents/144_004.pdf]

Puri VP (1984) Effect of crystallinity and degree of polymerization of cellulose on enzymatic saccharification. Biotechnol. Bioeng. 26:1219-1222

Queyroy S, Muller-Plathe F, Brown D (2004) Molecular dynamics simulations of cellulose oligomers: Conformational analysis. Macromol. Theory Simul. 13:427-440

Rabemanolonstsoa H, Saka S (2013) Comparative study on chemical composition of various biomass species. RSC Advances 3:3946-3956

Reese ET, Segal L, Tripp VW (1957) The effect of cellulose on the degree of polymerization of cellulose and hydrocellulose. Text. Res. J. 27:626-632

REN21 Renewable Energy Policy Network (2005) Renewables 2005 Global Status Report. Washington, DC: Worldwatch Institute

Ribeiro KS, Kobayashi S, Beuthe M, Gasca J, Greene D, Lee DS, Muromachi Y, Newton PJ, Plotkin S, Sperling D, Wit R, Zhou PJ (2007) Transport and its infrastructure. In Climate Change 2007: Mitigation. Contribution of Working Group III to the Fourth Assessment Report of the Intergovernmental Panel on Climate Change [Metz B, Davidson OR, Bosch PR, Dave R, Meyer LA

(eds)], Cambridge University Press, Cambridge, United Kingdom and New York, NY, USA

Roche E, Chanzy H (1981) Electron microscopy study of the transformation of cellulose I into cellulose III_I in *Valonia*. Int. J. Biol. Macromol. 3:201-206

Roelofsen PA (1965) Ultrastructure of the wall in growing cells and its relation to the direction of the growth. Ad. Bot. Res. 2:69-149

Rogalinski T, Ingram T, Brunner G (2008) Hydrolysis of lignocellulosics biomass in water under elevated temperatures and pressures. J. of Supercrit. Fluids 47:54-63

Saka S, Ueno T (1999) Chemical conversion of various celluloses to glucose and its derivatives in supercritical water. Cellulose 6:177-191

Sakaki T, Shibata M, Sumi T, Yasuda S (2002) Saccharification of cellulose using a hot-compressed water-flow reactor. Ind. Eng. Chem. Res. 41: 661-665

Sarko A, Southwick J, Hayashi J (1976) Packing analysis of carbohydrates and polysaccharides. 7. Crystal structure of cellulose III_I and its relationship to other cellulose polymorphs. Macromolecules 9:857-863

Sasaki T, Tanaka T, Nanbu N, Sato Y, Kainuma K (1979) Correlation between X-ray diffraction measurements of cellulose crystalline structure and the susceptibility to microbial cellulose. Biotechnol. Bioeng. 21:1031-1042

Sasaki M, Kabyemela B, Malaluan R, Hirose S, Takeda N, Adschiri T, Arai K (1998) Cellulose hydrolysis in subcritical and supercritical water. J. Supercrit. Fluids 13:261-268

Sasaki M, Fang Z, Fukushima Y, Adschiri T, Arai K (2000) Dissolution and hydrolysis of cellulose in subcritical and supercritical water. Ind. Eng. Chem. Res. 30:2883-2890

Sasaki M, Furukawa M, Minami M, Adschiri T, Arai K (2002) Kinetics and mechanism of cellobiose hydrolysis and retro-aldol condensation in subcritical and supercritical water. Ind. Eng. Chem. Res. 41:6642-6649

Sasaki M, Adschiri T, Arai K (2003) Production of cellulose II from native cellulose by near- and supercritical water solubilization. J. Agric. Food Chem. 51:5376-5381

Sasaki M, Adschiri T, Arai K (2004) Kinetics of cellulose conversion at 25 MPa in sub- and supercritical water. J. Amer. Inst. Chem. Engrs. 50:192-202

Savage PE (1999) Organic chemical reactions in supercritical water. Chem. Rev. 99:603-621

Schacht C, Zetzl C, Brunner G (2008) From plant materials to ethanol by means of supercritical fluid technology. J. Supercrit. Fluids 46:299-321

Schulz GV, Husemann E (1942) Uber die Verteilung der Molekulargewichte in abgebauten cellulosen und ein periodisches aufbauprinzip im cellulosemolekul. Z. Phys. Chem. B 52:23–49

Shen T, Langan P, French AD, Johnson GP, Gnanakaran S (2009) Conformational flexibility of soluble cellulose oligomers: chain length and temperature dependence. J. Am. Chem. Soc. 131:14786-14794

Shibazaki H, Kuga S, Okano T (1997) Mercerization and acid hydrolysis of bacterial cellulose. Cellulose 4:75-87

Sievers C, Valenzuela-Olarte MB, Marzialetti T, Musin I, Agrawal PK, Christopher WJ (2009) Ionic-liquid-phase hydrolysis of pine wood. Ind. Eng. Chem. Res. 48:1277-1286

Sihtola H, Kyrklund B, Laamanen L, Palenius I (1963) Comparison and conversion of viscosity and DP-values determined by different methods. Paperi ja Puu 45:225-232

Sivers MV, Zacchi G (1995) A techno-economical comparison of three processes for the production of ethanol from pine. Bioresour. Technol. 51:43-52

Srokol Z, Bouche AG, Estrik AV, Strik RCJ, Maschmeyer T, Peters JA (2004) Hydrothermal upgrading of biomass to fuel; studies on some monosaccharide model compounds. Carbohydr. Res. 339:1717-1726

Stenberg D (1976) Production of cellulose by *Trichoderma*. Biotechnol. Bioeng. Symp. 6:35-53

Stone B (2005) Cellulose: Structure and distribution. In: eLS. John Wiley & Sons Ltd, Chichester. Retrieved June 2014 [http://onlinelibrary.wiley.com/doi /10.1038/npg.els.0003892/full]

Sueoka A, Hayashi J, Watanabe S (1973) Differences between native cellulose I and regenerated cellulose I (I') (in Japanese). Nippon Kagaku Kaishi 3:594-602

Sugiyama J, Vuong R, Chanzy H (1991a) Electron diffraction study on the two crystalline phases occurring in native cellulose from an algal cell wall. Macromolecules 24:4168-4175

Sugiyama J, Persson J, Chanzy H (1991b) Combined infrared and electron diffraction study of the polymorphism of native celluloses. Macromolecules 24:2461-2466

Sun Y, Cheng J (2002) Hydrolysis of lignocellulosic materials for ethanol production: a review. Bioresour. Technol. 83:1-11

Tanaka F, Fukui N (2004) The behavior of cellulose molecules in aqueous environments. Cellulose 11:33-38

TAPPI Standard Methods T230 om-82 (1982)

Tirtowidjojo S, Sarkanen KV, Pla F, McCarthy JL (1988) Kinetics of organosolv delignification in batch and flow-through reactors. Holzforschung 42:177-183

Tolonen LK, Zuckerstätter G, Penttilä PA, Milacher W, Habicht W, Serimaa R, Kruse A, Sixta H (2011) Structural changes in microcrystalline cellulose in subcritical water treatment. Biomacromolecules 12:2544-2551

UNEP, United Nations Environment Programme (2009). Toward sustainable production and use of resources: Assessing biofuels. Retrieved June 2014 [http://www.unep.org/pdf/biofuels/Assessing_Biofuels_Full_Report.pdf]

Uto T, Hosoya T, Hayashi S, Yui T (2013) Partial crystalline transformation of solvated cellulose III_I crystals reproduced by theoretical calculations. Cellulose 20:605-612

U.S. EPA, U.S. Environmental Protection Agency (2011) Biofuels and the environment: The first triennial report to congress (External Review Draft). U.S. Environmental Protection Agency, Washington, DC, EPA/600/R-10/183A

Van Wyk JPH (1997) Cellulose hydrolysis and cellulose adsorption after pretreatment of cellulose materials. Biotechnol. Tech. 11:443-335

Vanderghem C, Boquel P, Blecker C, Paquot M (2010) A multistage process to enhance cellobiose production from cellulosic materials. Appl. Biochem. Biotechnol. 160:2300-2307

Van Der Spoel D, Lindahl E, Hess B, Groenhof G, Mark AE, Berendsen HJC (2005) GROMACS: Fast, Flexible and Free. J. Comput. Chem. 26:1701-1719

Wada M (2001) In situ observation of the crystalline transformation from cellulose III_I to I_β. Macromolecules 34:3271-3275

Wada M, Heux L, Isogai A, Nishiyama Y, Chanzy H, Sugiyama J (2001) Improved structural data of cellulose III_I prepared in supercritical ammonia. Macromolecules 34:1237-1243

Wada M, Heux L, Sugiyama J (2004a) Polymorphism of cellulose I family: Reinvestigation of cellulose IV. Biomacromolecules 5:1385-1391

Wada M, Chanzy H, Nishiyama Y, Langan P (2004b) Cellulose III_I crystal structure and hydrogen bonding by synchrotron X-ray and neutron fiber diffraction. Macromolecules 37:8548-8555

Wada M, Kwon GU, Nishiyama Y (2008) Structure and thermal behavior of a cellulose I-ethylenediamine complex. Biomacromolecules 9:2898-2904

Wada M, Ike M, Tokuyasu K (2010) Enzymatic hydrolysis of cellulose I is greatly accelerated via its conversion to the cellulose II hydrate form. Polym. Degrad. Stab. 95:543-548

Wang WM, Cai ZS, Yu JY (2008) Study on the chemical modification process of jute fiber. J. Eng. Fiber. Fabr. 3:1-11

Ward RJ (2011) Cellulase engineering for biomass saccharification. In: Buckeridge MS, Goldman GH (eds) Routes to cellulosic ethanol. Springer, New York, p135-151

Weimer PJ, French AD, Calamari TA Jr (1991) Differential fermentation of cellulose allomorphs by ruminal cellulolytic bacteria. Appl. Environ. Microbiol. 57:3101-3106

Weimer PJ, Hackney JM, French AD (1995) Effects of chemical treatments and heating on the crystallinity of celluloses and their implications for evaluating the effect of crystallinity on cellulose biodegradation. Biotechnol. Bioeng. 48:169-178

Wheals AE, Basso LC, Alves DMG, Amorim HV (1999) Fuel ethanol after 25 years. Trends Biotechnol. 17:482-487

Whittaker RH (1970) Communities and ecosystems. The Macmillan Company, New York, p1-113

Woodcock C, Sarko A (1980) Packing analysis of carbohydrates and polysaccharides. 11. Molecular and crystal structure of native ramie cellulose. Macromolecules 13:1183-1187

Wright JD (1998) Ethanol from biomass by enzymatic hydrolysis. Chem. Eng. Prog., 84:62-74

Xiao LP, Sun ZJ, Shi ZJ, Xu F, Sun RC (2011) Impact of hot compressed water pretreatment on the structural changes of woody biomass for bioethanol production. Bioresources 6:1576-1598

Xin J, Imahara H, Saka S (2009) Kinetics on the oxidation of biodiesel stabilized with antioxidant. Fuel 88:282-286

Yamane C, Aoyagi T, Ago M, Sato K, Okajima K, Takahashi T (2006) Two different surface properties of regenerated cellulose due to structural anisotropy. Polym. J. 38: 819-826

Yamamoto H, Horii F, Odani H (1989) Structural-changes of native celluloses crystals induced by annealing in aqueous alkaline and acidic solutions at high-temperatures. Macromolecules 22:4130-4132

Yamamoto H, Horii F (1993) CP/MAS ^{13}C NMR analysis of the crystal transformation induced for *Valonia* cellulose by annealing at high temperatures. Macromolecules 22:1313-1317

Yang J, Zhang X, Yong Q, Yu S (2010) Three-stage hydrolysis to enhance enzymatic saccharification of steam-exploded corn stover. Bioresour. Technol. 101:4930-4935

Yatsu LY, Calamari TA, Jr and Benerito RR (1986) Conversion of cellulose I to stable cellulose III. Text. Res. J. 56:419-424

Yoshida K, Kusaki J, Ehara K, Saka S (2005) Characterization of low molecular weight organic acids from beech wood treated in supercritical water. Appl. Biochem. Biotechnol. 121-124:795-806

Yoshida M, Liu Y, Uchida S, Kawarada K, Ukagami Y, Ichinose H, Kaneko S, Fukuda K (2008) Effects of cellulose crystallinity, hemicellulose, and lignin on the enzymatic hydrolysis of *Miscanthus sinensis* to monosaccharides. Biosci. Biotechnol. Biochem. 72:805-810

Yu Y and Wu H (2009) Characteristics and precipitation of glucose oligomers in the fresh liquid products obtained from the hydrolysis of cellulose in hot-compressed water. Ind. Eng. Chem. Res. 48:10682-10690

Yu Y, Wu HW (2010) Understanding the primary liquid products of cellulose hydrolysis in hot-compressed water at various reaction temperatures. Energy Fuels 24:1963-1971

Yui T, Hayashi S (2007) Molecular dynamics simulations of solvated crystal models of cellulose I_{α} and III_{I}. Biomacromolecules 8:817-824

Yui T, Hayashi S (2009) Structural stability of the solvated cellulose III_{I} crystal models: a molecular dynamics study. Cellulose 16:151-165

Yui T (2012) Crystal structure conversions observed in cellulose III_{I} crystal models. Cellulose Commun. (In Japanese) 19:7-11

Zhang Q, Bulone V, Agren H, Tu Y (2011) A molecular dynamics study of the thermal response of crystalline cellulose I_{β}. Cellulose 18:207-22

Zhang YHP, Lynd LR (2004) Toward an aggregated understanding of enzymatic hydrolysis of cellulose: noncomplexed cellulose systems. Biotech. Bioeng. 88:797-824

Zhang YHP, Lynd LR (2005) Determination of the number-average degree of polymerization of cellodextrins and cellulose with application to enzymatic hydrolysis. Biomacromolecules 6:1510-1515

Zhu S, Wu Y, Chen Q, Yu Z, Wang C, Jin S, Ding Y, Wu G (2006) Dissolution of cellulose with ionic liquids and its application: a mini-review. Green Chem. 8:325-327

Zugenmaier P (2008) Crystalline cellulose and cellulose derivatives: characterization and structures. Springer, Heidelberg, Germany, p101-151

List of Publications and Award

Original papers

1. Abdullah R, Saka S (2012) Hydrolysis behavior of various crystalline celluloses from cotton linter as treated by one-step semi-flow hot-compressed water. In: Yao T (ed.) Zero-Carbon Energy Kyoto 2011, Green Energy and Technology, Springer, Tokyo, 141-146

2. Abdullah R, Saka S (2013) Transformation of crystalline cellulose III_I to cellulose I_β in semi-flow hot-compressed water treatment. In: Yao T (ed.) Zero-Carbon Energy Kyoto 2012, Green Energy and Technology, Springer, Tokyo, 105-111

3. Abdullah R, Ueda K, Saka S (2013) Decomposition behaviors of various crystalline celluloses as treated by semi-flow hot-compressed water. Cellulose 20:2321-2333

4. Abdullah R, Ueda K, Saka S (2014) Hydrothermal decomposition of various crystalline celluloses as treated by semi-flow hot-compressed water. J. Wood Sci. 60:278-286

5. Miyamoto H, Abdullah R, Tokimura H, Hayakawa D, Ueda K, Saka S Molecular dynamics simulation of dissociation behavior of various crystalline celluloses as treated with hot-compressed water. Cellulose DOI: 10.1007/s10570-014-0343-y (Published online: 08 July 2014)

6. Abdullah R, Saka S Hydrolysis behaviors of various crystalline celluloses as treated by cellulase of *Tricoderma viride*. Cellulose DOI: 10.1007/s10570-014-0410-4 (Published online: 26 August 2014)

Abstracts and Proceedings of International Conferences

1. Abdullah R, Saka S (2011) Hydrolysis behavior of various crystalline celluloses from cotton linter as treated by one-step semi-flow hot-compressed water. Abstracts of the 3rd GCOE International Symposium, August 18-19, 2011, Suwon, Korea, 96

2. Abdullah R, Saka S (2012) Observation on crystalline cellulose III_I transformed to I_β as treated by one-step semi-flow hot-compressed water. Abstracts of the 4th GCOE International Symposium, May 22-23, 2012, Bangkok, Thailand, 91

3. Abdullah R, Saka S (2012) Decomposition of various crystalline celluloses treated by semi-flow hot-compressed water. Abstracts of the 4th GCOE International Symposium, May 22-23, 2012, Bangkok, Thailand, 51

4. Miyamoto H, Abdullah R, Tokimura H, Hayakawa D, Saka S, Ueda K (2014) Molecular dynamics simulation on dissociation behaviors of various crystalline celluloses treated by hot-compressed water. Proceedings of the International Symposium organized by the Institute for Chemical Research, March 10-12, 2014, Kyoto, Japan, 138-139

5. Abdullah R, Ueda K, Saka S (2014) Comparative study of various crystalline celluloses in their decomposition behaviors as treated by semi-flow hot-compressed water. Proceedings of the Grand Renewable Energy 2014 International Conference and Exhibition, July 27-August 1, 2014, Tokyo, Japan, 207

Abstracts and Proceedings in Domestic Meetings

1. Abdullah R, Saka S (2012) One-step hydrolyses of various crystalline celluloses from cotton linter as treated by semi-flow hot-compressed water. Abstracts of the 62nd Annual Meeting of the Japan Wood Research Society, March 15-17, 2012, Sapporo, Japan, 161

2. Abdullah R, Saka S (2012) Hydrolyses of cotton linter in various crystalline forms as treated by one-step semi-flow hot-compressed water. Abstracts of the 19th Annual Meeting of the Cellulose Society of Japan, Nagoya, Japan, 2012, July 12-13, 7-8

3. Abdullah R, Ueda K, Saka S (2013) Decomposition behaviors of various crystalline celluloses as treated by semi-flow hot-compressed water. Abstracts of the 20th Annual Meeting of the Cellulose Society of Japan, July 18-19, 2013, Kyoto, Japan, 27-28

4. Abdullah R, Saka S (2014) Hydrolysis behaviors of various crystalline structures by enzymatic saccharification. Abstracts of the 21st Annual Meeting of the Cellulose Society of Japan, July 17-18, 2014, Kagoshimia, Japan, 121

Award

1. Best Group Research Presentation Award in the GCOE Group Presentation Session, August 3, 2012, Kyoto, Japan
   (Presentation title: Hour-by-hour simulation of an energy-independent office building)

Copyrights on original papers

The author would like to express her sincere appreciations to Springer for its kind permission in using the accepted manuscripts of the original papers for her dissertation. Each chapter concerned is acknowledged by providing the original source of publication and link to the published article on Springer's website.

Acknowledgments

In the name of Allah, the Most Gracious and the Most Merciful.

First and foremost, I would like to thank Allah for all the blessings that have been bestowed upon me to be able to pursue and complete this study.

I would like to convey my sincere gratitude to my advisor Professor Shiro Saka of the Laboratory of Energy Ecosystems, Department of Socio-Environmental Energy Science, Graduate School of Energy Science, Kyoto University, who is incredibly supportive with all dissertation, professional and personal issues. His continued guidance, discussion, motivation and support throughout my research training in the laboratory are very much appreciated and remembered, otherwise, the completion of this work would have been impossible. Meeting him for the first time at the biomass seminar in Jakarta back in 2009 gave the impression that he was a strict person and I actually felt a little scared and anxious in the beginning. Even so, I was determined to work under his supervision and became his research student. All the way through, my thoughts about him were wrong, in fact, knowing him has been a very great pleasure indeed.

I wish to express my appreciation to Associate Professor Haruo Kawamoto of Laboratory of Energy Ecosystems, Department of Socio-Environmental Energy Science, Graduate School of Energy Science, Kyoto University, for his constructive comments and valuable suggestions, particularly, during weekly student seminars. My appreciation also goes to Professor Junji Sugiyama, Division of Forest and Biomaterials Science, Graduate School of Agriculture, Kyoto University, for his advice and considerations toward the betterment of this dissertation.

For the former GCOE Specific Assistant Professor Kazuchika Yamauchi, I thank him for his contribution and help, especially on equipment troubleshooting. His friendly and approachable character in assisting the nitty-gritty part of my *nihongo-wakarimasen* experiences in the lab is very much treasured. For Assistant

Professor Eiji Minami of Laboratory of Energy Ecosystems, Department of Socio-Environmental Energy Science, Graduate School of Energy Science, Kyoto University, his comments and suggestions are very much valued.

A token of appreciation goes to Professor Kazuyoshi Ueda, Dr Hitomi Miyamoto and the group members of the Department of Advanced Materials Chemistry, Graduate School of Engineering, Yokohama National University, who have been very supportive and accommodating in conducting the collaborative works. Hopefully, they would not be the last ones.

My special thanks to the government of Brunei for generously funding my four years of study in Kyoto University, as well as the staff members of the Embassy of Brunei in Japan for their help in everything. In addition, I would like to thank the GCOE Program from the Graduate School of Energy Science, Kyoto University for the research funds.

To dear colleagues, Dr Nathanoon, Dr Pramila, Dr Harifara, Dr Fadjar, Dr Zul Ilham, Dr Asmadi, Dr Mahendra, Mai Ogura, Phoo, Takada, Nakahara, Fukutome, Sugami and the rest of Saka lab members, I am thankful for their assistances, moral and emotional supports. To amazing friends Az, Deejah, Erne, Ezan, Siti, Suzi, Zab, Shaheeda and Sabrina thanks for your invariable love and support. To my FOS PhD colleagues Zimah, Arif, Rozy, Daphne, Elvy, Hussein and Hong your constant support in my pursuit of a PhD is very much treasured. For the charming and *kawaii* Ms Nakanishi, Ms Senoue, Ms Kyomi and Ms Shibayama, I thank them for their kindness and help with the logistic, academic and financial matters.

On a personal note, my sincere thanks extended to my parents and parents-in-law for their supports beyond measure during my transition period here and always been there for my family back at home. To my beloved husband, Pg. Hazman Pg. Jaludin, I am truly grateful for his sacrifices in carrying out the family responsibilities during my absence. To my precious munchkins, Haziq Izzuddin,

Zahra Zulaikha and Aleesya Zaira, the love and smiles from all of them through Skype/Face Time have always been a source of rejuvenation after long, exhaustive lab works and they all deserve credit for all my achievements. I am sorry that I have missed your growing years. They all have supported me wholeheartedly in all my endeavours. I also wish to thank the entire family members for their love and support. I love them all dearly.

To my late grandmother, she will remain as the source of inspiration throughout my life, and I will always remember her words – "Knowledge is everything". She had inculcated the fighting spirit in me. How I wish she was here… I miss her…

Last but not least, I would like to thank the others who are not mentioned here for their continued support and being a part of this journey.

Alhamdulillah….

Rosnah Abdullah
2014